NI

NASA CR 165368

(NASA-CR-165368) THE DESIGN OF AN ULTRA-LOW SIDELOBE OFFSET-FED 1.22m ANTENNA FOR USE IN THE BROADCASTING SATELLITE SERVICE (Edutel Communications and Development, Inc.) 156 p HC A08/MF A01 CSCL 17B G3/32

N81-28312

Unclas 27036

THE DESIGN OF AN ULTRA-LOW SIDELOBE OFFSET-FED 1.22M ANTENNA FOR USE IN THE BROADCASTING SATELLITE SERVICE

by James M. Janky

EDUTEL Communications and Development, Inc.

prepared for

NATIONAL AERONAUTICS AND SPACE ADMINISTRATION

NASA Lewis Research Center

Contract NAS 3-22344

NASA CR 165368

THE DESIGN OF AN ULTRA-LOW SIDELOBE OFFSET-FED 1.22M ANTENNA FOR USE IN THE BROADCASTING SATELLITE SERVICE

by James M. Janky

EDUTEL Communications and Development, Inc.

prepared for

NATIONAL AERONAUTICS AND SPACE ADMINISTRATION

NASA Lewis Research Center

Contract NAS 3-22344

TABLE OF CONTENTS

TABLE OF CONTENTS (continued)

LIST OF FIGURES

LIST OF FIGURES (continued)

LIST OF TABLES

APPENDIX

ACKNOWLEDGEMENTS

The assistance of Dr. Steven P. Russell and Dr. William T. Zaumen in the analysis and programming is gratefully acknowledged, as is the mechanical design and cost estimating by Mr. Robert Lathrop and Mr. Claus Suberknopp.

SUMMARY

The purpose of this research effort is to determine a feed design and reflector geometry for an ultra-low sidelobe offset fed 1.22 meter antenna suitable for use in the 12 GHz Broadcasting Satellite Service. A particular set of arbitrary constraints was used to evaluate the relative merits of the feed horns and range of f/D geometries. These constraints are: minimum efficiency of 55%, -30 dB first sidelobe level (relative to on-axis gain), a 0 dBi plateau beyond the near-in sidelobe region, and a Chebyshev polynomial-based envelope (borrowed from filter theory) for the region from the -3 dB beamwidth points to the 0 dBi plateau region. This envelope is extremely stringent but the results of this research effort indicate that two types of corrugated feed and a cluster array of small 1λ horns do meet the constraints. If an evaluation program using these feeds is successful in attaining this performance, it means that a significant decrease in the orbital slot spacing between broadcasting satellites (and Fixed Service satellites) is possible, because of the greatly increased discrimination in the off-axis angle region from 1° to 12°.

A set of performance specifications and a mechanical design suitable for a consumer-oriented market in the Broadcasting Satellite Service was developed. Costs for production quantities of 10,000 units per year are estimated to be around $150, with a sale price in the range of $400 - $500.

SYMBOLS and DEFINITIONS

dB	decibel = 10 log P_1/P_2
dBi	dB relative to isotropic
f	focal length
D	diameter of parent parabola
$G(\theta)$	the Chebyshev envelope
$G(0)$	on-axis gain of antenna
θ_0	½ of the full 3 dB beamwidth in degrees
E	$[10^{R/10} - 1]^{\frac{1}{2}}$, a parameter
R	the ripple factor borrowed from filter theory in dB
$C_n(k\theta/\theta_0)$	$\cosh [n \cosh^{-1}(k\theta/\theta_0)]$
n	the order of the polynomial, 1, 2, . . .
k	the normalizing constant which matches the envelope to the 3 dB point at the 3 dB beamwidth θ_0 $= \cosh \left[\frac{\cosh^{-1}(1/E)}{n}\right]$
θ	angle relative to boresight axis of antenna
ϕ	azimuth angle measured from vertical reference axis on aperture of antenna
λ	wavelength
θ_F	feed angle relative to boresight axis

1.0 INTRODUCTION

1.1 Background

The importance of obtaining lower sidelobe levels from ground station antennas used in the broadcasting satellite service has been described [1]. The customary method for describing sidelobe levels is through the use of an envelope which starts at some off-axis angle just beyond the main beam [2]. The envelope currently adopted by the CCIR for use in international planning and interference analysis results in 6° orbital slot allocations. With the results of the WARC-77 requiring the Fixed Satellite Service (FSS) and the Broadcasting Satellite Service (BSS) to share the orbital arc as well as some portions of the 12 GHz band [2], and with a growing demand for FSS and BSS orbital slots, obtaining improved sidelobe performance and envelopes become even more important.

The new, high performance envelope proposed by NASA [3] is given by a Chebyshev type of equation derived from filter theory. The present CCIR envelope and two Chebyshev envelopes with n=2 and 3 are given in Figure 1-1, and discussed in subsequent paragraphs.

The reluctance of the CCIR administrations to adopt more stringent sidelobe envelopes in the past can be traced in part to a lack of specific hardware with measured test pattern results and corresponding high volume for production cost estimates.

1.2 Objective

The purpose of this effort is to remedy this perceived situation by designing an ultra-low sidelobe antenna suitable for use in the Broadcast Satellite Service with a Chebyshev envelope performance. The actual design will be fabricated and tested in a subsequent effort.

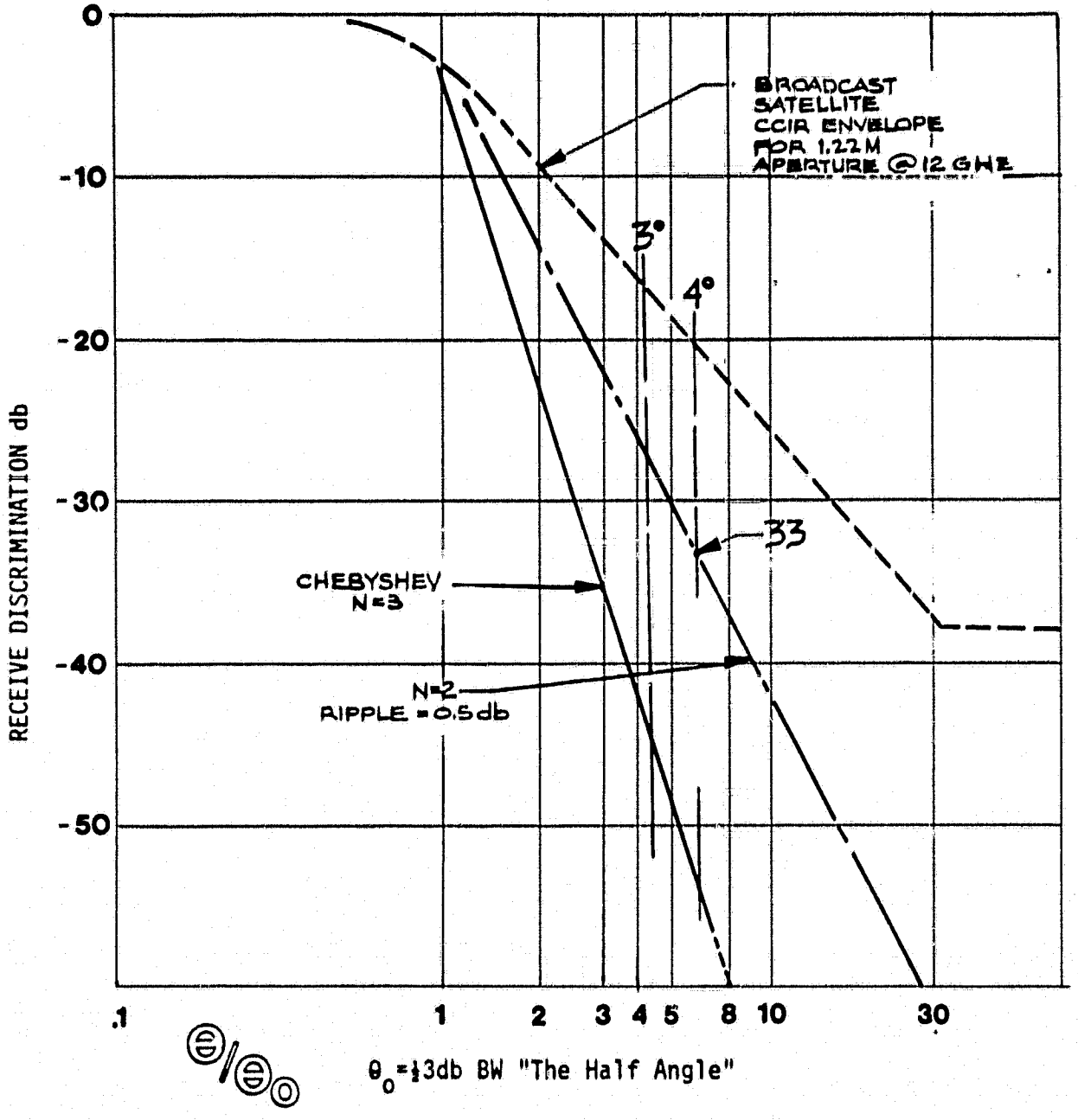

FIGURE 1-1 Sidelobe Envelopes

The baseline design for a Broadcasting Satellite Service (BSS) system calls for a 1.22m antenna. Further, it has been shown in previous theoretical work that, in order to obtain any significant improvement in sidelobe levels, an unblocked aperture is desirable (CWRU showed it could be done).

Blockage due to the feed and its supports introduces increases in both the near-in and far-out sidelobes due to the inverse transform of the blockage, and scattering, respectively [1]. Although antennas as small as 3m have met the CCIR/FCC (32-25 log θ) sidelobe envelope at 6 GHz ($D/\lambda = 60$, the Prodelin Co., Hightstown, N.J.) averaging of the sidelobe levels is usually required and the designs are usually complicated and expensive. This need for an unblocked aperture leads to the requirement for an offset-fed configuration. For simplicity of design and for minimizing the expected manufacturing cost, we will address only prime-focus offset-fed antennas.

1.3 Relevance of Previous Work

In previous work [1], the ideal illumination function for an arbitrary far-field pattern was calculated. This far-field pattern was constrained to fit under an envelope given by a second or third-order Chebyshev envelope down to a plateau of 10, 0, or -10 dBi. The basic conclusion of that preliminary theoretical work was that there is a tradeoff available between sidelobe level and aperture efficiency. Sidelobe levels can be made arbitrarily small if efficiency is not constrained to some peak performance specification like 60 to 70%. This is easily done by under-illuminating the dish, i.e., by letting the edge illumination taper increase from a typical -10 dB to -20 dB. Ref. [1] considered only the ideal illumination function and only for an axi-symmetric parabola. Synthesizing that ideal primary illumination function for an offset-fed configuration with a physically realizable feed that also has excellent sidelobes itself (in order that the feed spillover be low enough to

meet the plateau-level requirement of -10 dBi) is one of the major requirements addressed in this report.

As a result of using actual feed patterns from physically realizable horns, the actual efficiency is expected to be slightly better than was predicted in the previous study. Further improvements may be possible through the use of more complicated feeds such as cluster arrays of 1λ horns. These possibilities are also investigated.

1.4 Approach

We investigated three radically different approaches in analyzing the basic problem which is that of determining the best feed for realizing a Chebyshev envelope with a 1.22m offset-fed antenna.

1.4.1 The Analytic Approach: Pure Mode Synthesis

The first and most complicated approach as proposed in the original work statement is to work backward from the desired far-field pattern to the aperture illumination function and then to the far-field feed pattern function or to the focal fields distribution at the aperture of the feed. This approach is very difficult because of the non-uniqueness of the far-field phase pattern and the complex nature of the focal field distribution. On top of that, once the focal field distribution is obtained, it is extremely difficult to synthesize that exact field distribution by the normal method of superimposing a number of different modes in a feed horn. And then there is the added difficulty of actually physically building a feed that introduces the right amplitude and phase of the various number of modes required. Analytically, this is a very tough process and we did not pursue it to its conclusion.

We did, however, make a start by doing the transformation from the desired aperture distribution to the far-field illumination pattern of the feed horn. We thus have an idea of the degree of ellipticity that the feed horn must have to produce a prescribed $J_1(u)/u$ aperture distribution. We assumed a range of edge illumination tapers so that the relative beamwidth of the $J_1(u)u$ function varied accordingly. The extent of the ellipticity is extremely small for reasonable f/D ratios. The results of this effort are contained in Appendix 1.

1.4.2 The Experiential Approach: Use Of A Circular Symmetric Corrugated Horn

A second approach relies on the more familiar techniques of working forward with a known feed function and examining what the sidelobe levels are in the far-field. The advantages of this technique are many. In the first place, using a known feed function guarantees that there will be few surprises when an actual test is done on a test range. Based on our experience and thorough literature search, we know that the basic feed requirements must include the use of a nearly axially symmetric feed function and that this function in itself must have very low sidelobes. This implies immediately the use of a circular corrugated horn which produces the hybrid balanced HE_{11} mode, (i.e., a combination of the TE_{11} and the TM_{11} modes). So, by assuming this type of feed function at first and examining the far field, we can establish a baseline of performance with which we can compare other analysis techniques and feed realization techniques.

It is well known that the use of a corrugated horn in a prime focus antenna produces very low sidelobes because of the axial symmetry that horn's primary pattern possesses, and because the corrugated horn itself has very low sidelobes, usually 30 - 40 dB below beam center. This is very important

for the off-axis angles beyond 60° for a center-fed prime focus antenna because of "spillover". Spillover refers to reception by the primary feed horn of signals that are incident from other than the surface of the dish. Typically, angles off the bore-sight axis from 60° to 90° are the worst cases for spillover reception. By using a corrugated horn and assuming a very good feed pattern, we have simplified the range and breadth of the analysis necessary to determine a reasonable solution. We limit the variations in feed horn parameters to a range over which known good performances can be obtained.* We have examined the case for a 3λ and a 4λ horn and the results are described in the next section of this report.

Since the aperture of the feed horn has now been fixed at 3λ and 4λ, the resulting primary radiation patterns are also fixed. This leaves only the focal length to diameter ratio (f/D) as the last variable. By varying the f/D we can effectively change the edge illumination taper. The essential difference between this approach and the analytic approach is that we have no axial asymmetry in the feed pattern as we know we must have from the initial analytic effort (Appendix 1). Thus, we know that we haven't provided a perfect match to illuminate the aperture plane exactly with the type of function described in our previous work. However, because of the inherently good performance obtained from a corrugated horn, and since the degree of asymmetry needed for a practical and efficient design will be small, we have established a reasonable baseline reference design to which other approaches can be compared.

1.4.3 The Synthetic Approach: Use Of A Cluster Array

With this method, we use an entirely different approach to synthesis. We assume the use of a cluster array of small diameter (1λ) horns. By assuming a linear superposition of

---

* The relative size of the corrugated horn aperture must be at least 2 wavelengths in diameter in order to properly launch the hybrid mode.

multiple single point sources, we can calculate the far field pattern due to each individual horn. Since each small horn has an illumination function that is very broad, the resulting far field pattern may be assumed to look like $J_1(u)/u$. This is the mathematically simple transform of a uniform illumination pattern. Experimentally, this approximation has been found to be very useful. We have analyzed and synthesized a seven element cluster array. Examination of the magnitude and phase of each individual element of the array reveals the slight asymmetry postulated earlier as being necessary for perfect illumination. The results for these two cases are summarized in a subsequent section.

Finally, if we wish to revisit the possibility of using a multimode horn to synthesize the far field pattern, we must determine the focal field distribution in more detail than is possible with a seven element approximation. Based on the experience obtained from the array analysis, we have expanded the number of elements from seven to nineteen. The results of this analysis permit a more accurate, unique definition of the focal field strength, and thus provide a way to develop a multimode horn. The design of this type of horn is beyond the scope of the present effort.

1.5 Far Field Analysis Procedure

We have used a far field pattern analysis procedure based on the result of Mentzer, et al., and described in their report entitled "Pattern Analysis of an Offset-Fed Parabolic Reflector Antenna" [4]. The importance of this type of analysis using the Geometric Theory of Diffraction cannot be over-emphasized in this type of work with relatively small apertures. Beyond the first 10 sidelobes, the usual Fourier transform theory approach will not give accurate or useful results; in fact, it will provide extremely optimistic results which would not be borne out on the test range. The results of Section 2 for the baseline design were all determined with this type of program.

1.6 The Chebyshev Envelope and Specification Limits

1.6.1 The Chebyshev Envelope

The envelopes used to guide our design work are given by the following equation:

$$G(k\theta/\theta_0) = G(0) - 10 \log_{10} \{1 + E^2 C_n^2 (k\theta/\theta_0)\} \text{ dB}$$

where

$G(\ )$ = the Chebyshev envelope

$G(0)$ = the on-axis gain of the antenna

θ_0 = ½ of the full 3 dB beamwidth in degrees

E = $\{10^{R/10} - 1\}^{\frac{1}{2}}$, a parameter

R = the ripple factor borrowed from filter theory in dB

$C_n(k\theta/\theta_0)$ = $\cosh \{(n \cosh^{-1}(k\theta/\theta_0))\}$

n = the order of the polynomial, 1, 2, . . .

k = the normalizing constant which matches the envelope to the 3 dB point at the 3 dB beamwidth $\cdot \theta_0$

$$= \cosh \left\{\frac{\cosh^{-1}(1/E)}{n}\right\}$$

This equation gives the envelope relative to the peak on-axis gain. Through the constant k we arrange so that the Chebyshev envelopes are coincident with the 3 dB point at $\theta=\theta_o$. We have examined a range of ripple factors. For the sake of argument, we have selected a ripple factor, R, of 0.5 dB. The ripple factor is useful in adjusting the rate of decay of the envelope over some small range. The factor n has much greater influence, largely because of the use of integer values. The ripple factor has little real relevance to the antenna work herein because we are not concerned with shaping or specifying the main beam. For a zero ripple factor, the equations are slightly different. The main effect of increasing the ripple factor is to increase the rate of decay, and so could be used to fine-tune an envelope to match measured results with predicted and/or desired performance. The limits on this range of envelope parameters are related to other factors as follows.

1.6.2 Envelope Parameters

For the broadcasting satellite service, a maximum protection ratio (or discrimination from unwanted signals) of 40 dB is likely to be entirely adequate. This can be inferred from the CCIR documents* on Protection Ratios among the various services. Consequently, we have adopted a plateau of 0 dB as a baseline performance goal. If better performance can be obtained, this limit may be reconsidered after verification on the test range.

One of the major ingredients in the realization of very low sidelobes is the edge taper of the illumination function. We are interested in severe under-illumination, and so the main beamwidth and the location of the nulls and near-in sidelobes will be larger than for the limiting case of uniform illumination. The choice of envelope parameters must be such that the envelope is above the main beam. As a result, the order of the Chebyshev envelope can be no higher than 2 for simple feeds.

1.6.3 Gain and Efficiency

In the previous work [1], it was shown that sidelobes could be made arbitrarily low at the expense of overall efficiency. To obtain a certain gain level and a specified sidelobe envelope, the diameter of the reflector would have to increase. The conclusion of that report argued that for a penalty of about 10% increase in diameter (20% decrease in efficiency), a much lower sidelobe level could be had. But in the Broadcasting Satellite Service, overall efficiency is very important because of the impact on system cost. Larger dishes cost more. Therefore, we have constrained the efficiency to be no less than the historically experienced levels of 50 - 60%. This is also less than what is feasible with corrugated feeds today, but the compromise is likely to work out well in that much better sidelobes can be obtained.

---

*Subjectively Measured Interference Protection Ratios for Planning Television Broadcasting Systems, Rep. 634, Vol. XI, CCIR Documents, XIV Plenary Assembly, 1978, Kyoto.

1.6.4 First Sidelobe Level

The first and second sidelobes occur at ±2.4° and ±3.6°, respectively for an under-illuminated system. The contract specifications require that the first sidelobes be at least 30 dB below the on-axis gain.

1.6.5 Equivalence to Other Envelope Descriptions

The Chebyshev type of envelope can be related to the more familiar form of specifying the absolute gain according to the equaion:

$$G(\theta) = a + b \log \theta/\theta_o \qquad (2)$$

For n=2 and for a nominal gain of 42 dB, the equivalent expression is:

$$G(\theta) = 39\text{-}39.6 \log (\theta/\theta_o) \text{ dBi} \qquad (3)$$

For n=3, it is:

$$G(\theta) = 39\text{-}63 \log (\theta/\theta_o) \text{ dBi} \qquad (4)$$

When put in this form it is easy to see why it is so difficult to use n=3.

1.7 Implications of the Goals and Constraints

The results of this set of goals and specifications is that the only dependent variables available are the f/D ratio and the feed illumination function. In order to make a start, we shall fix the illumination functions and examine what occurs as the f/D ratios vary.

2.0 THE BASELINE DESIGN
A CIRCULAR SYMMETRIC CORRUGATED FEED

2.1 Rationale

The original approach to developing an optimum low sidelobe design required the determination of a large number of optimum feed horn illumination functions, i.e., one for each f/D under consideration. Once this data is obtained, we could attempt to synthesize the feed horn pattern for each case, assuming that a number of modes could be excited in the proper phase and amplitude. An "optimum" design for this type of approach might be one in which the best fit to the design feed horn pattern is obtained with the fewest number of modes. However, any real feed horn would have some error of fit with respect to our derived optimum, and so we would want to determine the expected far-field pattern based on the real feed horn to examine how well the objective of gain, first sidelobe level, and far-out sidelobes were met. In doing so, we would be using real patterns, with little regard for our original ideal illumination functions. Accordingly, we altered the original approach.

Instead, we have assumed the use of a corrugated feed horn which produced excellent primary patterns, as shown by inspection of the data in Tables 2-1 and 2-2. These horns both have a flare angle of 30°and are 3λ and 4λ in aperture width. We used these parameters because we wanted first of all to get good primary patterns with low sidelobes and excellent symmetry. Also, this is actual measured data. The design of the feed to be used in a test antenna is described in a subsequent section. Also, it is very difficult to synthesize a corrugated design with a prescribed beam width (illumination taper) and with prescribed sidelobe levels.

Table 2-1 — FAR FIELD PATTERN FOR
THREE LAMBDA DIAMETER CORRUGATED HORN

THETA	INPUT PATTERN IN DBi	NORMALIZED PATTERN GAIN, dB
0	17.87	0
5.0	17.40	- 0.47
10.0	15.97	- 1.90
15.0	13.51	- 4.36
20.0	9.86	- 8.01
25.0	4.66	-13.21
30.0	- 3.19	-21.06
35.0	-19.61	-37.48
40.0	-13.08	-30.95
45.0	-10.93	-28.80
50.0	-12.49	-30.36
55.0	-16.25	-34.12
60.0	-22.53	-40.40
65.0	-35.52	-53.39
70.0	-32.73	-50.60
75.0	-27.40	-45.27
80.0	-25.86	-43.73
85.0	-25.64	-43.51
90.0	-26.13	-44.00
95.0	-27.17	-45.04
100.0	-28.93	-46.30
105.0	-32.05	-49.92
110.0	-39.17	-57.04
115.0	-44.17	-62.04
120.0	-32.14	-50.01
125.0	-27.63	-45.50
130.0	-25.78	-43.65
135.0	-26.31	-44.18
140.0	-30.90	-48.77
145.0	-43.16	-61.03
150.0	-26.16	-44.03

Table 2-2 — FAR FIELD PATTERN FOR
FOUR LAMBDA DIAMETER CORRUGATED HORN

THETA	INPUT PATTERN IN dBi	NORMALIZED PATTERN GAIN, dB
0.	20.36	0
5.0	19.53	- 0.83
10.0	16.96	- 3.41
15.0	12.31	- 8.05
20.0	4.50	-15.86
25.0	-12.27	-32.63
30.0	- 8.39	-28.75
35.0	- 9.02	-29.38
40.0	-17.09	-37.45
45.0	-26.61	-46.97
50.0	-18.27	-38.63
55.0	-18.57	-38.93
60.0	-22.27	-42.63
65.0	-29.74	-50.11
70.0	-48.51	-68.87
75.0	-33.55	-53.91
80.0	-30.43	-50.79
85.0	-29.74	-50.10
90.0	-30.11	-50.47
95.0	-31.26	-51.62
100.0	-33.50	-53.86
105.0	-38.22	-58.58
110.0	-60.34	-80.70
115.0	-37.65	-58.01
120.0	-31.83	-52.19
125.0	-29.93	-50.29
130.0	-31.58	-51.94

The utility of this approach is two-fold. First, we minimize problems due to spillover from horn design. Ultimately, this need for low spillover would fall out of any analysis which sought to predict the optimum feed function. By using a good known pattern from the start, we establish a reference point from which to examine possible improvements. Second, we eliminate the need to design a large variety of different feed horns to suit the variations in illumination function we might encounter as we tried to optimize the feed pattern over the large range of f/D required.

2.2 Geometry

The circular aperture offset fed geometry analyzed herein is described in Figure 2-1. The range of f/D covers 0.15 to 1.30. The corresponding dimensions and angles are also given in Table 2-3. The f/D ratio is defined in terms of the parent parabola, and no allowance is made for the normal 1λ to 2λ offset to eliminate any feed blockage effects. Thus the parent parabola diameter is 2.44m for the 1.22m nominal case of interest. The offset for feed clearance is accounted for in subsequent sections.

2.3 Gain and First Sidelobe Levels

Figure 2-2 summarizes the essential tradeoffs between first sidelobe levels and efficiency as a function of f/D ratio with the horn size as a parameter. Inspection reveals a number of observations. First, attaining a very low first sidelobe level in the vicinity of -30 dB (relative to beam center) is a very sensitive function of f/D ratio for either horn diameter.

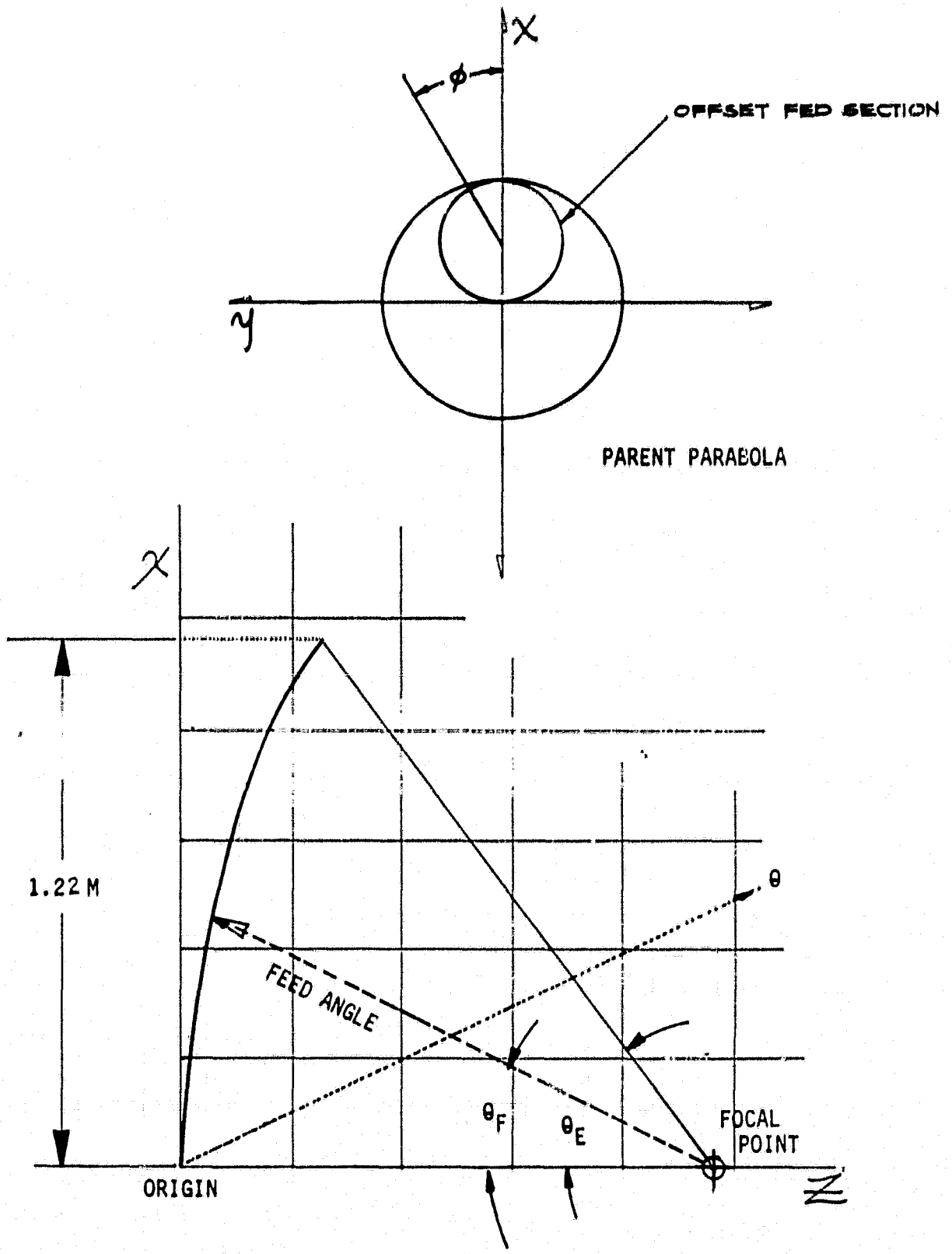

Figure 2-1. Geometry and definitions for the offset FED configuration.

Table 2-3 — REFLECTOR PARAMETERS

DATA SET	f/D	f,m	θ_F
A	0.15	0.36	79.6°
B	0.30	0.72	45.2°
C	0.50	1.20	28.1°
D	0.70	1.68	20.3°
E	0.90	2.16	15.8°
F	1.10	2.64	13.0°
G	1.30	3.12	11.0°

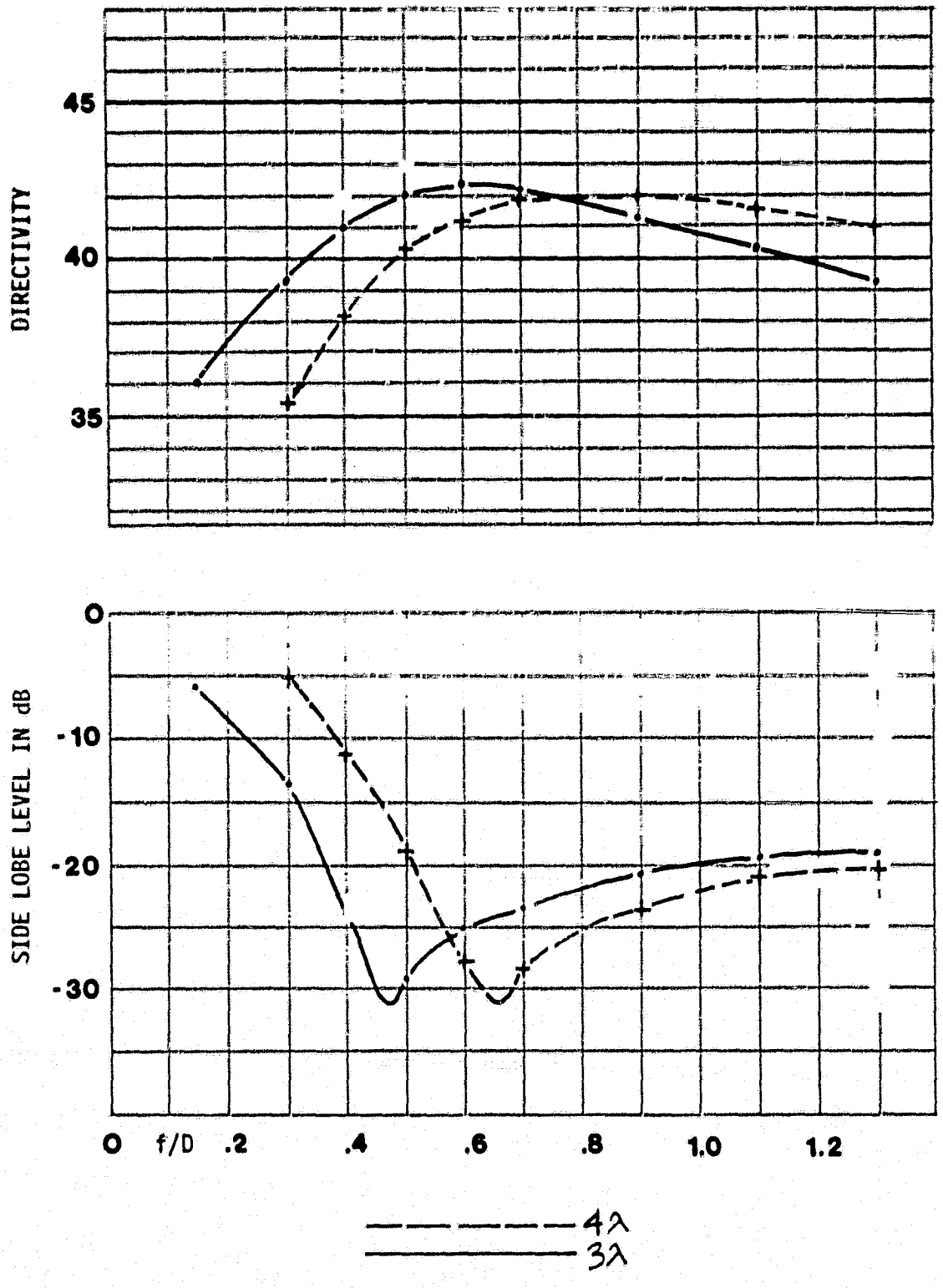

Figure 2-2. Relative Gain and First Sidelobe Level as a function of f/D Ratio with horn size as a parameter.

Second, the smaller aperture horn (3λ) attains its minimum sooner than the 4λ horn as f/D increases. From a mechanical/structural design standpoint, this is more desirable since it means the constraints on the feed horn support mechanism are less stringent. Also, the gain attains its maximum sooner for the smaller aperture horn, but the f/D point of maximum gain and minimum first sidelobe are not the same. The smaller horn should attain its maximum gain sooner, because its beamwidth is broader and therefore the illumination function edge taper is less steep. At the apparent first sidelobe minimum point for the 3λ horn, the gain is in excess of the specified limit, 41 dB. By contrast, the first sidelobe minimum for the 4λ horn occurs at an f/D ≅ 0.65, and the gain is also above our minimum. For an f/D = 0.5, the 4λ horn case has higher sidelobes and less gain than necessary.

By extension of this analysis, we might infer that a 2λ horn would attain the first sidelobe and gain specifications sooner as f/D increases, thereby lessening our mechanical constraints even further. However, we have not yet examined the complete far field data, and so it would be premature to make this conclusion. Further, the primary pattern of a smaller horn will have worse sidelobes itself and so the spillover levels will be worse.

The complete set of far-field patterns are shown in Figures 2-3A-G and 2-4A-G. For each f/D, there are four θ patterns corresponding to Ø = 0°, 45°, 90° and 135° about the boresight axis (as shown in Figure 2-1). Each pattern has the n = 2 Chebyshev envelope plotted on it down to a level of 0 dBi.

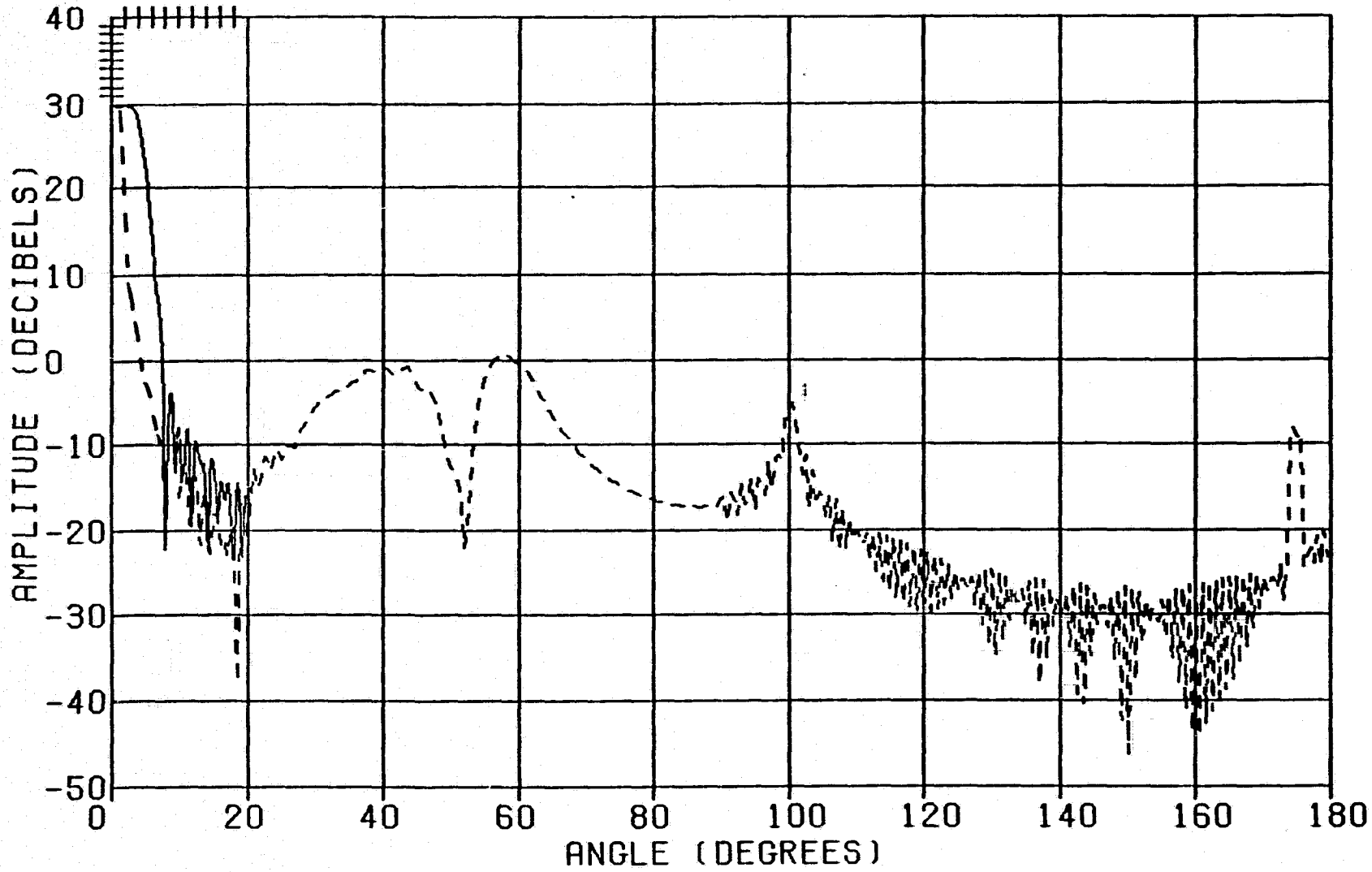

FOCAL LENGTH = 14.173, FEED ANGLE = 79.61, FREQ = 12.0 G
GPAT+GTD PATTERN PHI = 0.0, PRINCIPAL (XH)
GPAT(SOLID), GTD(DASHED)

FIGURE 2-3A-1 FAR FIELD PATTERN FOR 3 λ HORN WITH f/D=0.15 ϕ = 0°

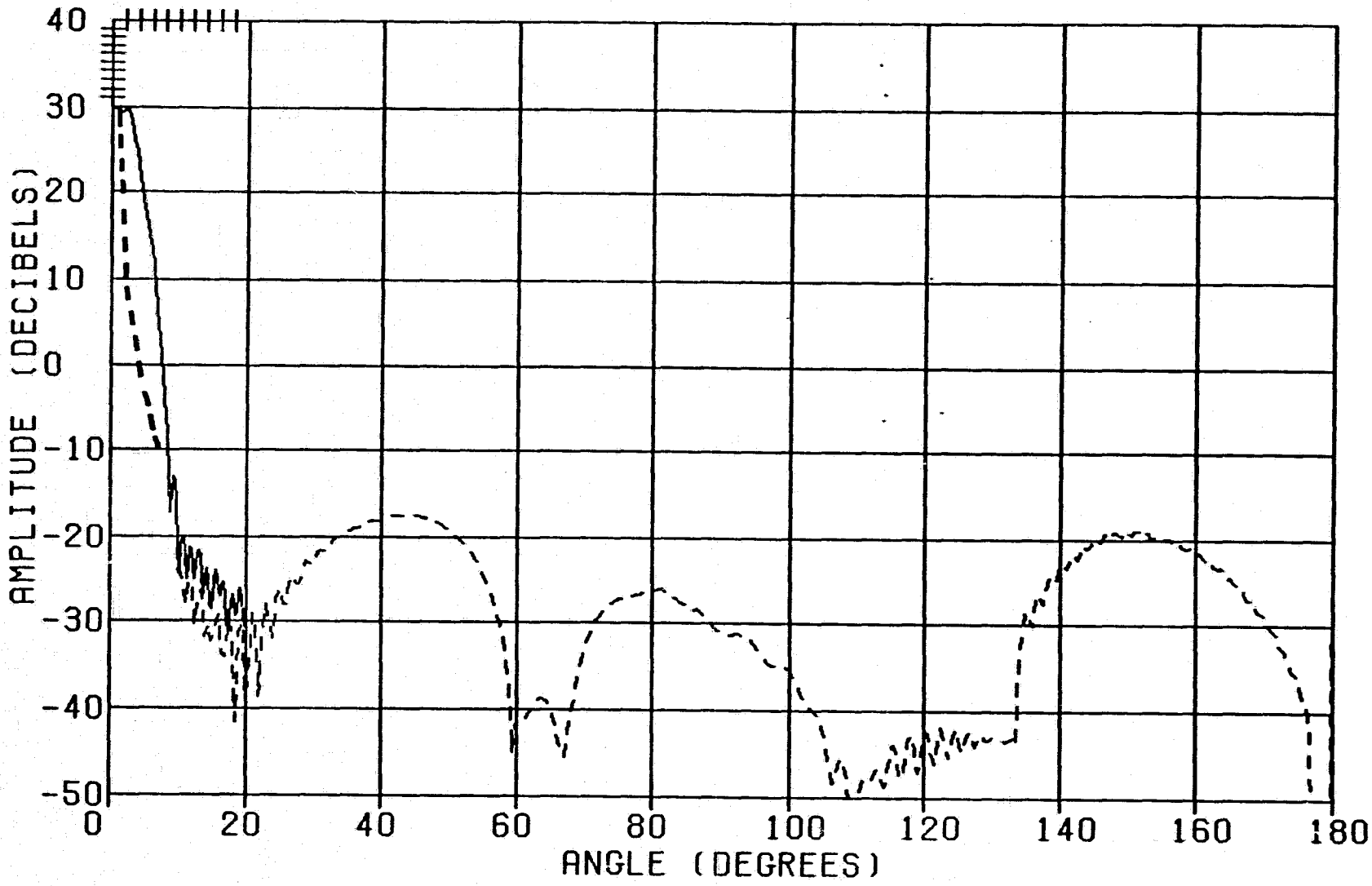

FIGURE 2-3A-2 FAR FIELD PATTERN FOR 3 λ HORN WITH f/D=0.15 Ø = 45°

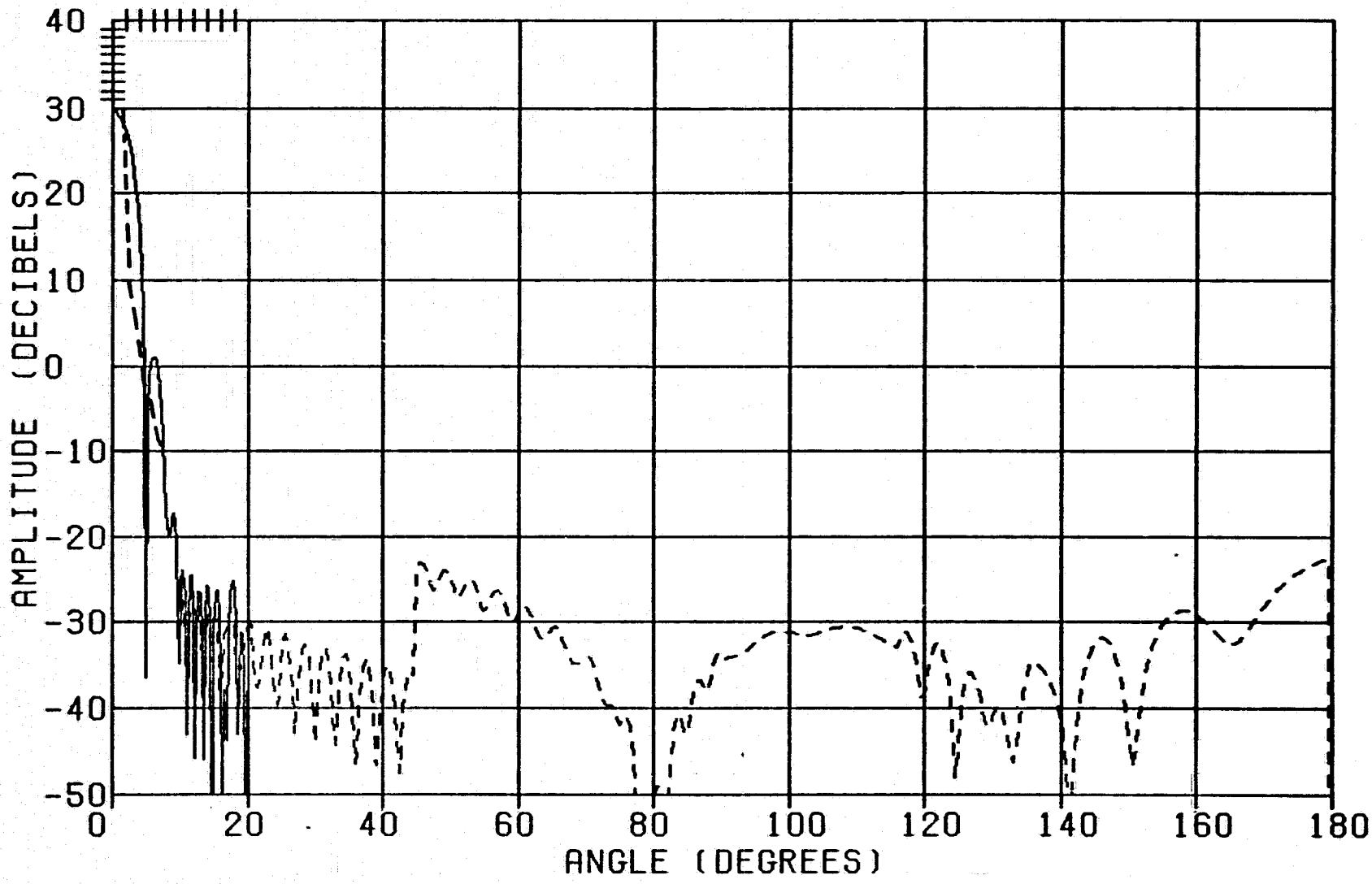

FOCAL LENGTH = 14.173, FEED ANGLE = 79.61, FREQ = 12.0 G
GPAT+GTD PATTERN PHI = 90.0, PRINCIPAL (XH)
GPAT(SOLID), GTD(DASHED)

FIGURE 2-3A-3 FAR FIELD PATTERN FOR 3 λ HORN WITH f/D=0.15 Ø = 90°

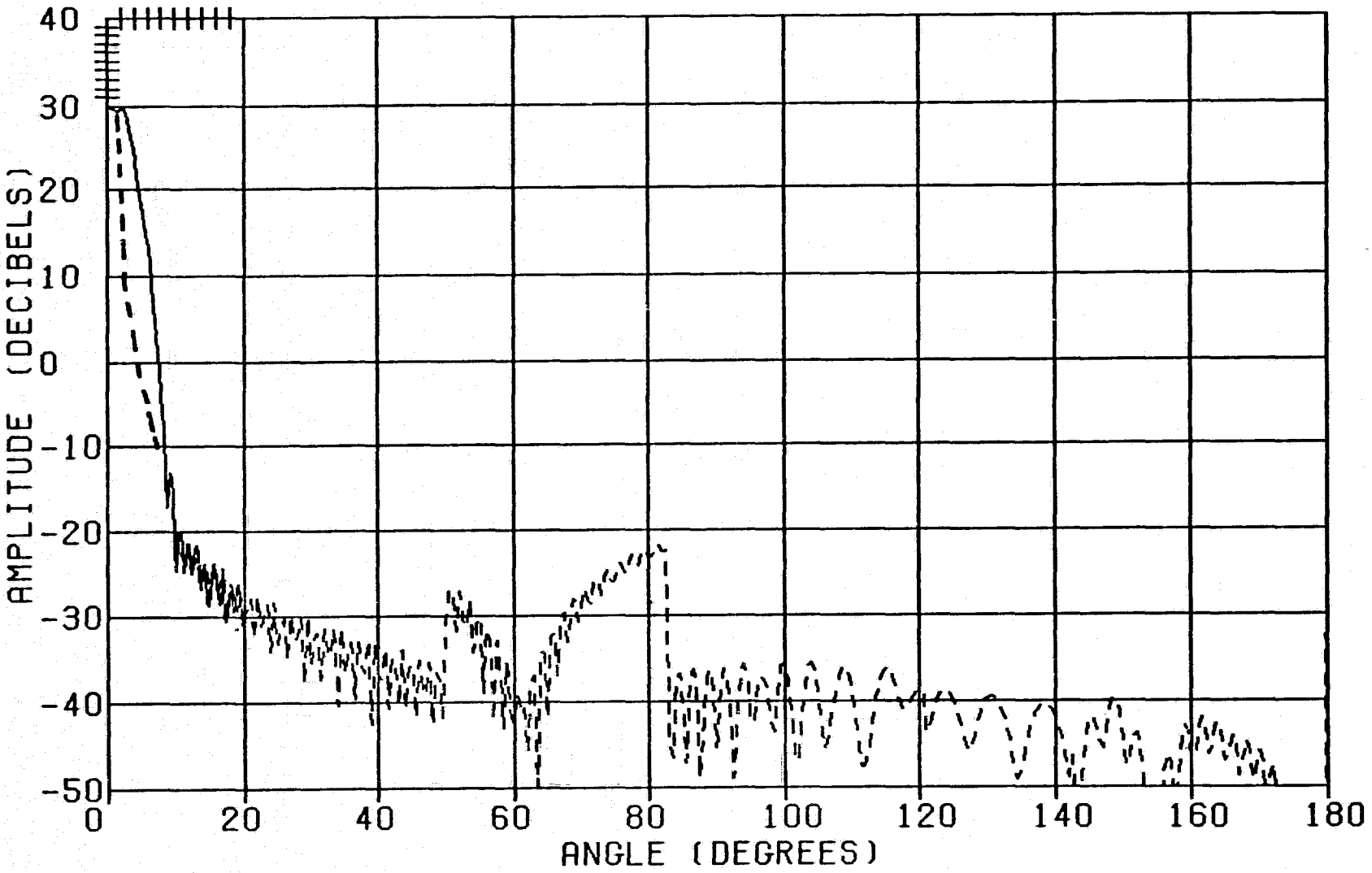

FOCAL LENGTH = 14.173, FEED ANGLE = 79.61, FREQ = 12.0 G
GPAT+GTD PATTERN PHI = 135.0, PRINCIPAL (XH)
GPAT(SOLID), GTD(DASHED)

FIGURE 2-3A-4 FAR FIELD PATTERN FOR 3 λ HORN WITH f/D=0.15 Ø = 135°

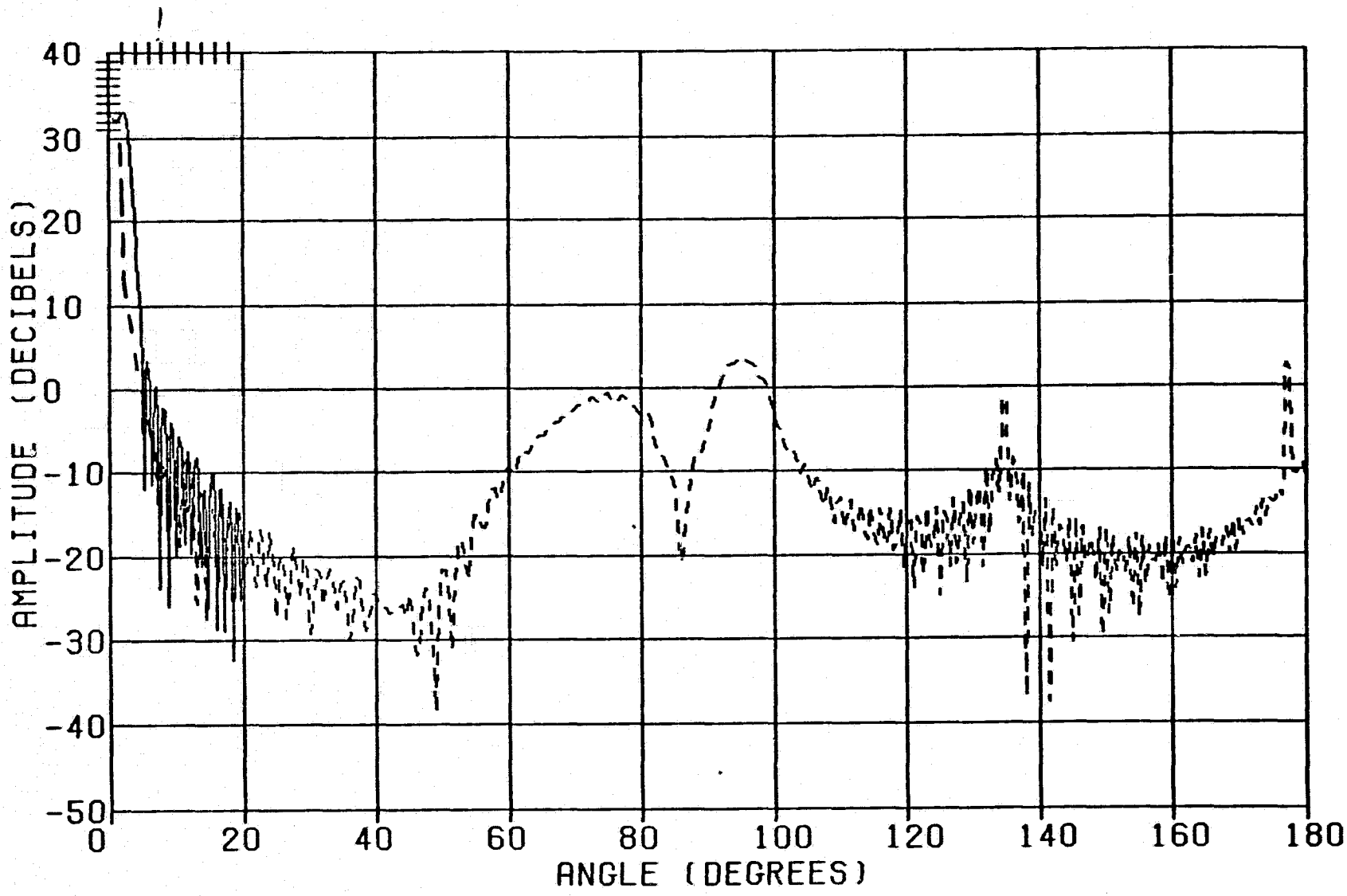

FOCAL LENGTH = 28.346. FEED ANGLE = 45.24. FREQ = 12.0 G
GPAT+GTD PATTERN PHI = 0.0, PRINCIPAL (XH)
GPAT(SOLID), GTD(DASHED)

FIGURE 2-3B-T FAR FIELD PATTERN FOR 3 λ HORN WITH f/D=0.30 Ø = 0°

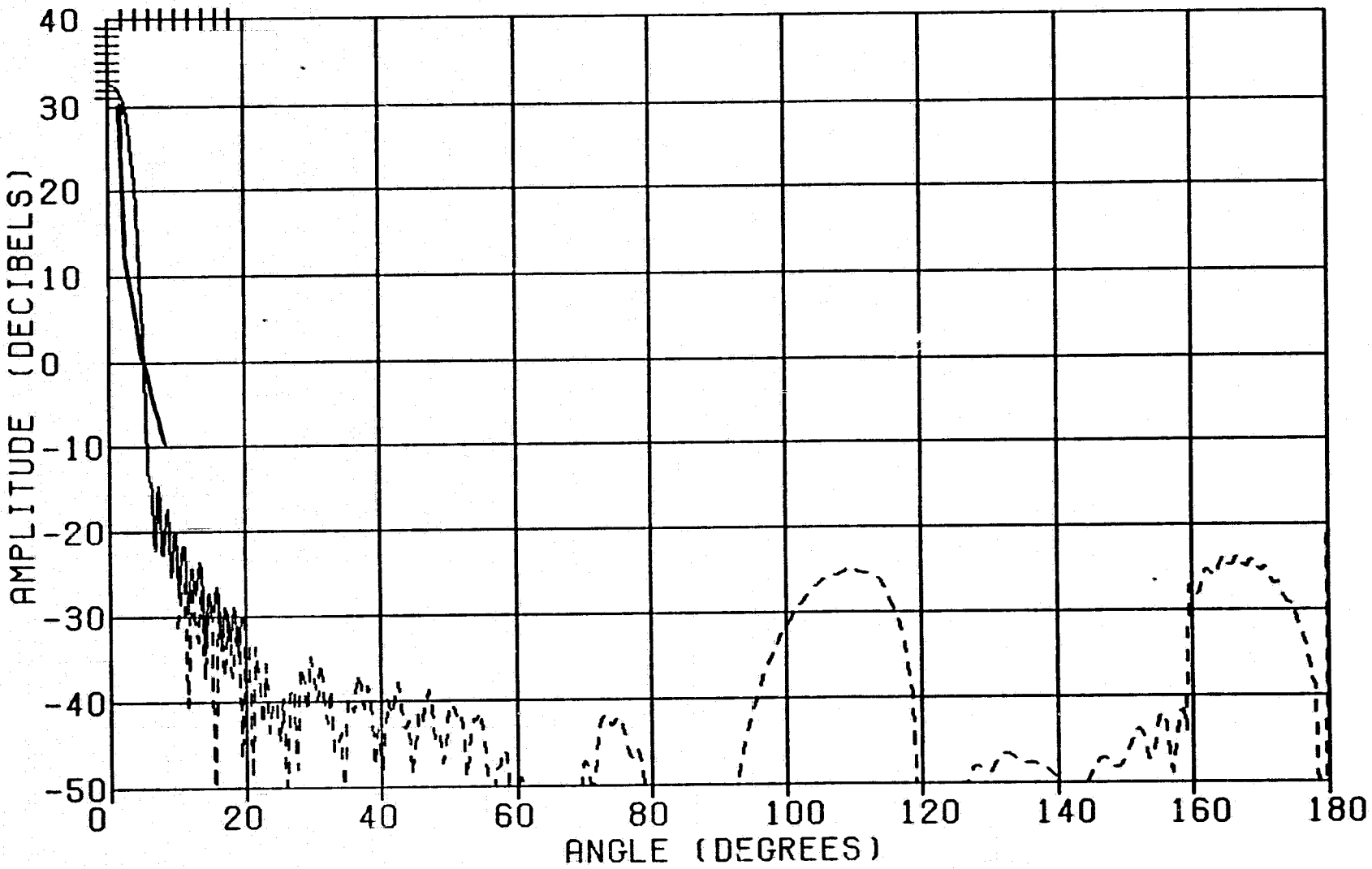

FOCAL LENGTH = 28.346, FEED ANGLE = 45.24, FREQ = 12.0 G
GPAT+GTD PATTERN PHI = 45.0, PRINCIPAL (XH)
GPAT(SOLID), GTD(DASHED)

FIGURE 2-3B-2 FAR FIELD PATTERN FOR 3 λ HORN f/D=0.30 · Ø = 45°

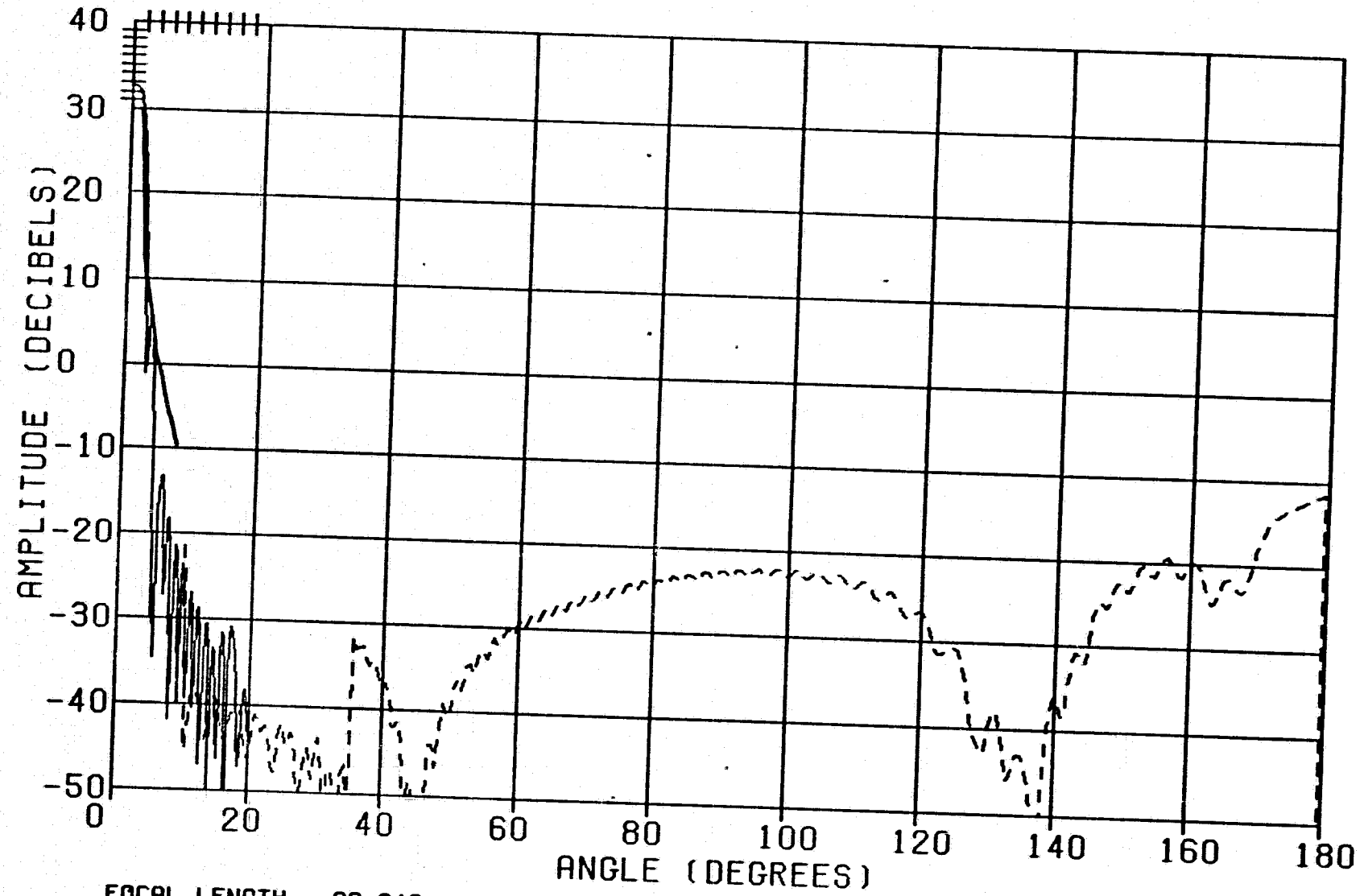

FOCAL LENGTH = 28.346, FEED ANGLE = 45.24, FREQ = 12.0 G
GPAT+GTD PATTERN PHI = 90.0, PRINCIPAL (XH)
GPAT(SOLID), GTD(DASHED)

FIGURE 2-3B-3 FAR FIELD PATTERN FOR 3 λ HORN WITH f/D=0.30 ϕ = 90°

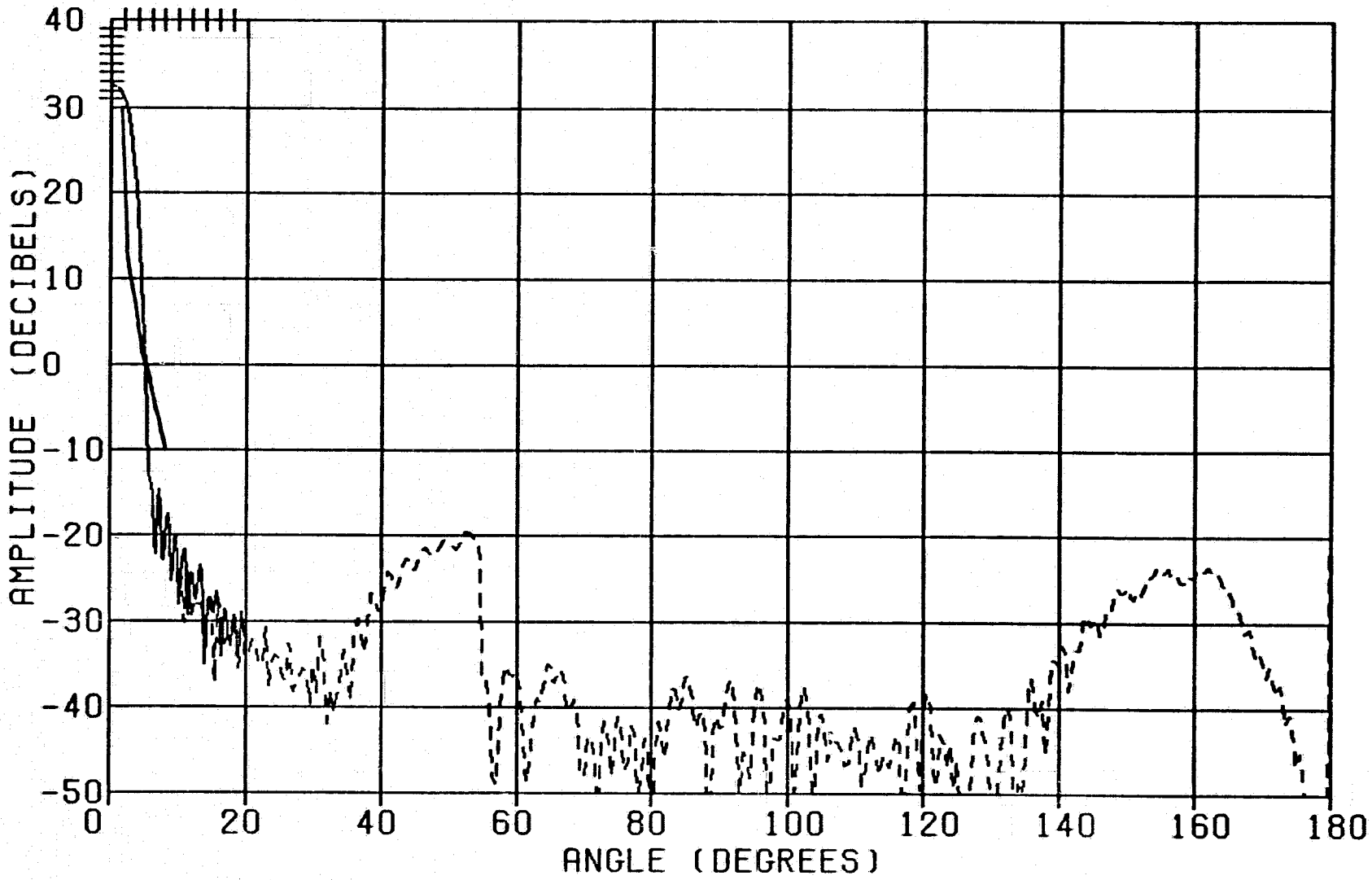

FOCAL LENGTH = 28.346, FEED ANGLE = 45.24, FREQ = 12.0 G
GPAT+GTD PATTERN PHI = 135.0, PRINCIPAL (XH)
GPAT(SOLID), GTD(DASHED)

FIGURE 2-3B-4 FAR FIELD PATTERN FOR 3 λ HORN WITH f/D=0.30 Ø = 135°

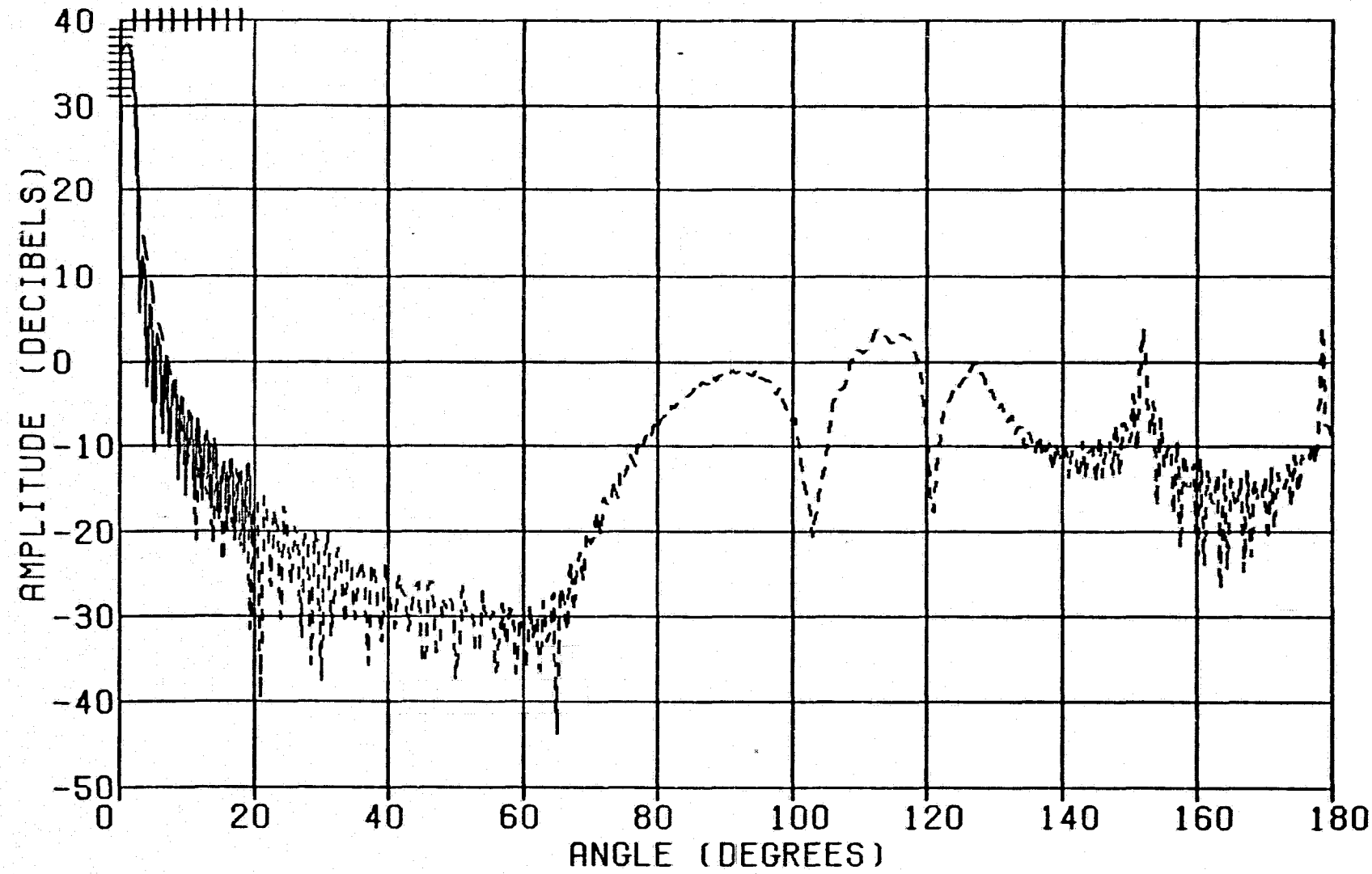

FOCAL LENGTH = 47.244. FEED ANGLE = 28.07. FREQ = 12.0 G
GPAT+GTD PATTERN PHI = 0.0, PRINCIPAL (XH)
GPAT(SOLID), GTD(DASHED)

FIGURE 2-3C-1 FAR FIELD PATTERN FOR 3λ HORN WITH f/D=0.50 ϕ = 0°

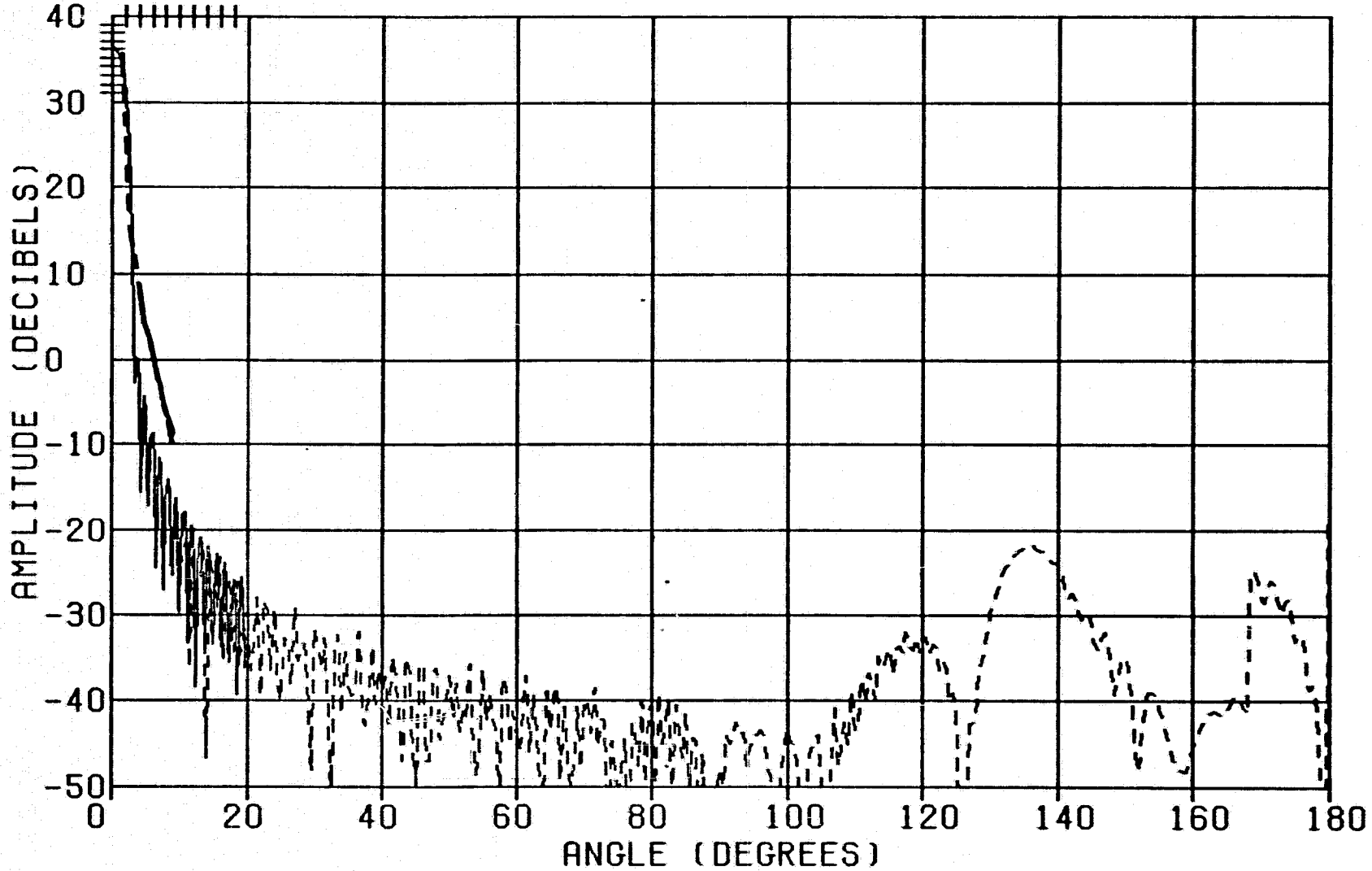

FOCAL LENGTH = 47.244. FEED ANGLE = 28.07. FREQ = 12.0 G
GPAT+GTD PATTERN PHI = 45.0, PRINCIPAL (XH)
GPAT(SOLID). GTD(DASHED)

FIGURE 2-3C-2 FAR FIELD PATTERN FOR 3λ HORN WITH f/D=0.50 ϕ = 45°

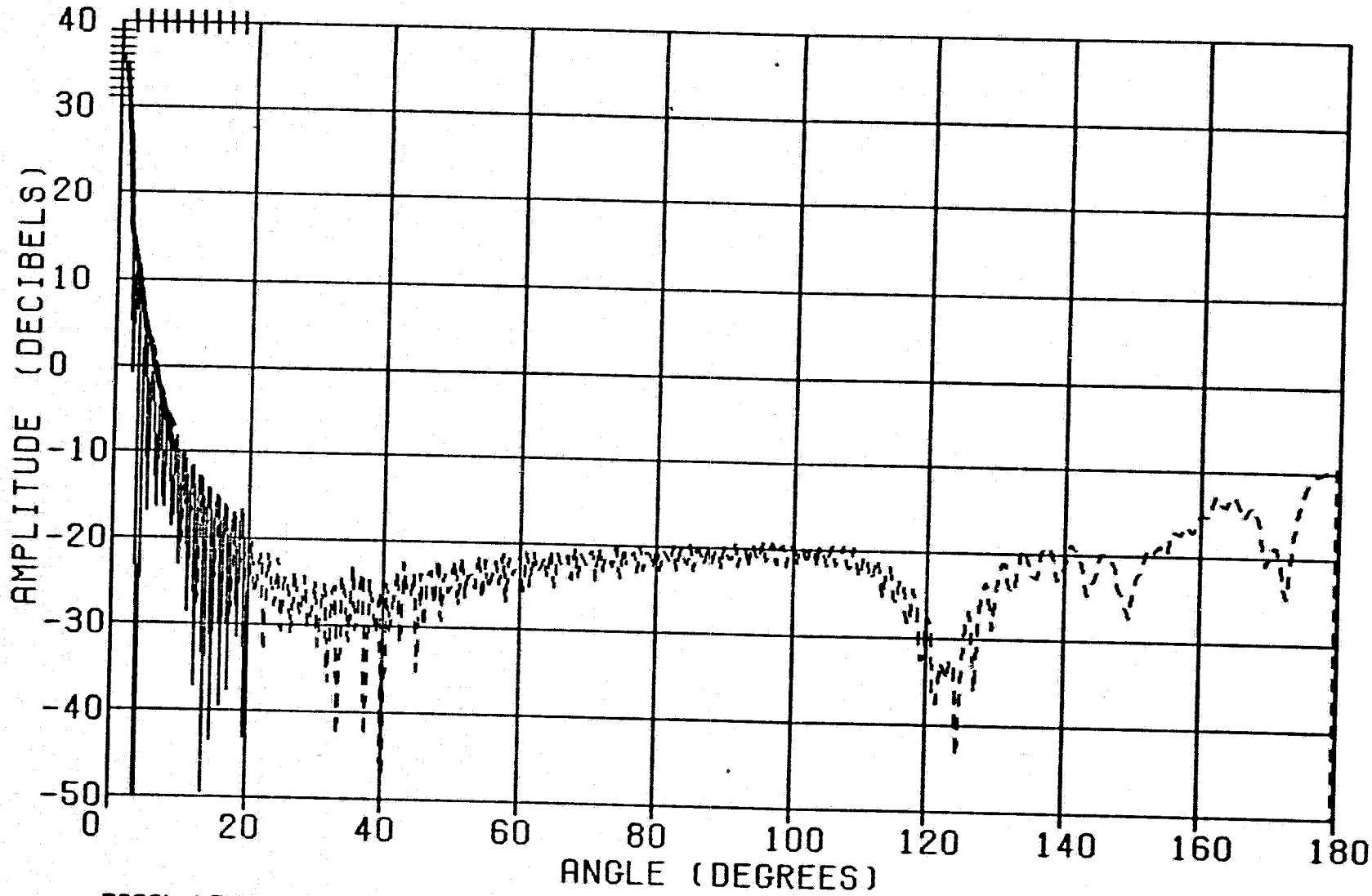

FOCAL LENGTH = 47.244. FEED ANGLE = 28.07. FREQ = 12.0 G
GPAT+GTD PATTERN PHI = 90.0, PRINCIPAL (XH)
GPAT(SOLID), GTD(DASHED)

FIGURE 2-3C-3 FAR FIELD PATTERN FOR 3λ HORN WITH f/D=0.50 Ø = 90°

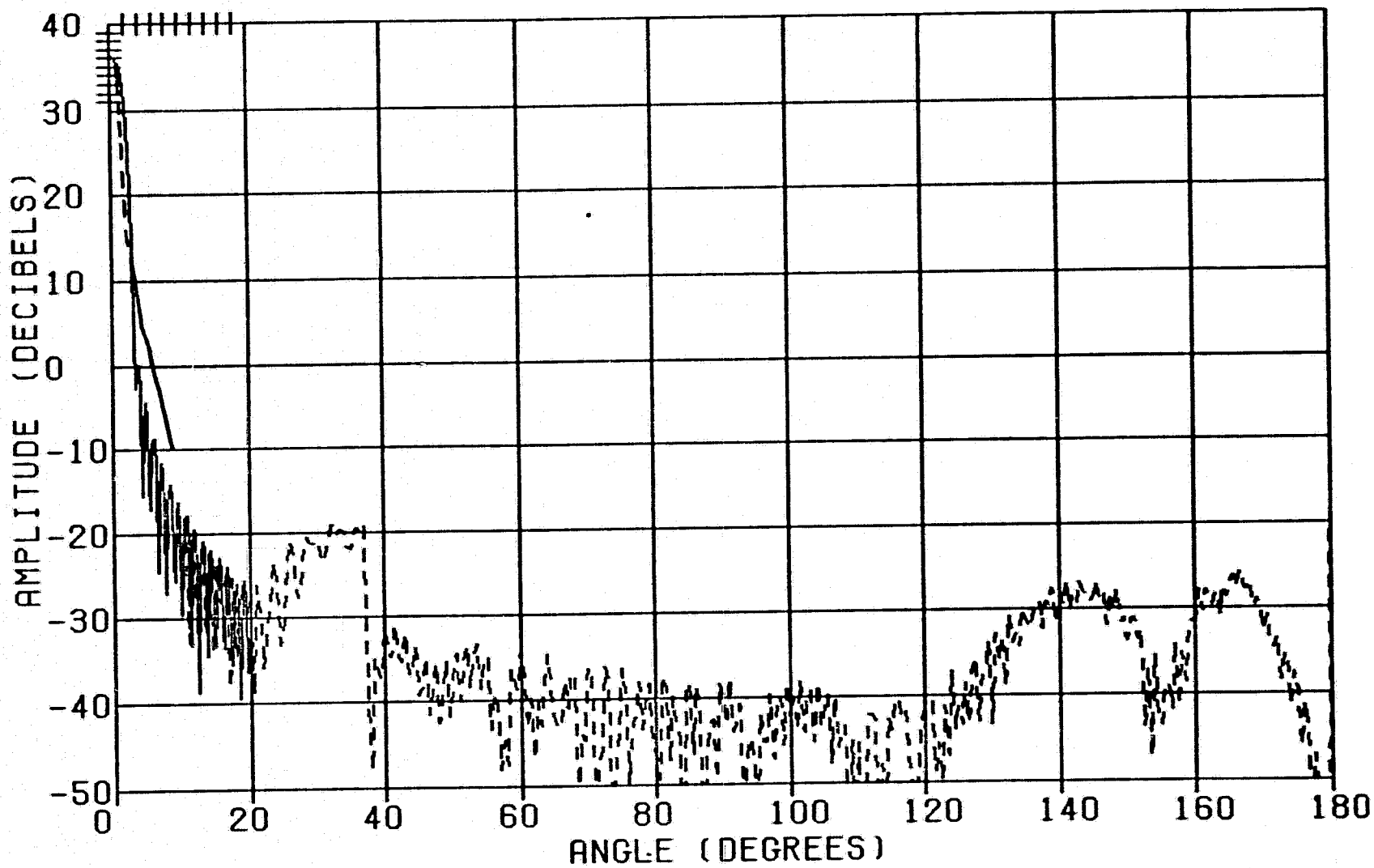

FOCAL LENGTH = 47.244. FEED ANGLE = 28.07. FREQ = 12.0 G
GPAT+GTD PATTERN PHI = 135.0, PRINCIPAL (XH)
GPAT(SOLID), GTD(DASHED)

FIGURE 2-3C-4 FAR FIELD PATTERN FOR 3λ HORN WITH f/D=0.50 Ø = 135°

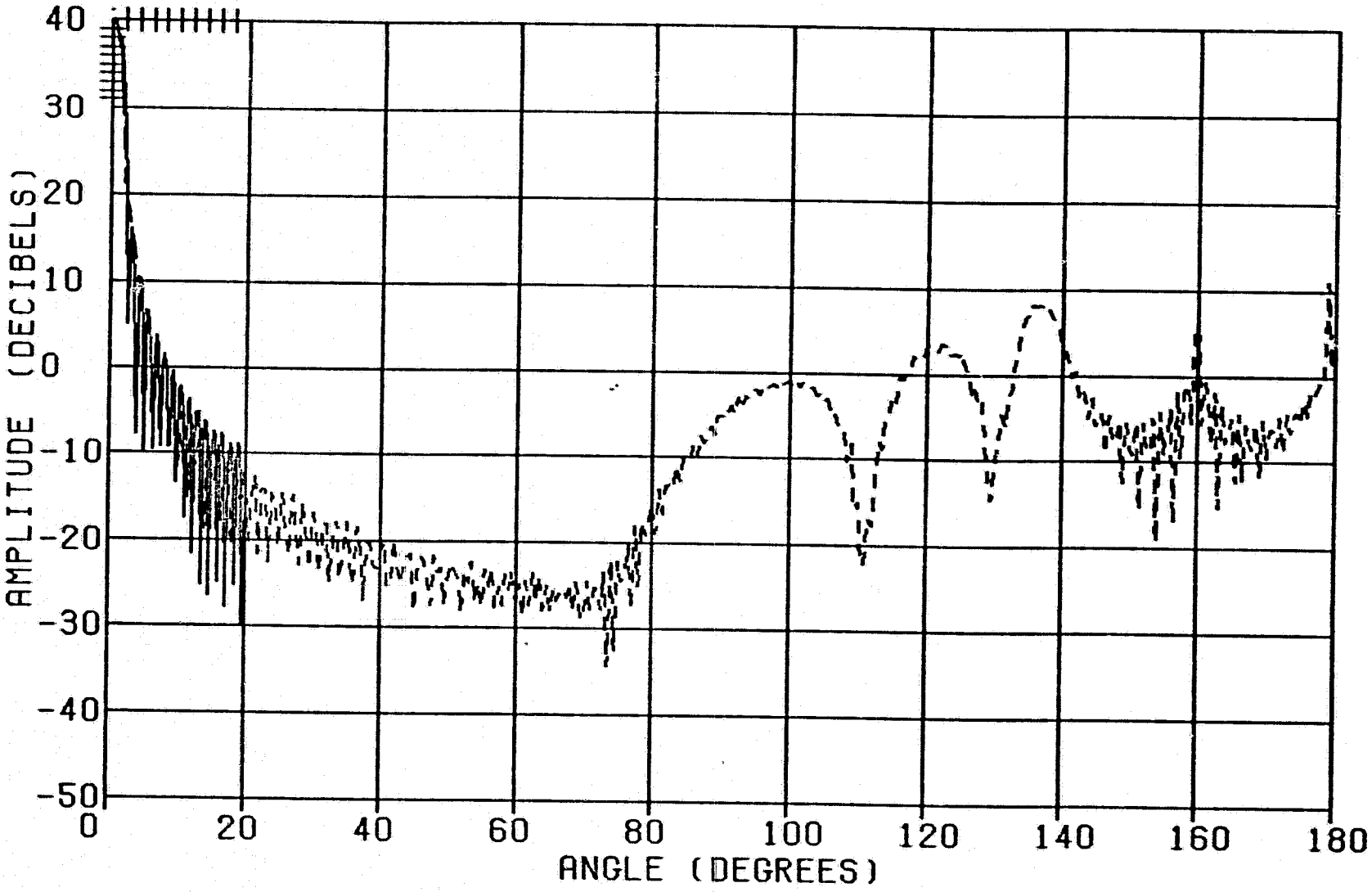

FOCAL LENGTH = 66.141, FEED ANGLE = 20.25, FREQ = 12.0 G
GPAT+GTD PATTERN PHI = 0.0, PRINCIPAL (XH)
GPAT(SOLID), GTD(DASHED)

FIGURE 2-3D-1 FAR FIELD PATTERN FOR 3 λ HORN WITH f/D=0.70 $\phi = 0°$

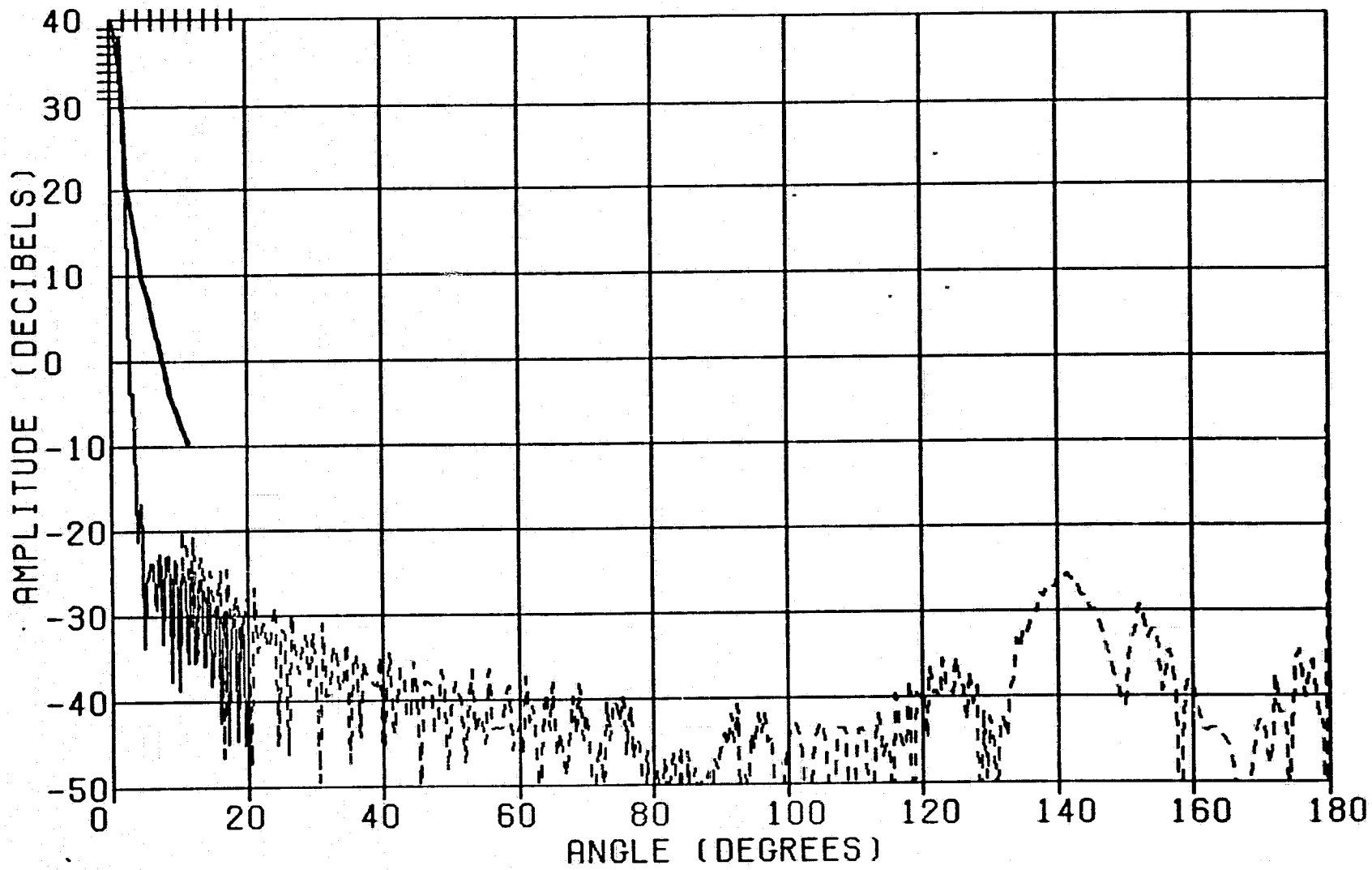

FOCAL LENGTH = 66.141, FEED ANGLE = 20.25, FREQ = 12.0 G
GPAT+GTD PATTERN PHI = 45.0, PRINCIPAL (XH)
GPAT(SOLID), GTD(DASHED)

FIGURE 2-3D-2 FAR FIELD PATTERN FOR 3 λ HORN WITH f/D=0.70 Ø = 45°

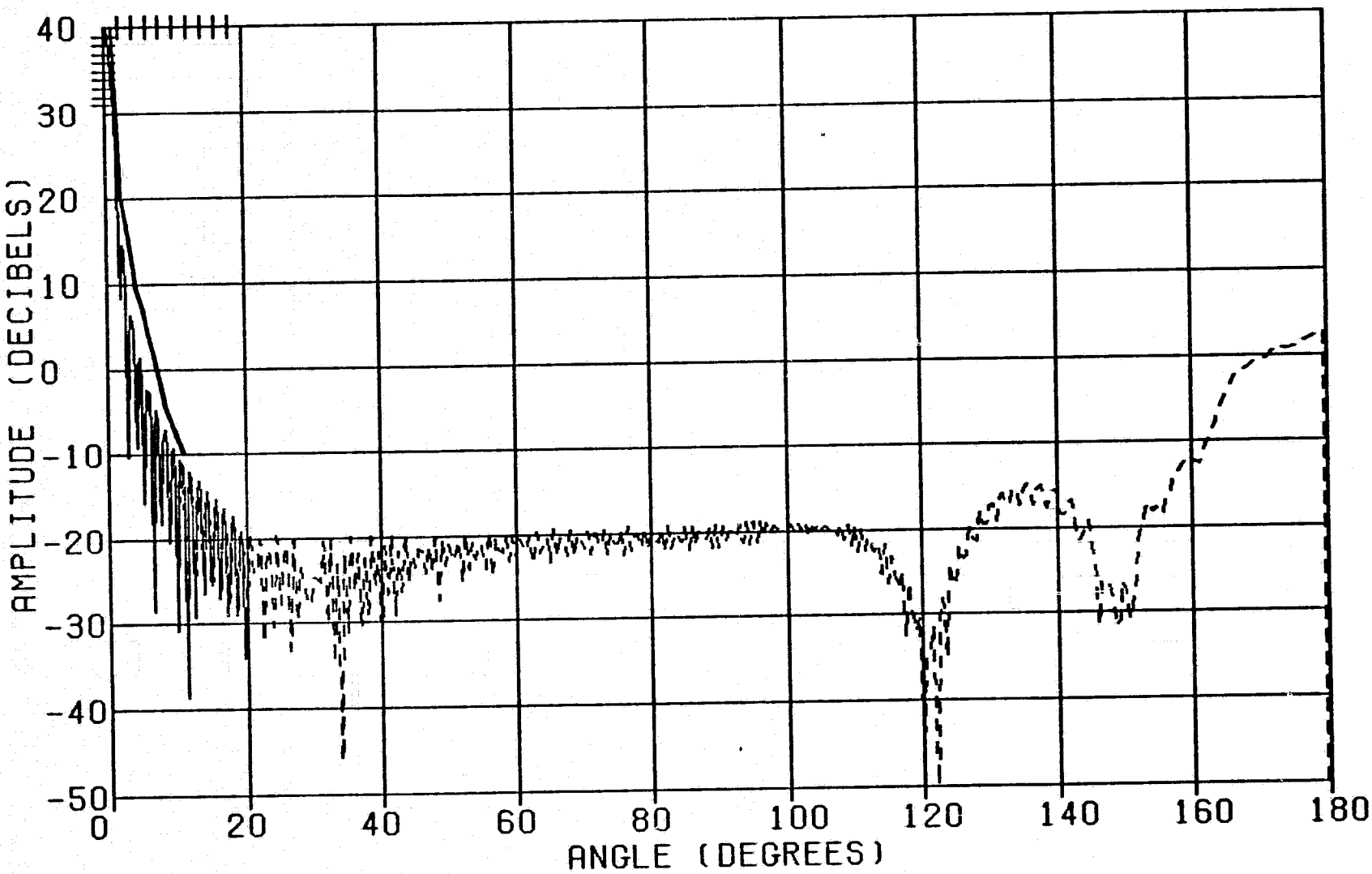

FOCAL LENGTH = 66.141, FEED ANGLE = 20.25, FREQ = 12.0 G
GPAT+GTD PATTERN PHI = 90.0, PRINCIPAL (XH)
GPAT(SOLID), GTD(DASHED)

FIRGURE 2-3D-3 FAR FIELD PATTERN FOR 3 λ HORN WITH f/D=0.70 Ø = 90°

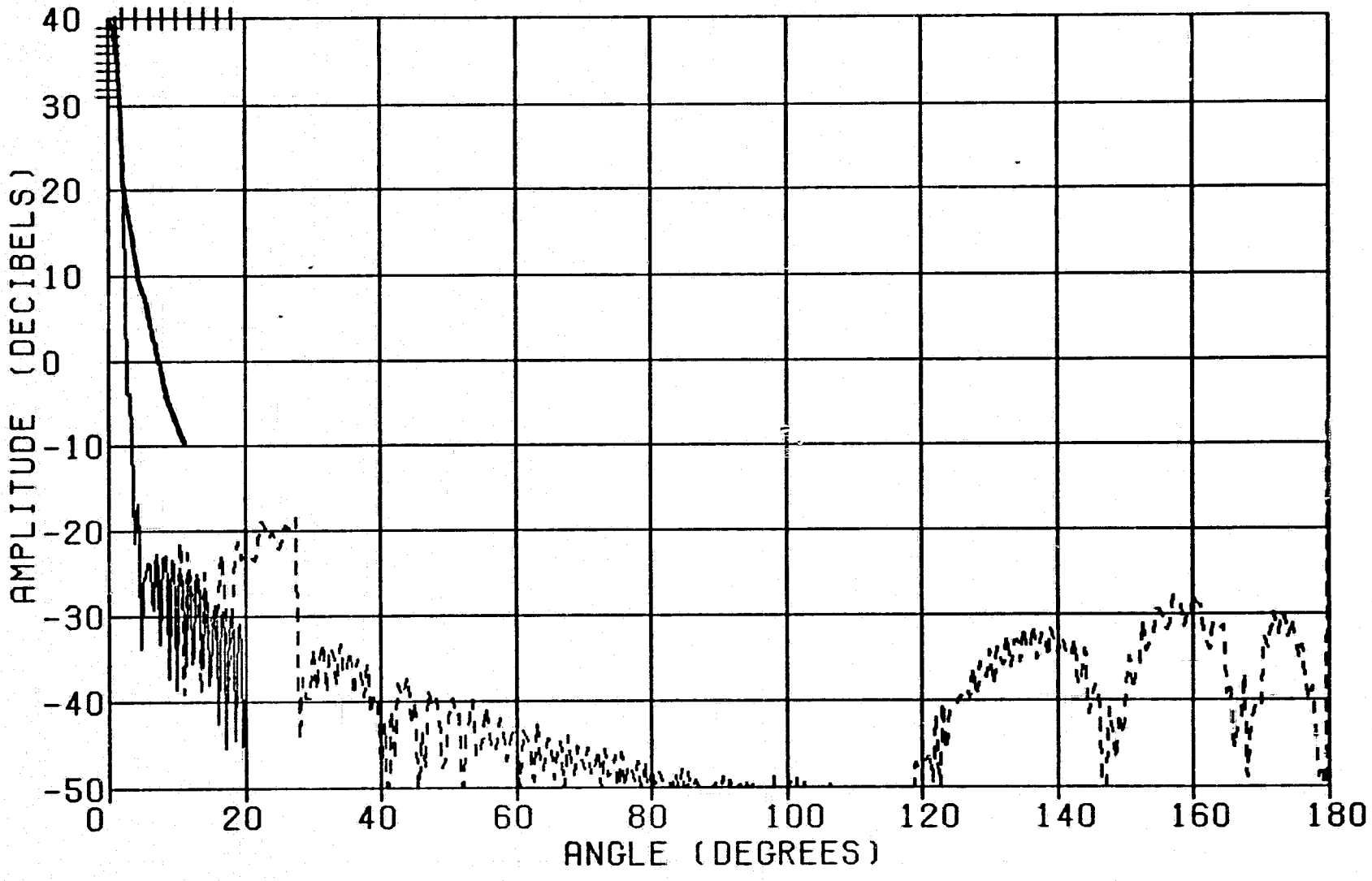

FOCAL LENGTH = 66.141, FEED ANGLE = 20.25, FREQ = 12.0 G
GPAT+GTD PATTERN PHI = 135.0, PRINCIPAL (XH)
GPAT(SOLID), GTD(DASHED)

FIGURE 2-3D-4 FAR FIELD PATTERN FOR 3 λ HORN WITH f/D=0.70 Ø = 135°

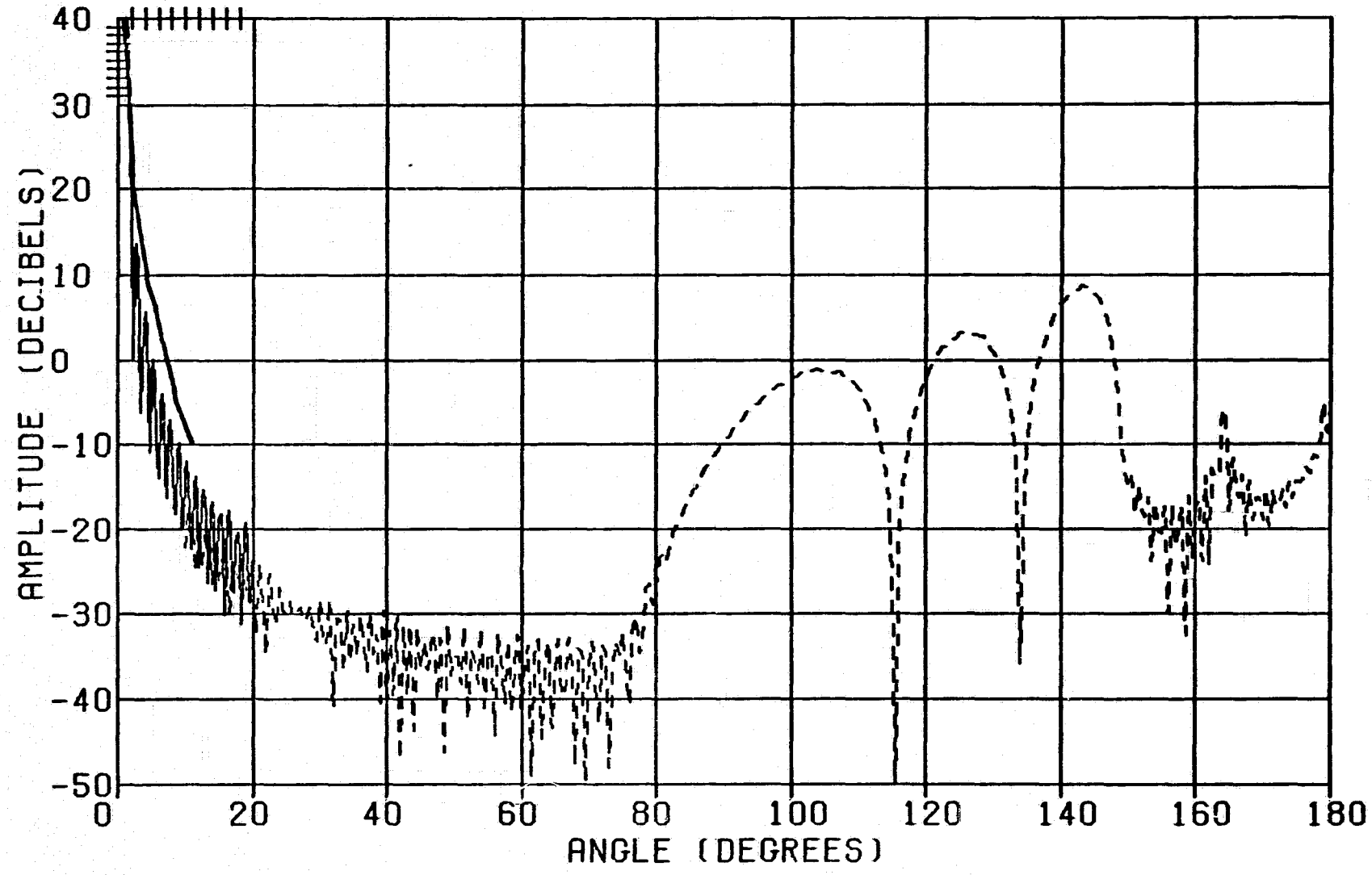

FOCAL LENGTH = 85.039, FEED ANGLE = 15.81, FREQ = 12.0 G
GPAT+GTD PATTERN PHI = 0.0, PRINCIPAL (XH)
GPAT(SOLID), GTD(DASHED)

FIGURE 2-3E-1 FAR FIELD PATTERN FOR 3 λ HORN WITH f/D=0.9 Ø = 0°

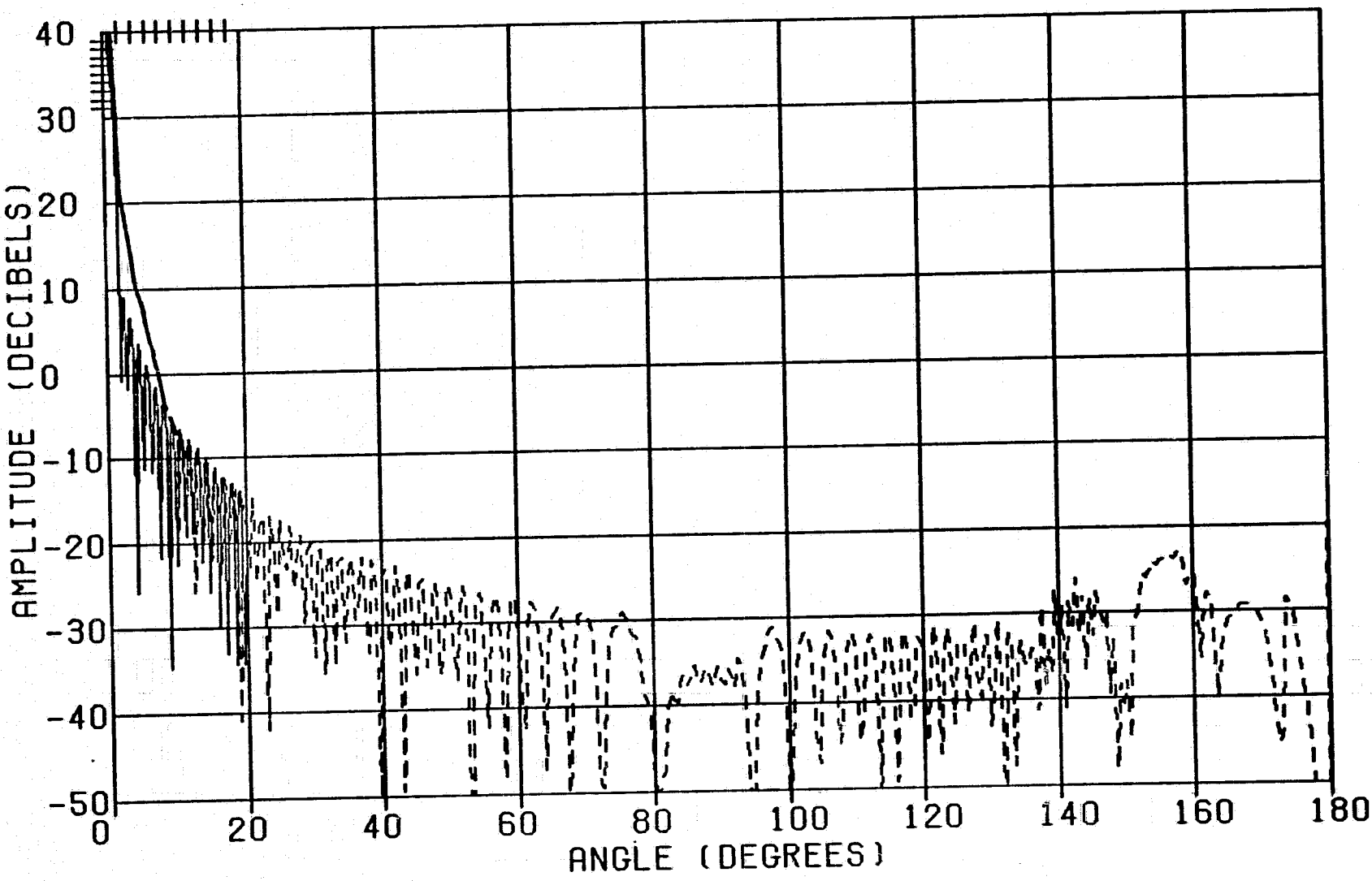

FOCAL LENGTH = 85.039, FEED ANGLE = 15.81, FREQ = 12.0 G
GPAT+GTD PATTERN PHI = 45.0, PRINCIPAL (XH)
GPAT(SOLID), GTD(DASHED)

FIGURE 2-3E-2 FAR FIELD PATTERN FOR 3 λ HORN WITH f/D=0.9 ϕ = 45°

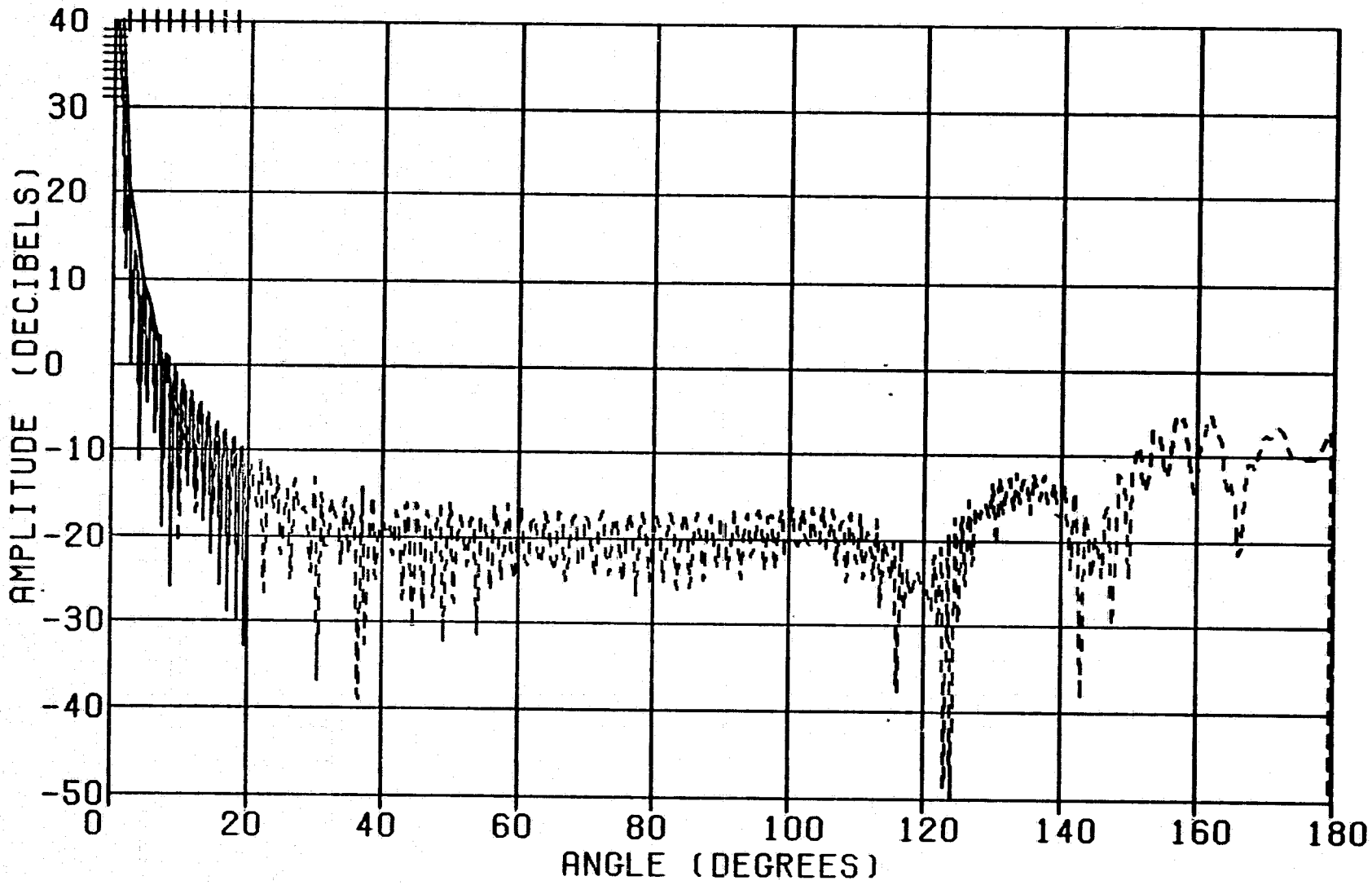

FOCAL LENGTH = 85.039, FEED ANGLE = 15.81, FREQ = 12.0 G
GPAT+GTD PATTERN PHI = 90.0, PRINCIPAL (XH)
GPAT(SOLID), GTD(DASHED)

FIGURE 2-3E-3 FAR FIELD PATTERN FOR 3 λ HORN WITH f/D=0.9 Ø = 90°

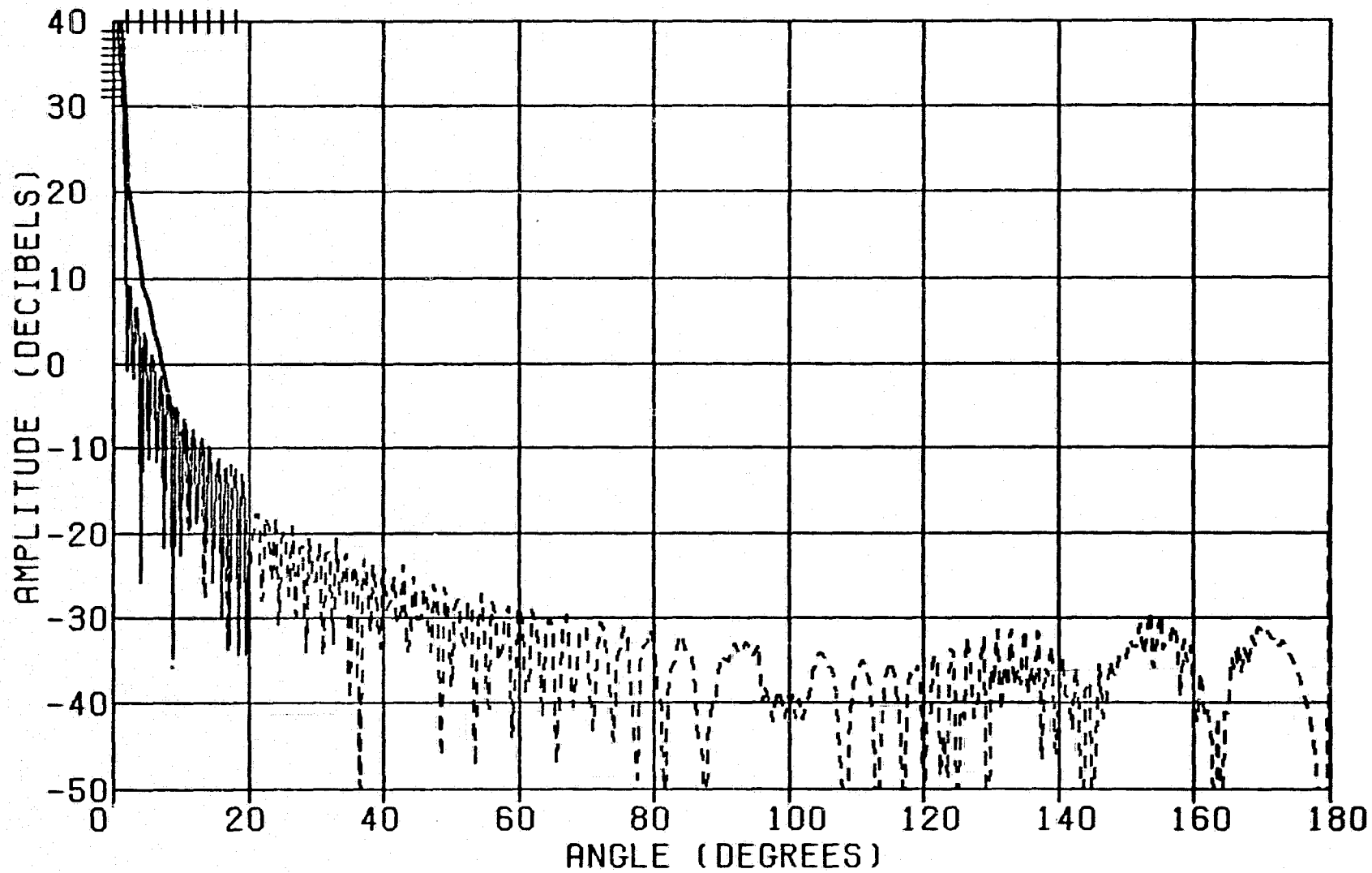

FOCAL LENGTH = 85.039, FEED ANGLE = 15.81, FREQ = 12.0 G
GPAT+GTD PATTERN PHI = 135.0, PRINCIPAL (XH)
GPAT(SOLID), GTD(DASHED)

FIGURE 2-3E-4 FAR FIELD PATTERN FOR 3 λ HORN WITH f/D=0.9 Ø = 135°

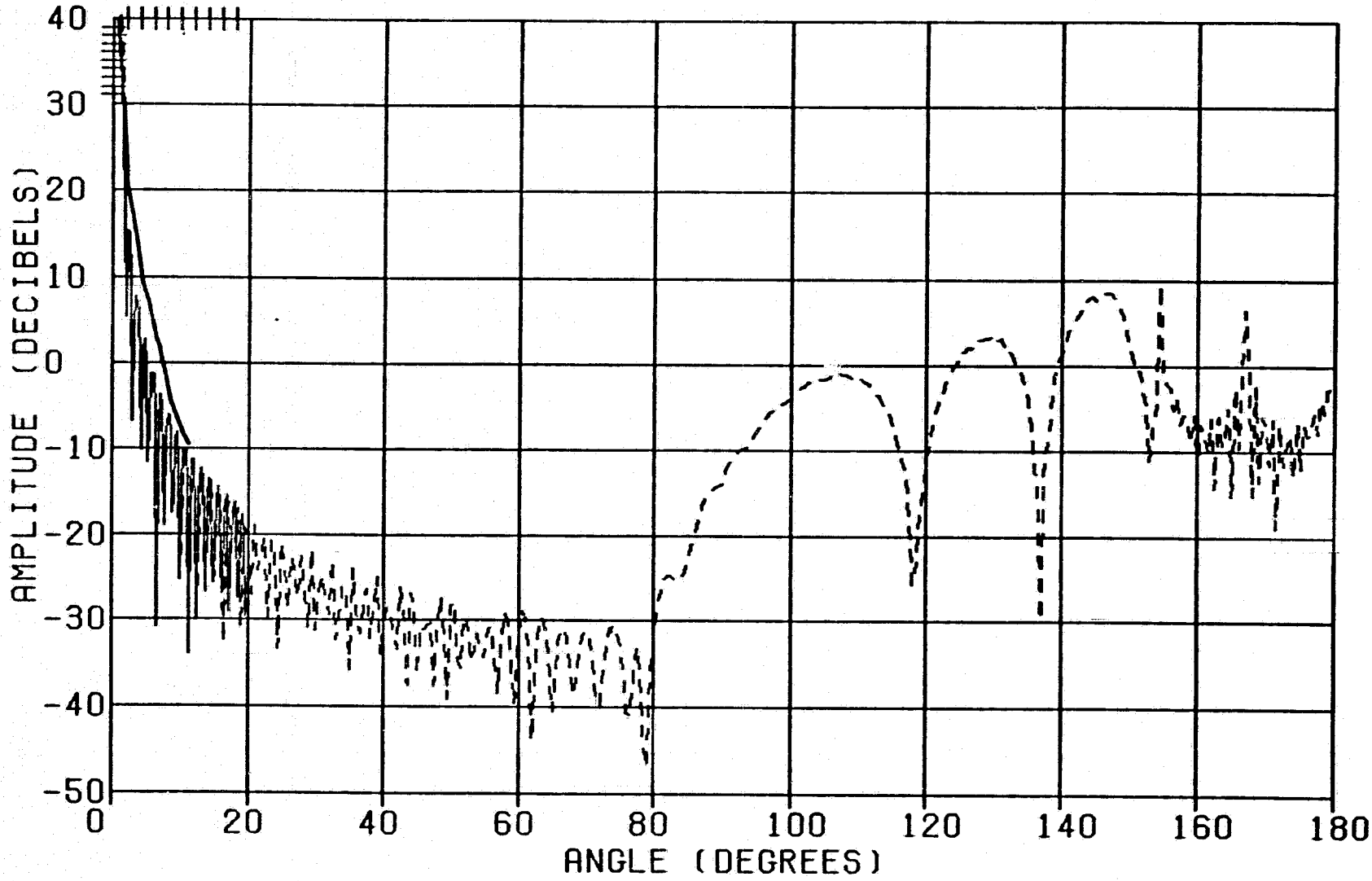

FOCAL LENGTH = 103.936, FEED ANGLE = 12.97, FREQ = 12.0
GPAT+GTD PATTERN PHI = 0.0, PRINCIPAL (XH)
GPAT(SOLID), GTD(DASHED)

FIGURE 2-3F-1 FAR FIELD PATTERN FOR 3 λ HORN WITH f/D=1.1 $\phi = 0°$

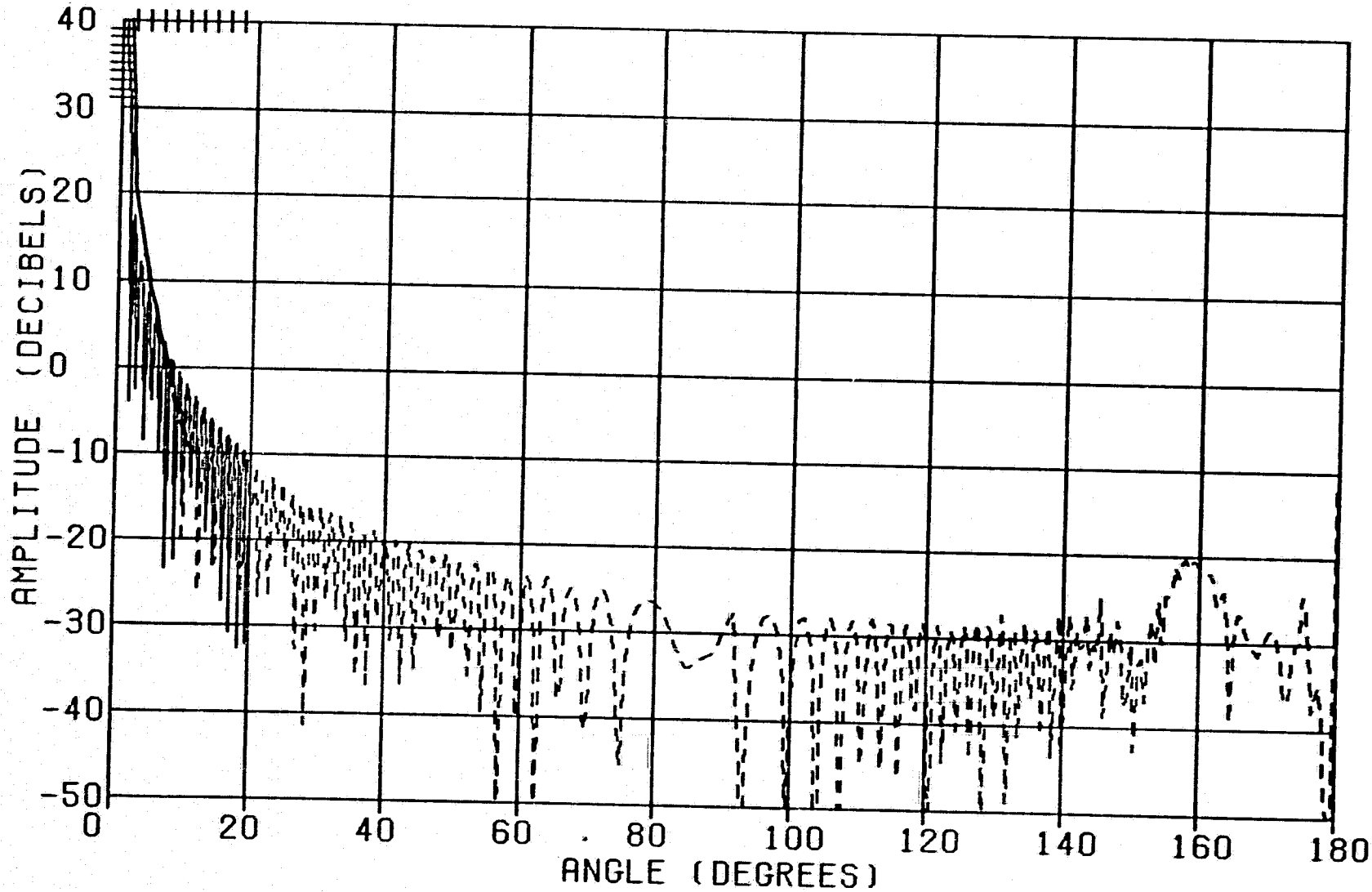

FIGURE 2-3F-2 FAR FIELD PATTERN FOR 3 λ HORN WITH f/D=1.1 ø = 45°

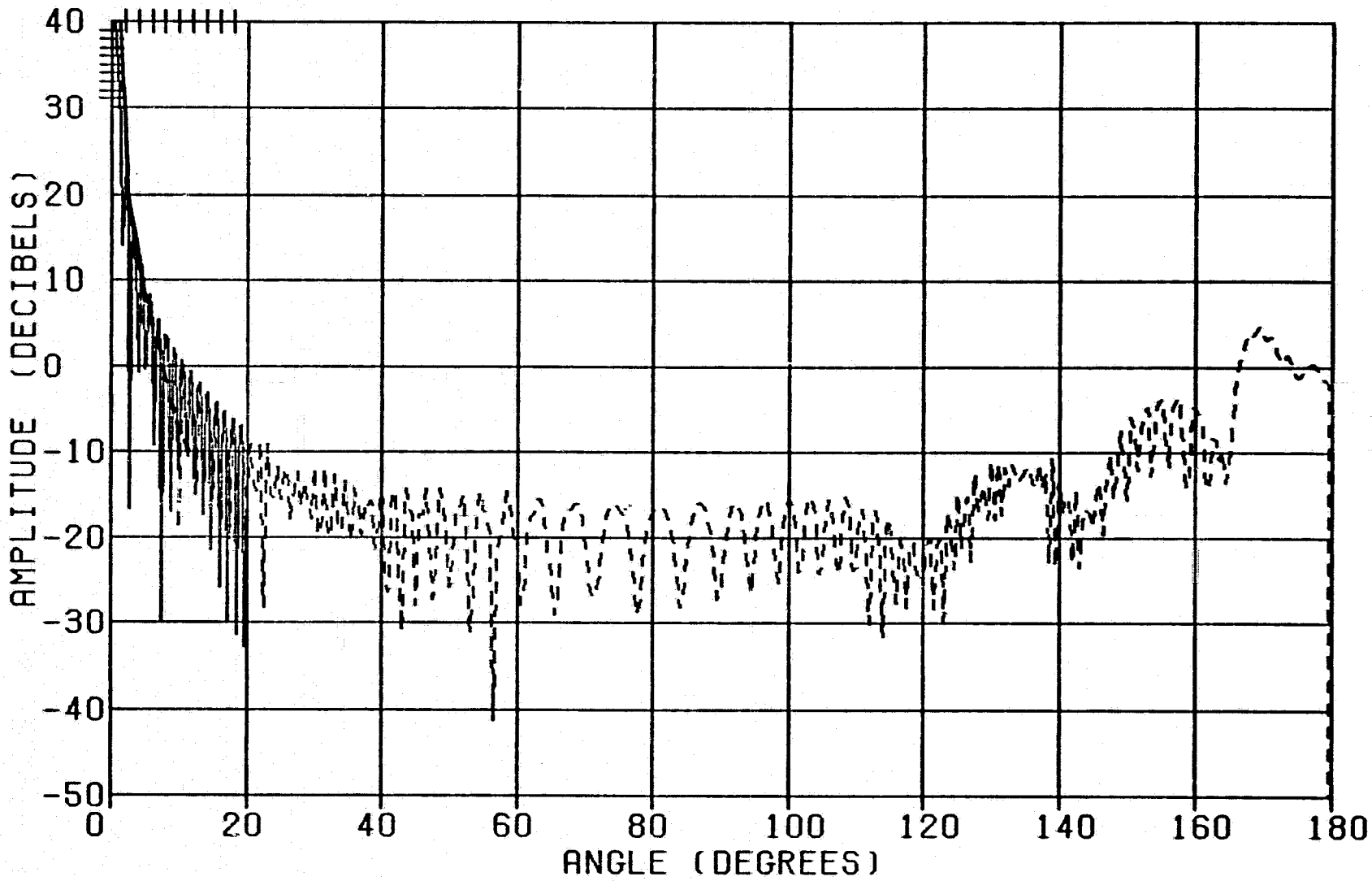

FOCAL LENGTH = 103.936. FEED ANGLE = 12.97. FREQ = 12.0
GPAT+GTD PATTERN PHI = 90.0. PRINCIPAL (XH)
GPAT(SOLID). GTD(DASHED)

FIGURE 2-3F-3 FAR FIELD PATTERN FOR 3 λ HORN WITH f/D=1.1 Ø = 90°

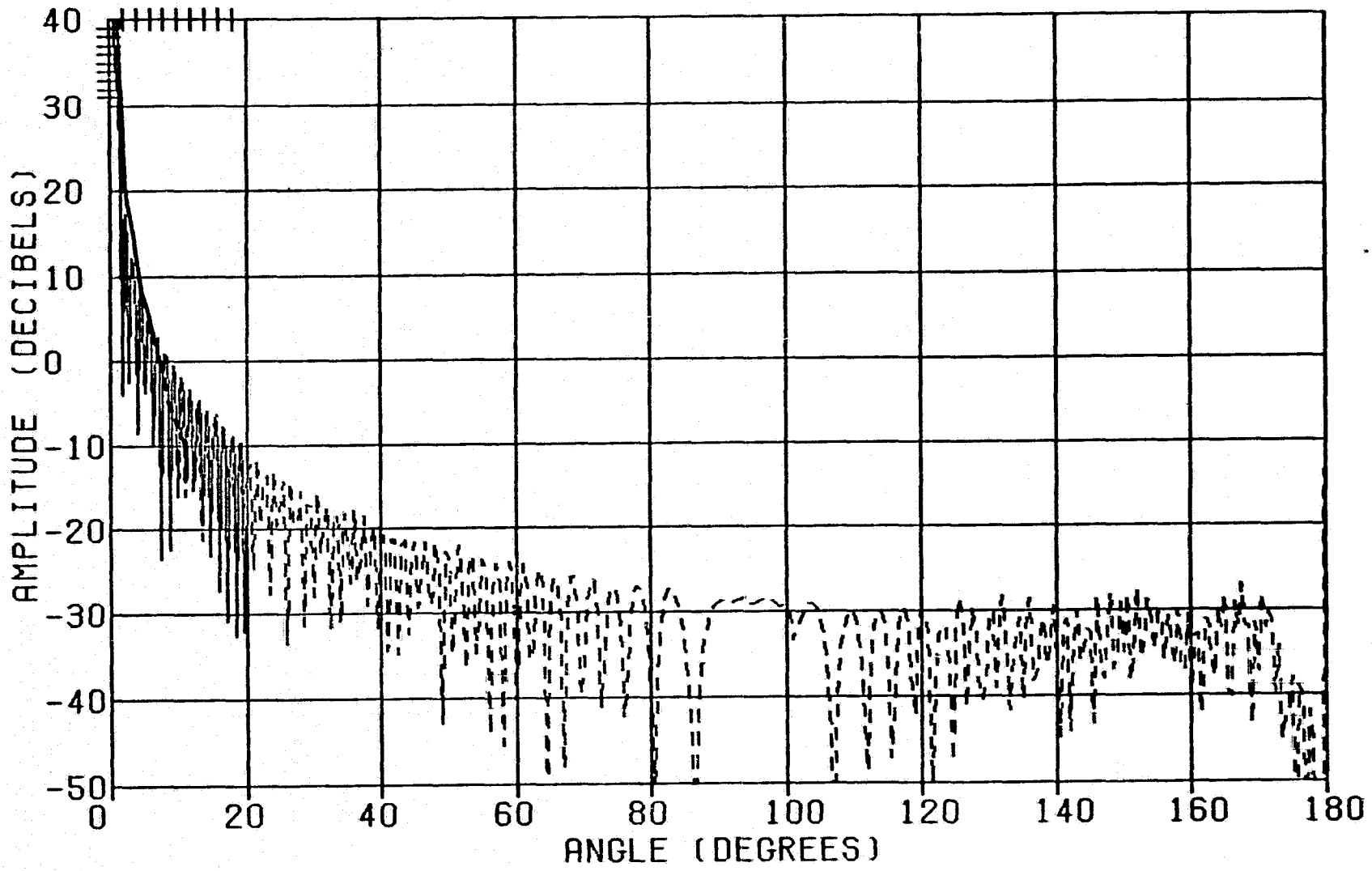

FOCAL LENGTH = 103.936, FEED ANGLE = 12.97, FREQ = 12.0
GPAT+GTD PATTERN PHI = 135.0, PRINCIPAL (XH)
GPAT(SOLID), GTD(DASHED)

FIGURE 2-3F-4 FAR FIELD PATTERN FOR 3 λ HORN WITH f/D=1.1 ϕ = 135°

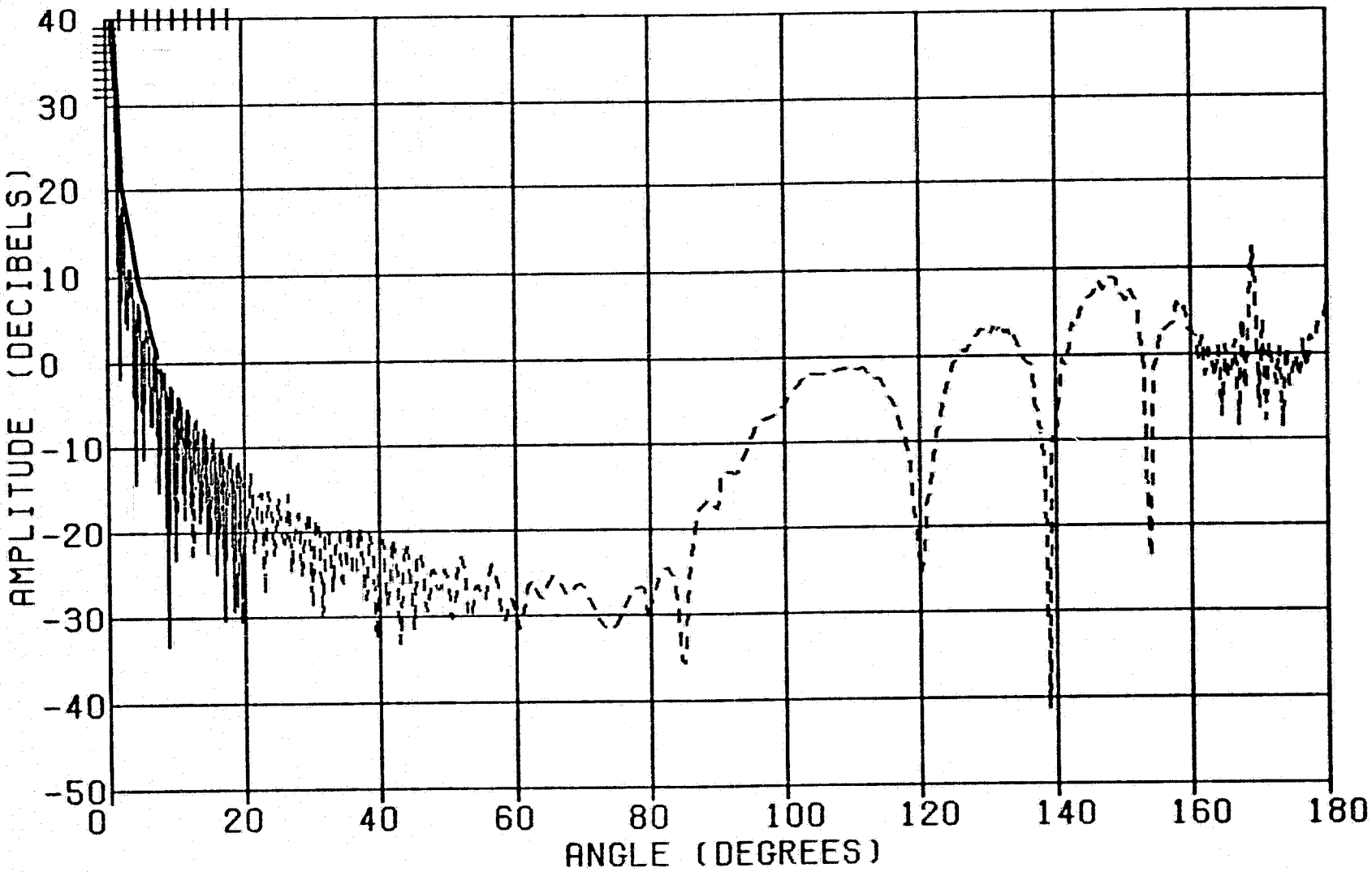

FOCAL LENGTH = 122.83, FEED ANGLE = 10.98, FREQ = 12.0 G
GPAT+GTD PATTERN PHI = 0.0, PRINCIPAL (XH)
GPAT(SOLID), GTD(DASHED)

FIGURE 2-3G-1 FAR FIELD PATTERN FOR 3λ HORN WITH f/D=1.3 $\phi = 0°$

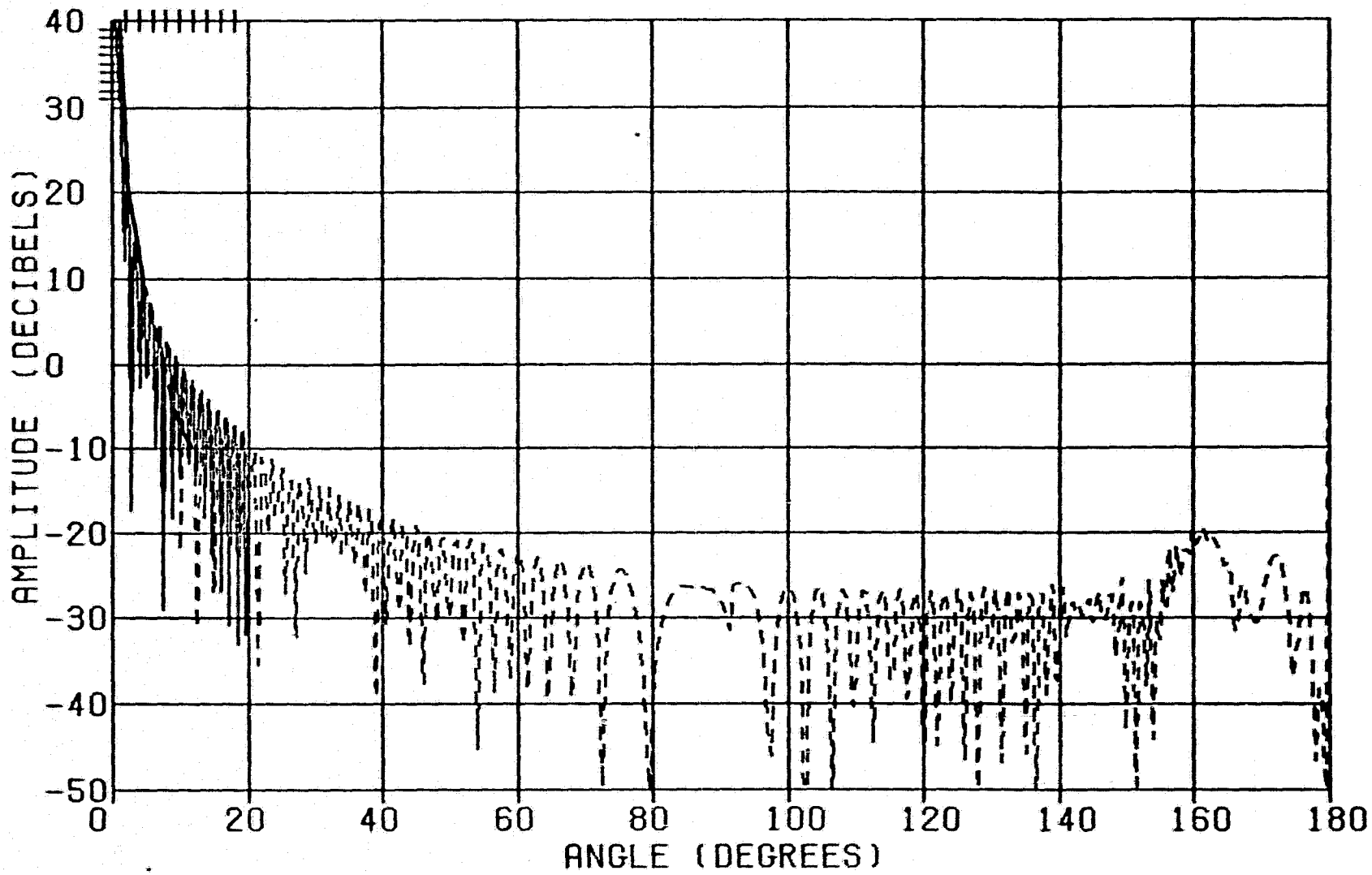

FOCAL LENGTH = 122.83. FEED ANGLE = 10.98. FREQ = 12.0 G
GPAT+GTD PATTERN PHI = 45.0. PRINCIPAL (XH)
GPAT(SOLID). GTD(DASHED)

FIGURE 2-3G-2 FAR FIELD PATTERN FOR 3 λ HORN WITH f/D=1.3 Ø = 45°

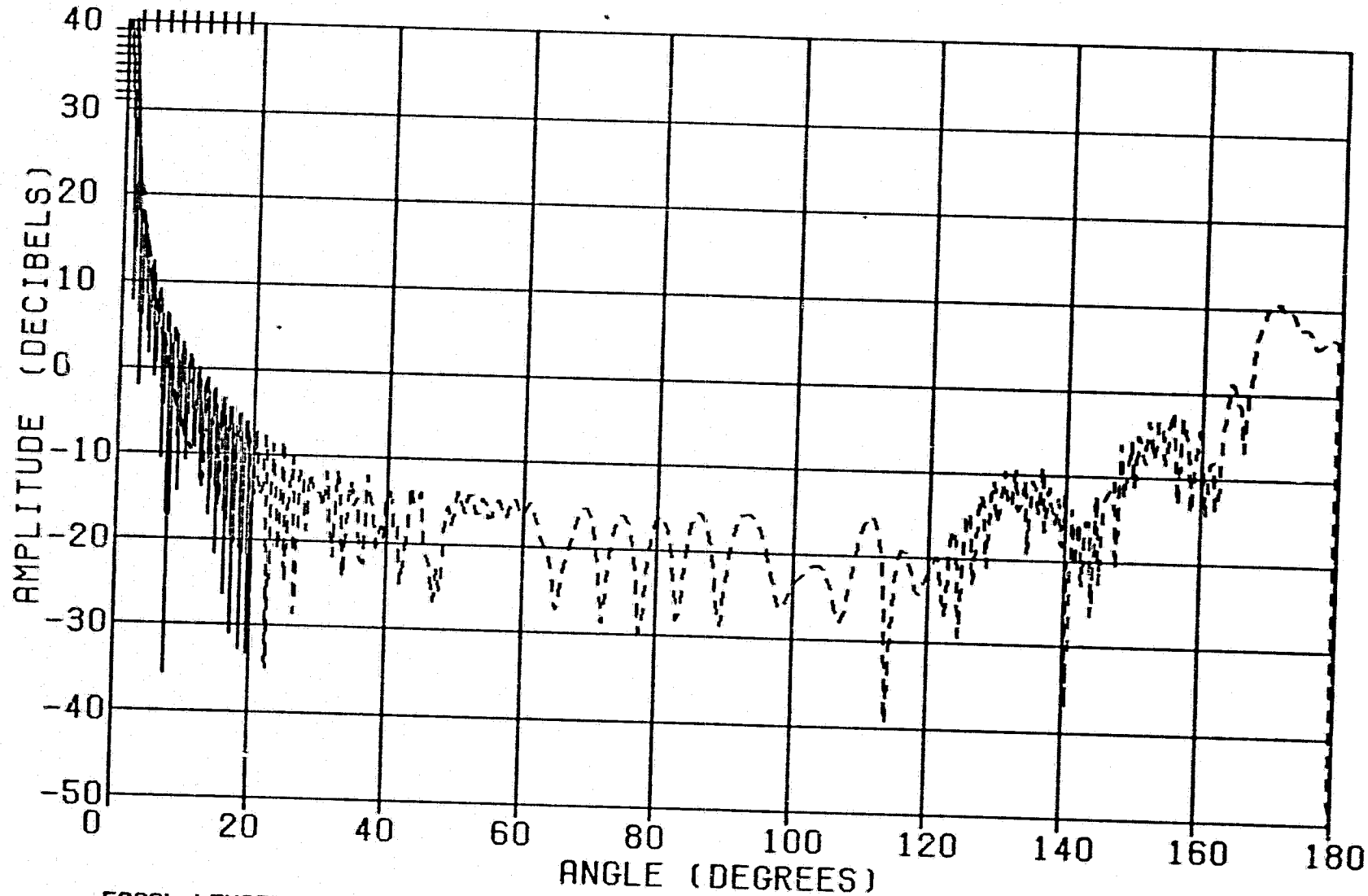

FIGURE 2-3G-3 FAR FIELD PATTERN FOR 3 λ HORN WITH f/D=1.3 Ø = 90°

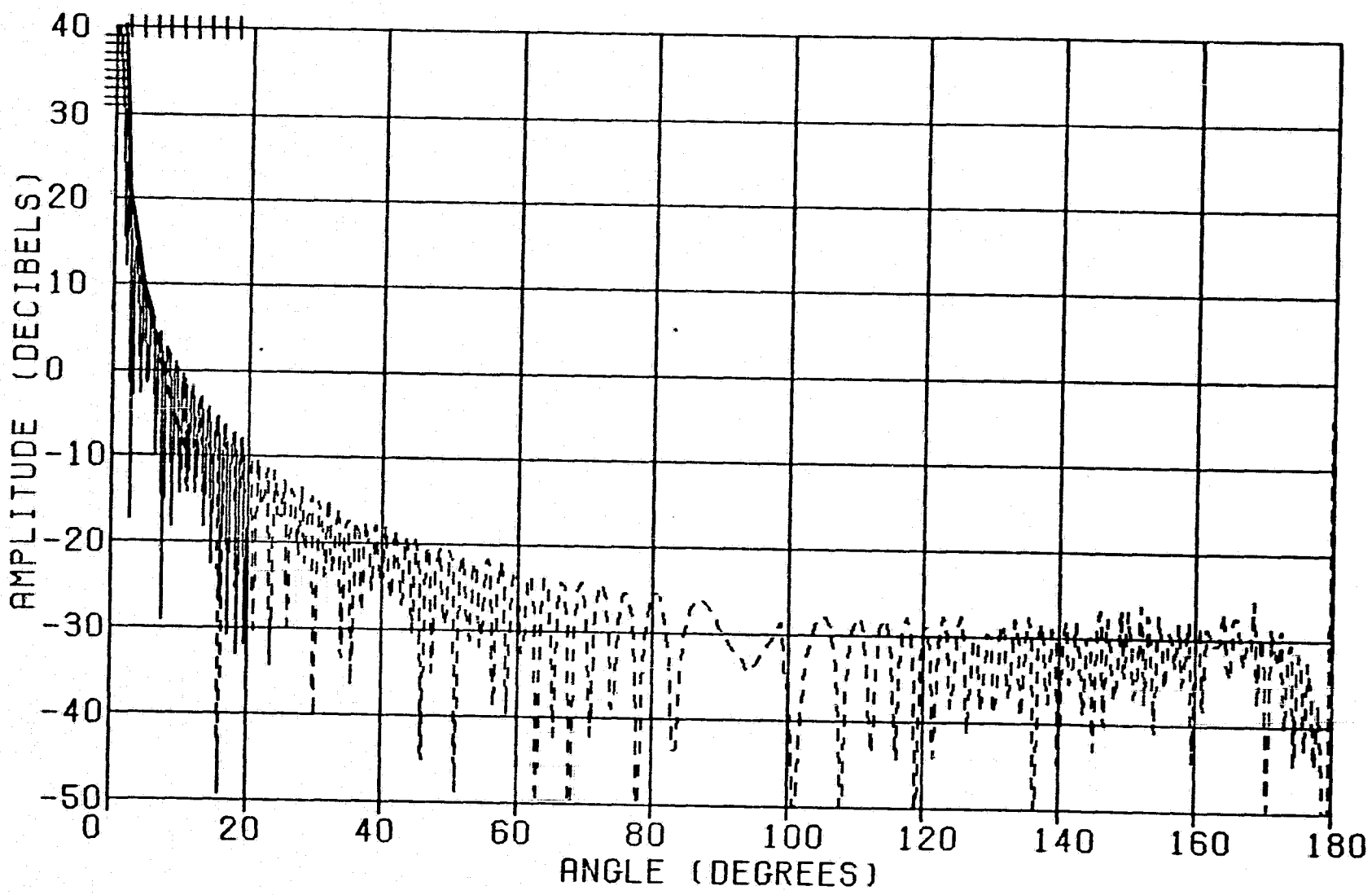

FOCAL LENGTH = 122.83, FEED ANGLE = 10.98, FREQ = 12.0 G
GPAT+GTD PATTERN PHI = 135.0, PRINCIPAL (XH)
GPAT(SOLID), GTD(DASHED)

FIGURE 2-3G-4 FAR FIELD PATTERN FOR 3 λ HORN WITH f/D=1.3 Ø = 135°

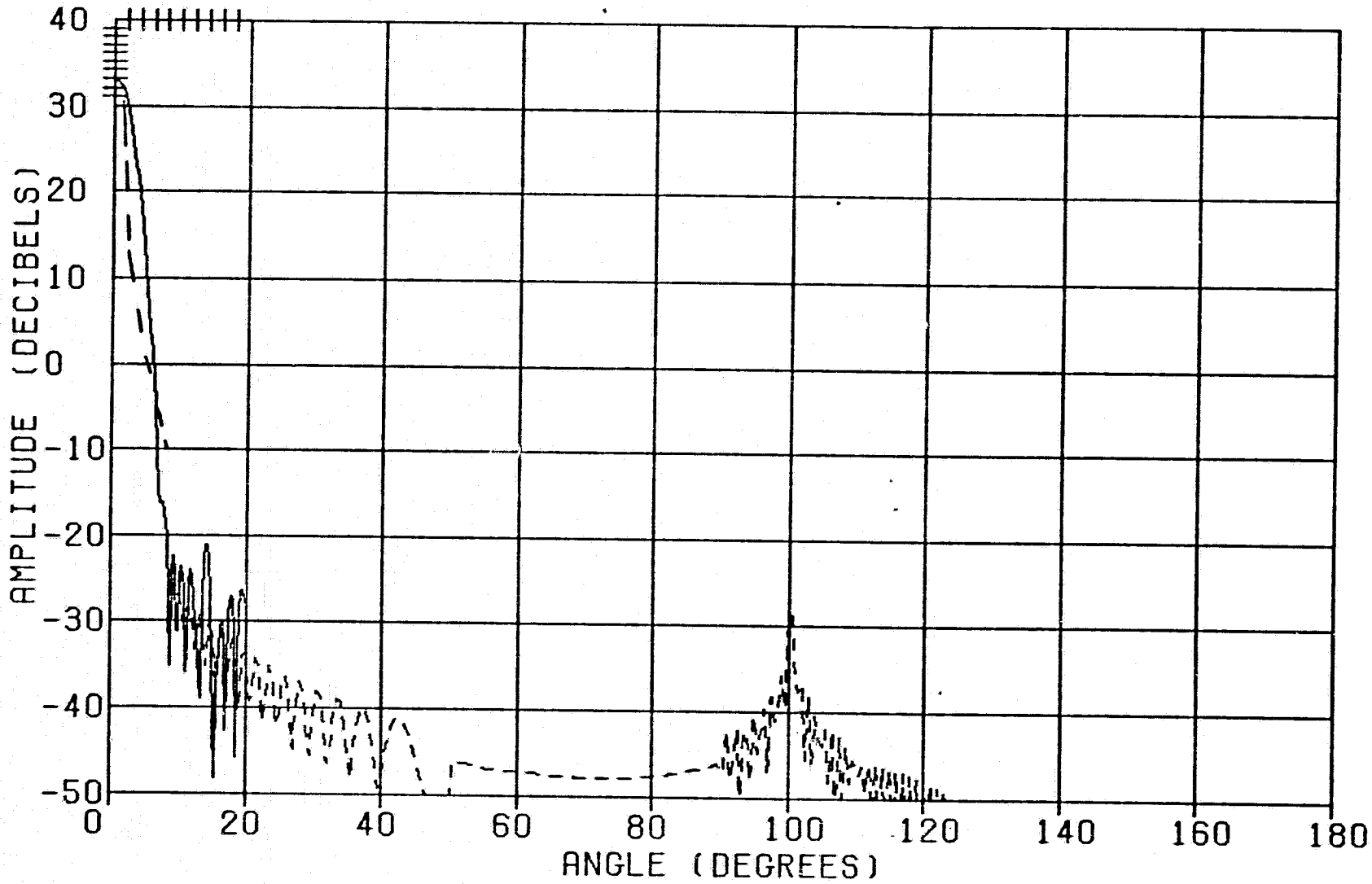

FOCAL LENGTH = 14.173, FEED ANGLE = 79.61, FREQ = 12.0 G
GPAT+GTD PATTERN PHI = 0.0, PRINCIPAL (4-LAMBDA)
GPAT(SOLID), GTD(DASHED)

FIGURE 2-4A-1 FAR FIELD PATTERN FOR 4 λ HORN WITH f/D=0.15 Ø = 0°

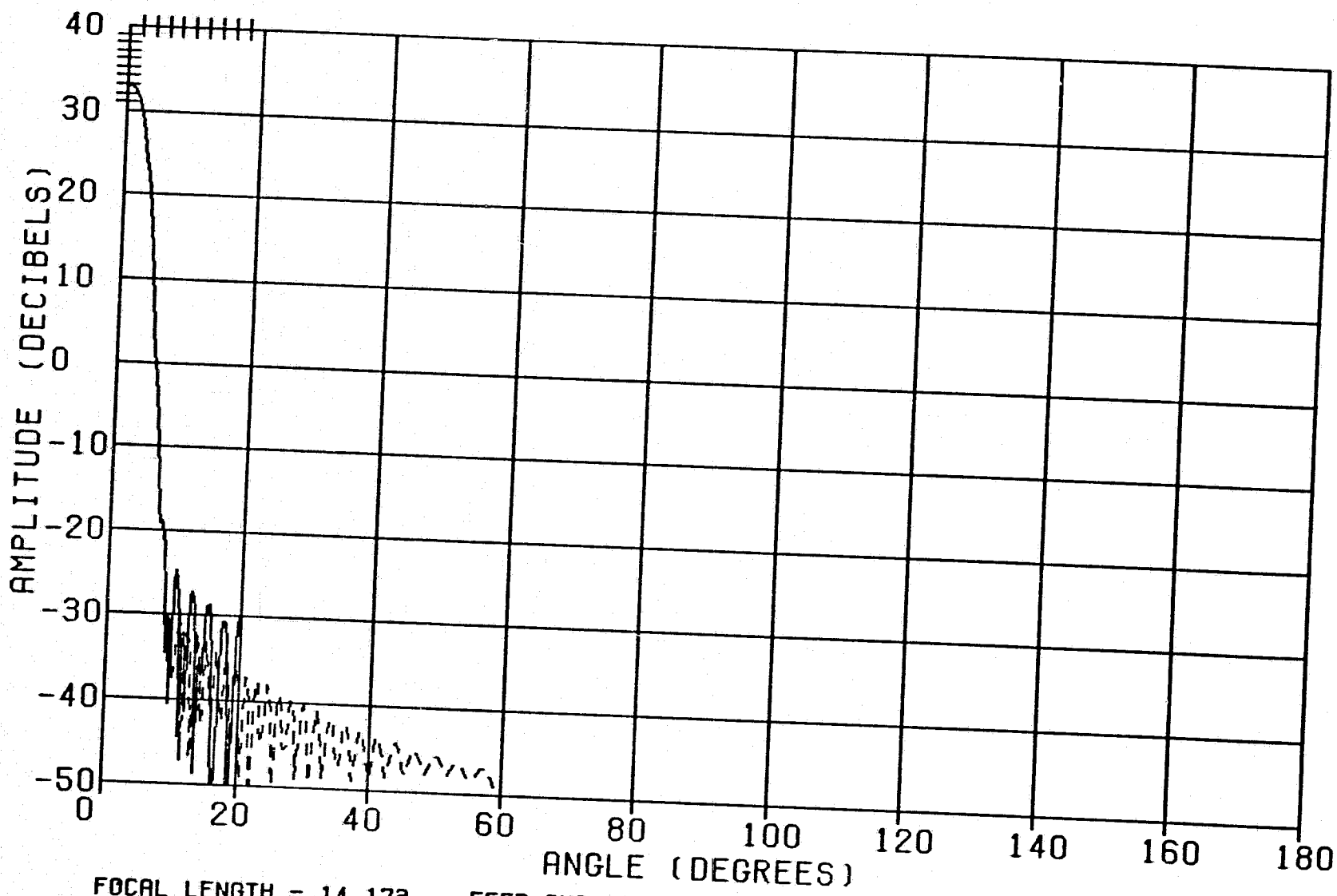

FOCAL LENGTH = 14.173, FEED ANGLE = 79.61, FREQ = 12.0 G
GPAT+GTD PATTERN PHI = 45.0, PRINCIPAL (4 LAMBDA)
GPAT(SOLID), GTD(DASHED)

FIGURE 2-4A-2 FAR FIELD PATTERN FOR 4 λ HORN WITH f/D=0.15 $\phi = 45°$

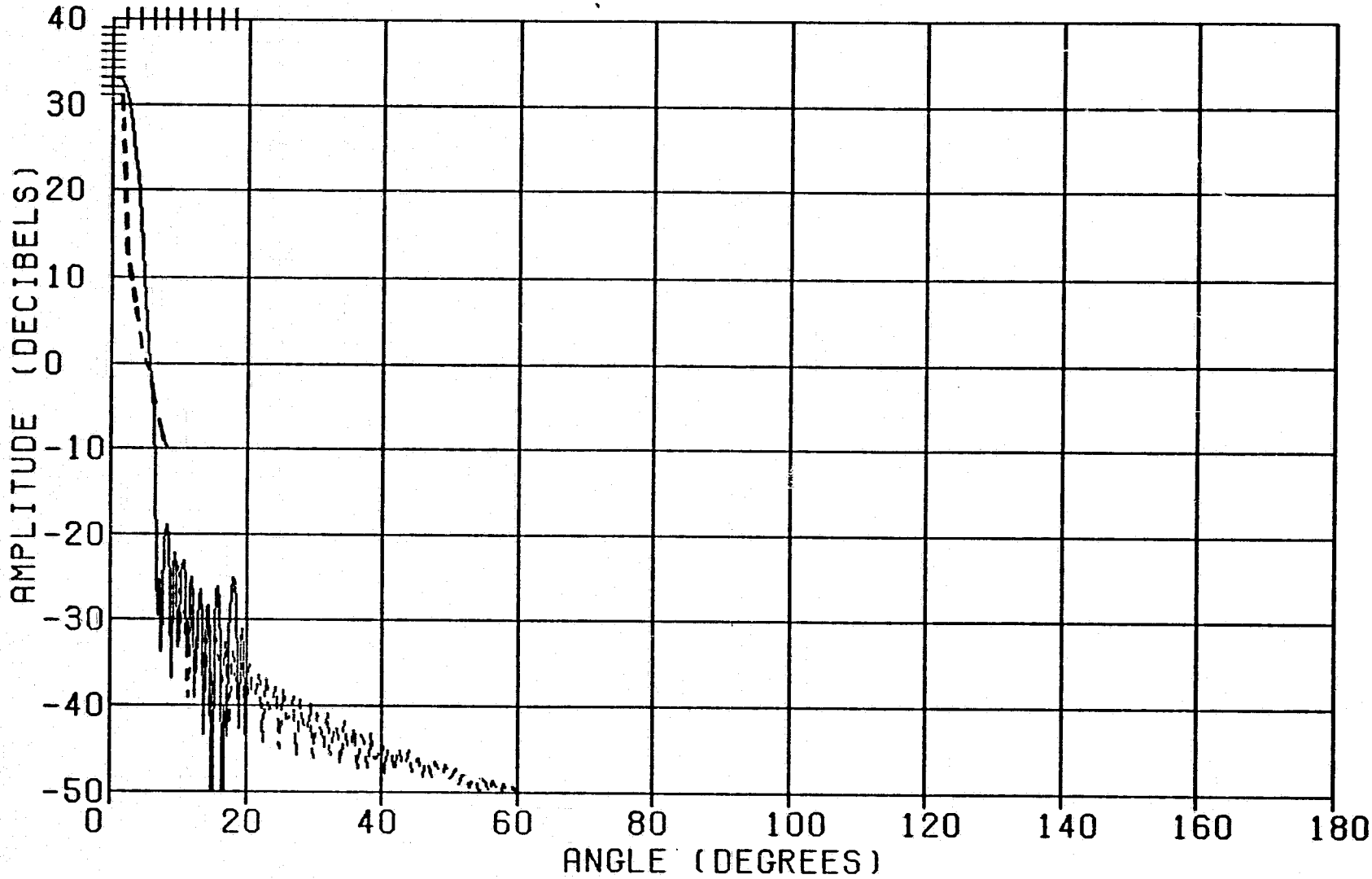

FIGURE 2-4A-3 FAR FIELD PATTERN FOR 4 λ HORN WITH f/D=0.15 ϕ = 90°

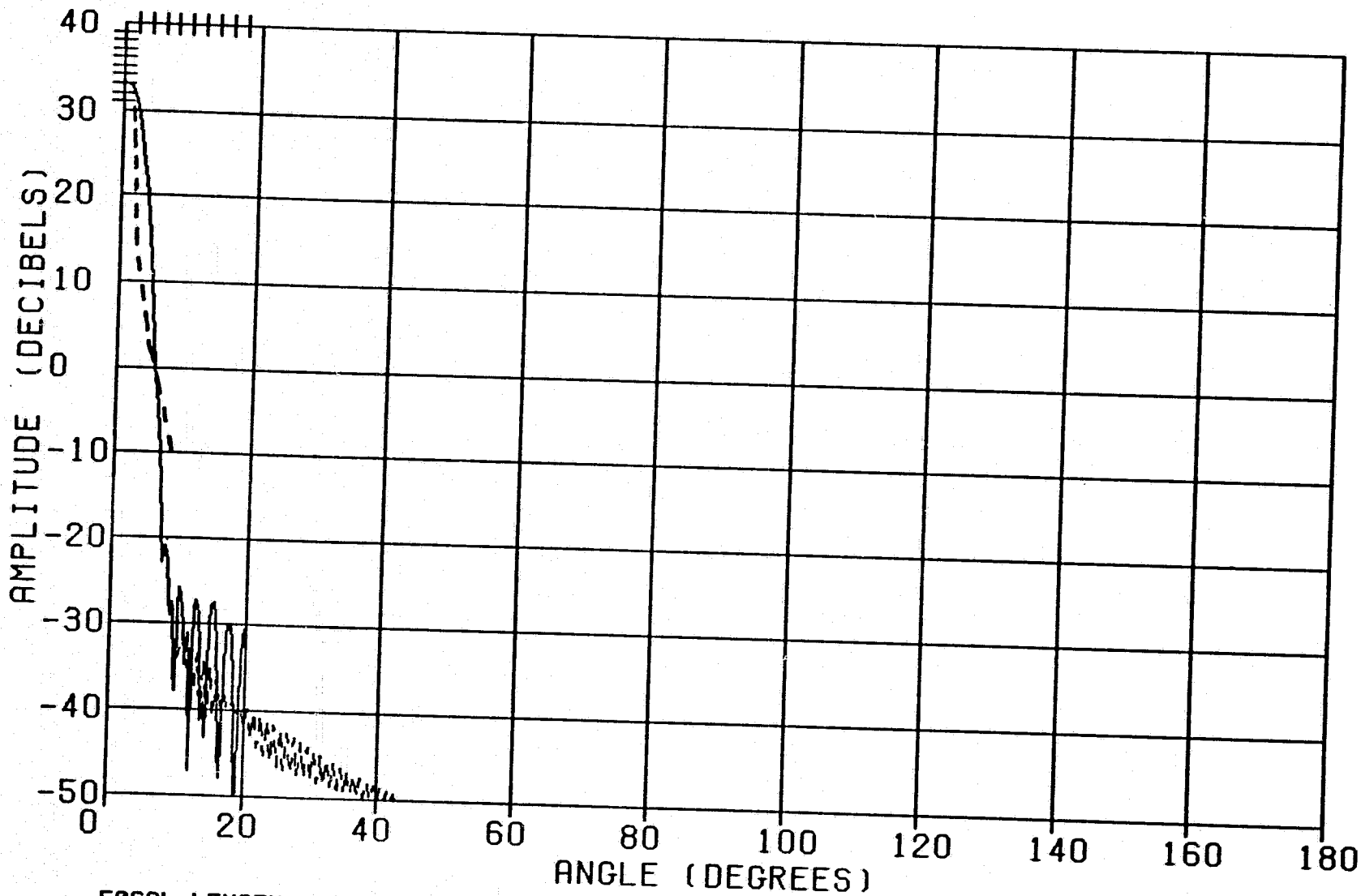

FIGURE 2-4A-4 FAR FIELD PATTERN FOR 4 λ HORN WITH f/D=0.15 ϕ = 135

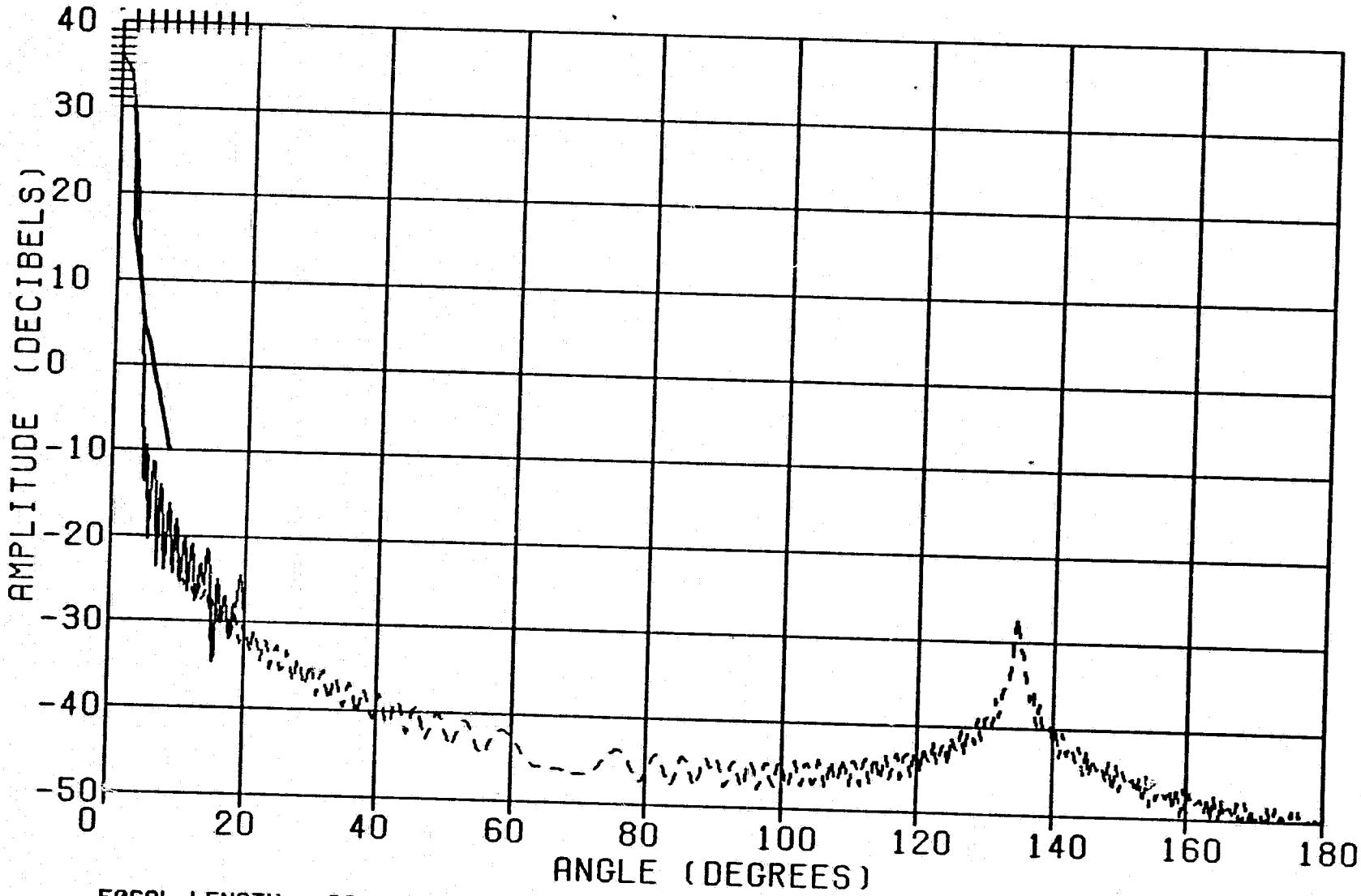

FOCAL LENGTH = 28.346. FEED ANGLE = 45.24. FREQ = 12.0 G
GPAT+GTD PATTERN PHI = 0.0. PRINCIPAL (4 LAMBDA)
GPAT(SOLID). GTD(DASHED)

FIGURE 2-4B-1 FAR FIELD PATTERN FOR 4 λ HORN WITH f/D=0.30 ϕ = 0°

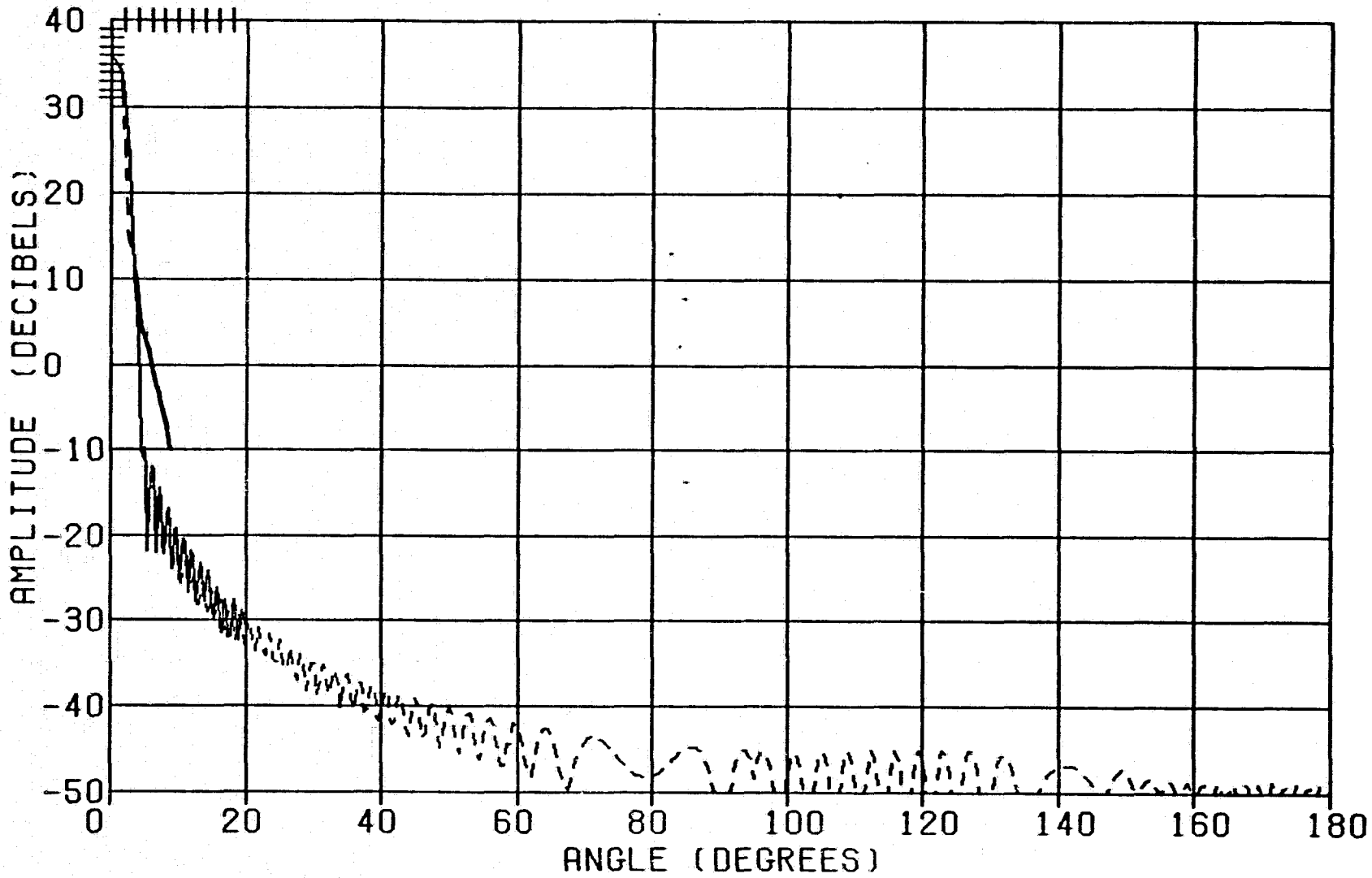

FOCAL LENGTH = 28.346, FEED ANGLE = 45.24, FREQ = 12.0 G
GPAT+GTD PATTERN PHI = 45.0, PRINCIPAL (4 LAMBDA)
GPAT(SOLID), GTD(DASHED)

FIGURE 2-4B-2 FAR FIELD PATTERN FOR 4 λ HORN WITH f/D=0.30 Ø = 45°

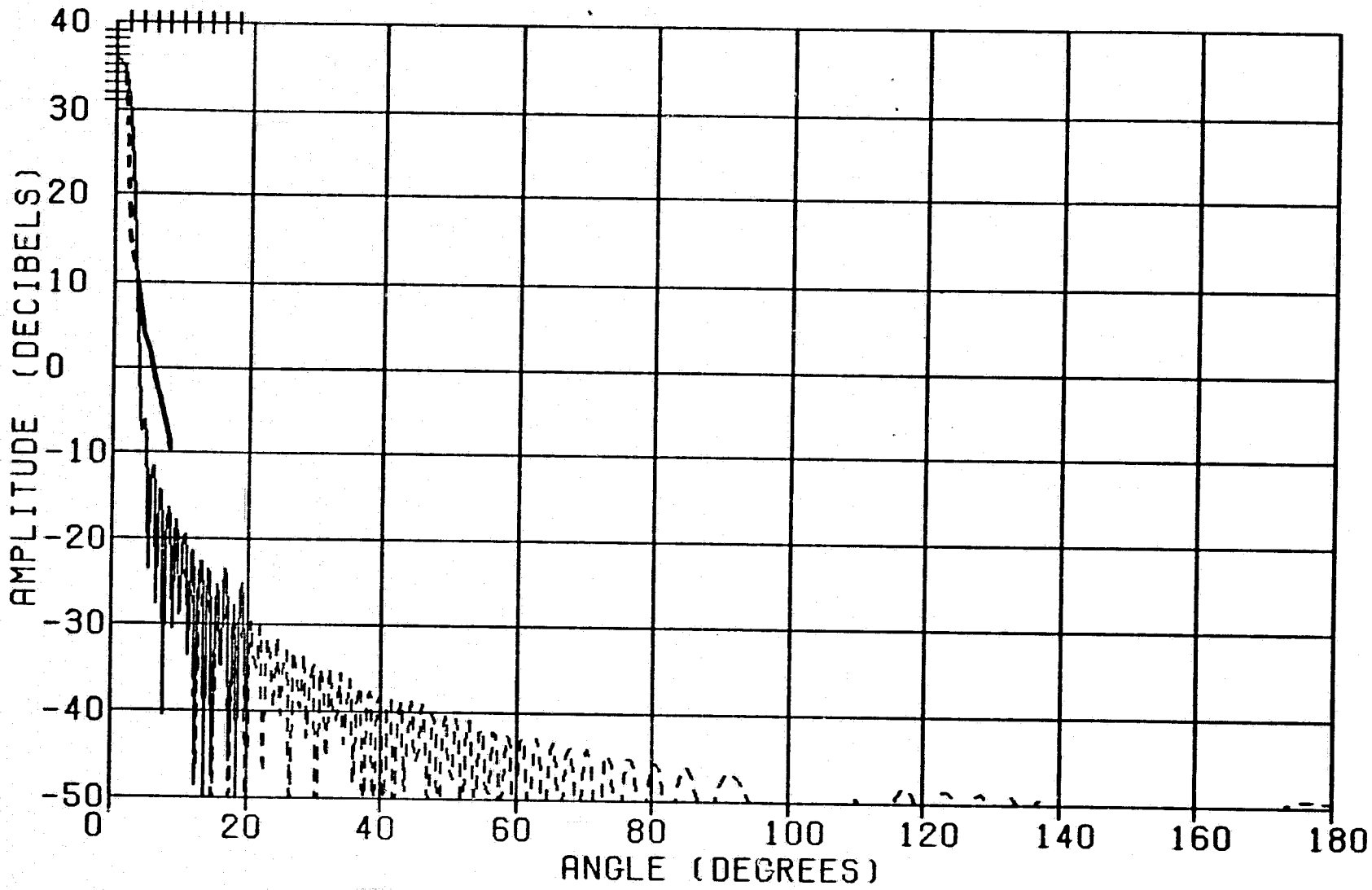

FIGURE 2-4B-3 FAR FIELD PATTERN FOR 4 λ HORN WITH f/D=0.30 ϕ = 90°

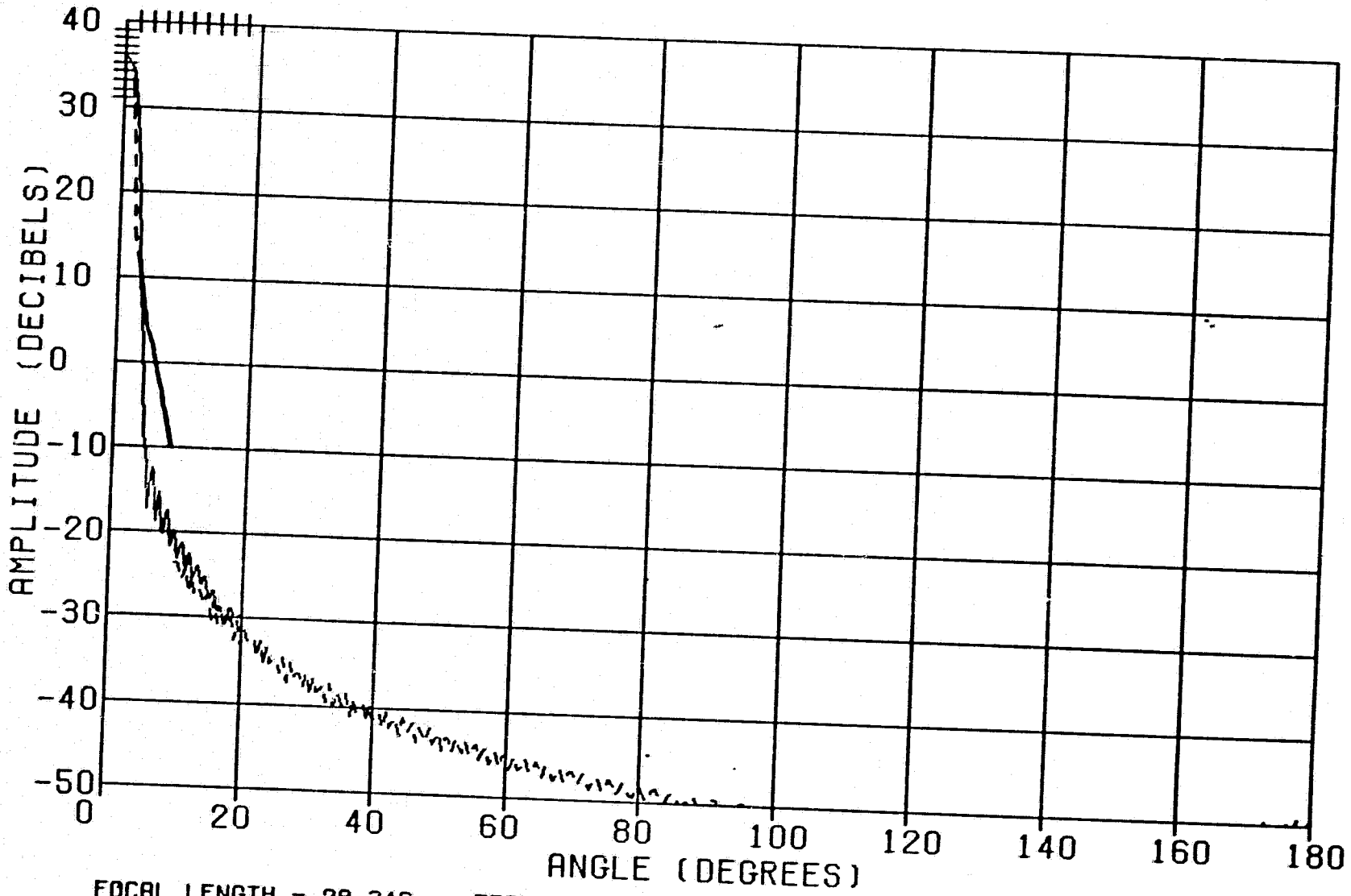

FIGURE 2-4B-4 FAR FIELD PATTERN FOR 4 λ HORN WITH f/D=0.30 ϕ = 135°

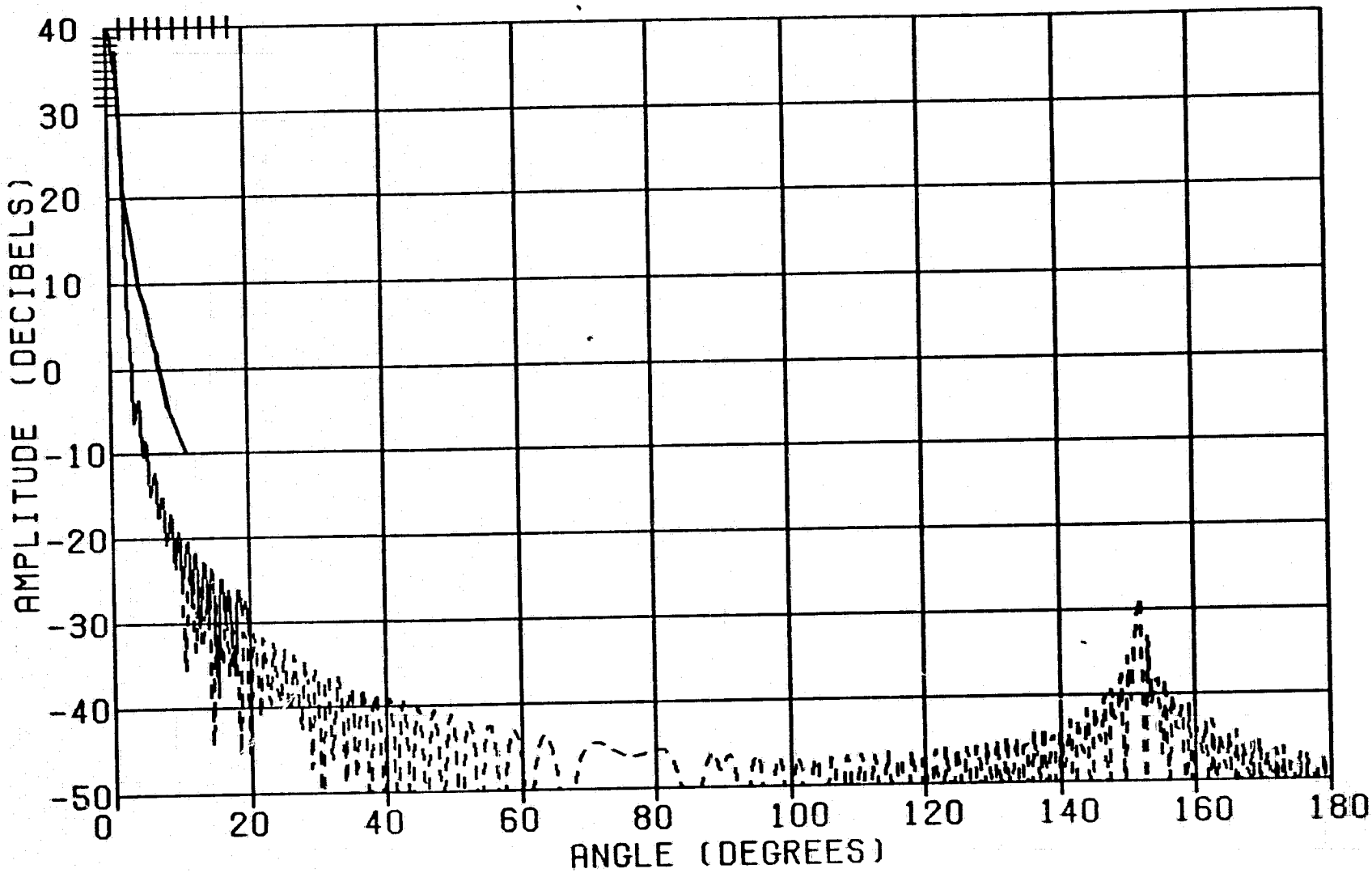

FOCAL LENGTH = 47.244. FEED ANGLE = 28.07. FREQ = 12.0 G
GPAT+GTD PATTERN PHI = 0.0. PRINCIPAL (4 LAMBDA)
GPAT(SOLID). GTD(DASHED)

FIGURE 2-4C-1 FAR FIELD PATTERN FOR 4 λ HORN WITH f/D=0.5 Ø = 0°

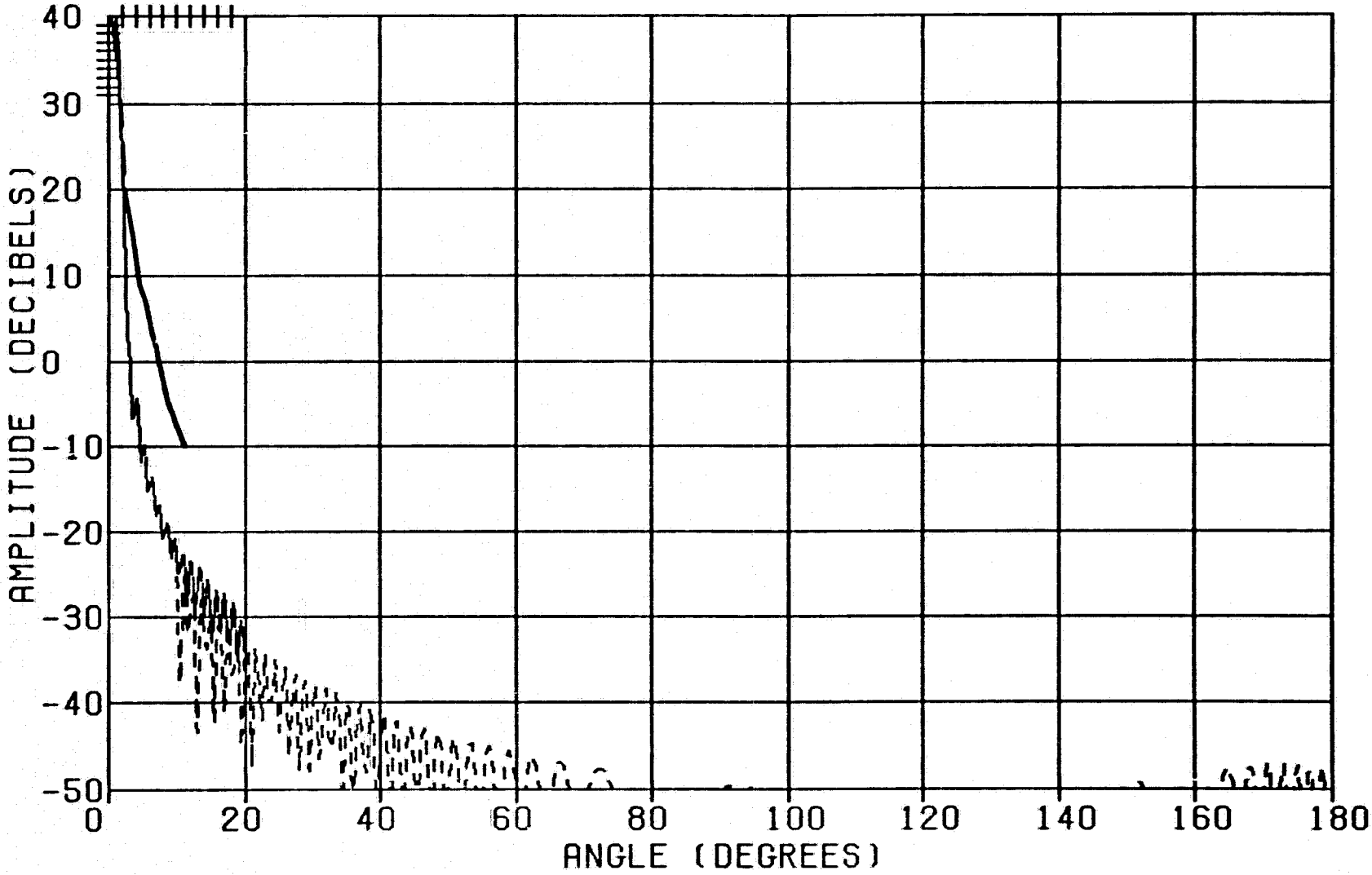

FOCAL LENGTH = 47.244. FEED ANGLE = 28.07. FREQ = 12.0 G
GPAT+GTD PATTERN PHI = 45.0. PRINCIPAL (4 LAMBDA)
GPAT(SOLID), GTD(DASHED)

FIGURE 2-4C-2 FAR FIELD PATTERN FOR 4 λ HORN WITH f/D=. 5 Ø = 45°

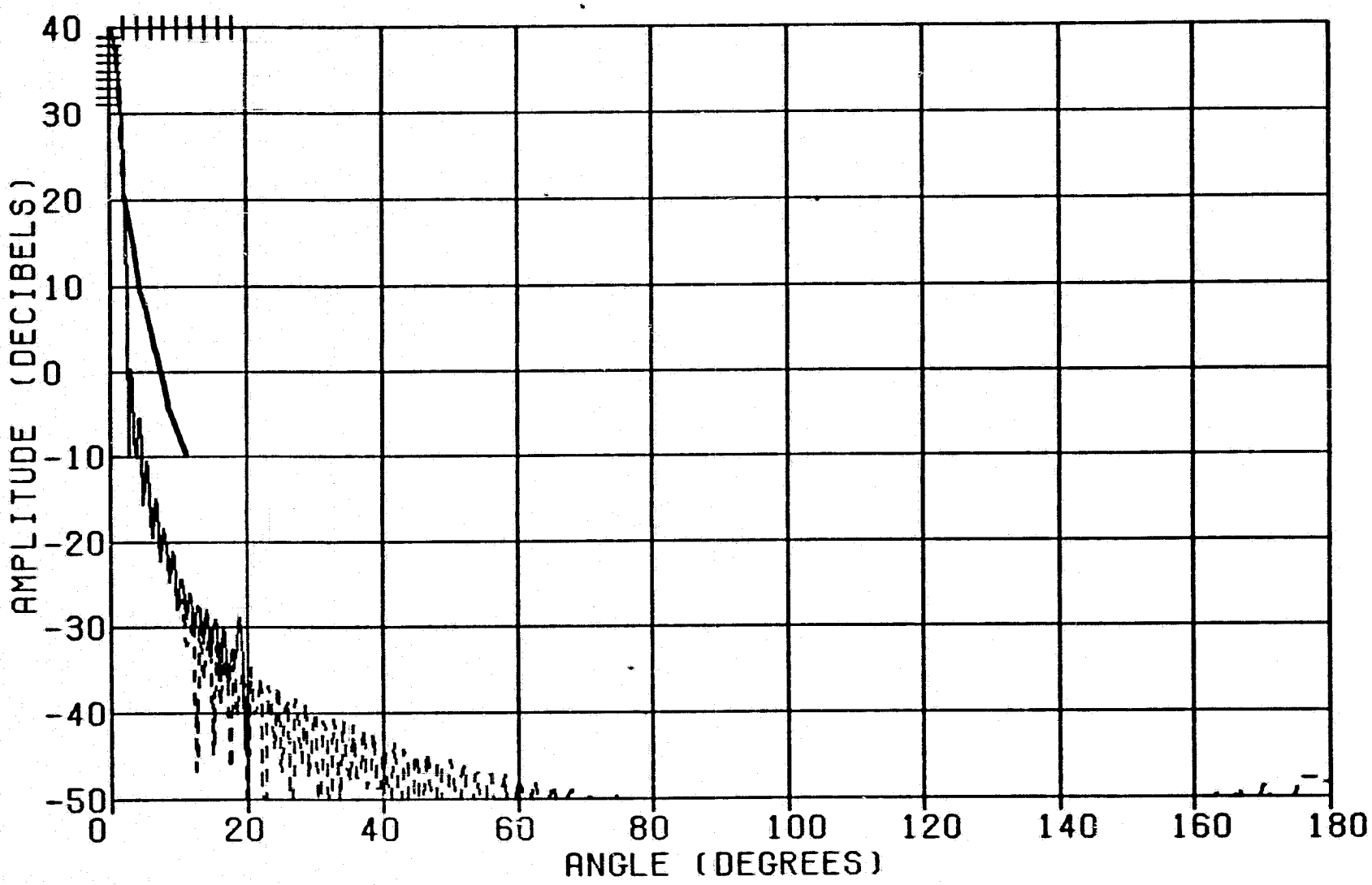

FOCAL LENGTH = 47.244, FEED ANGLE = 28.07, FREQ = 12.0 G
GPAT+GTD PATTERN PHI = 90.0, PRINCIPAL (4 LAMBDA)
GPAT(SOLID), GTD(DASHED)

FIGURE 2-4C-3 FAR FIELD PATTERN FOR 4λ HORN WITH f/D=0.5 ϕ = 90°

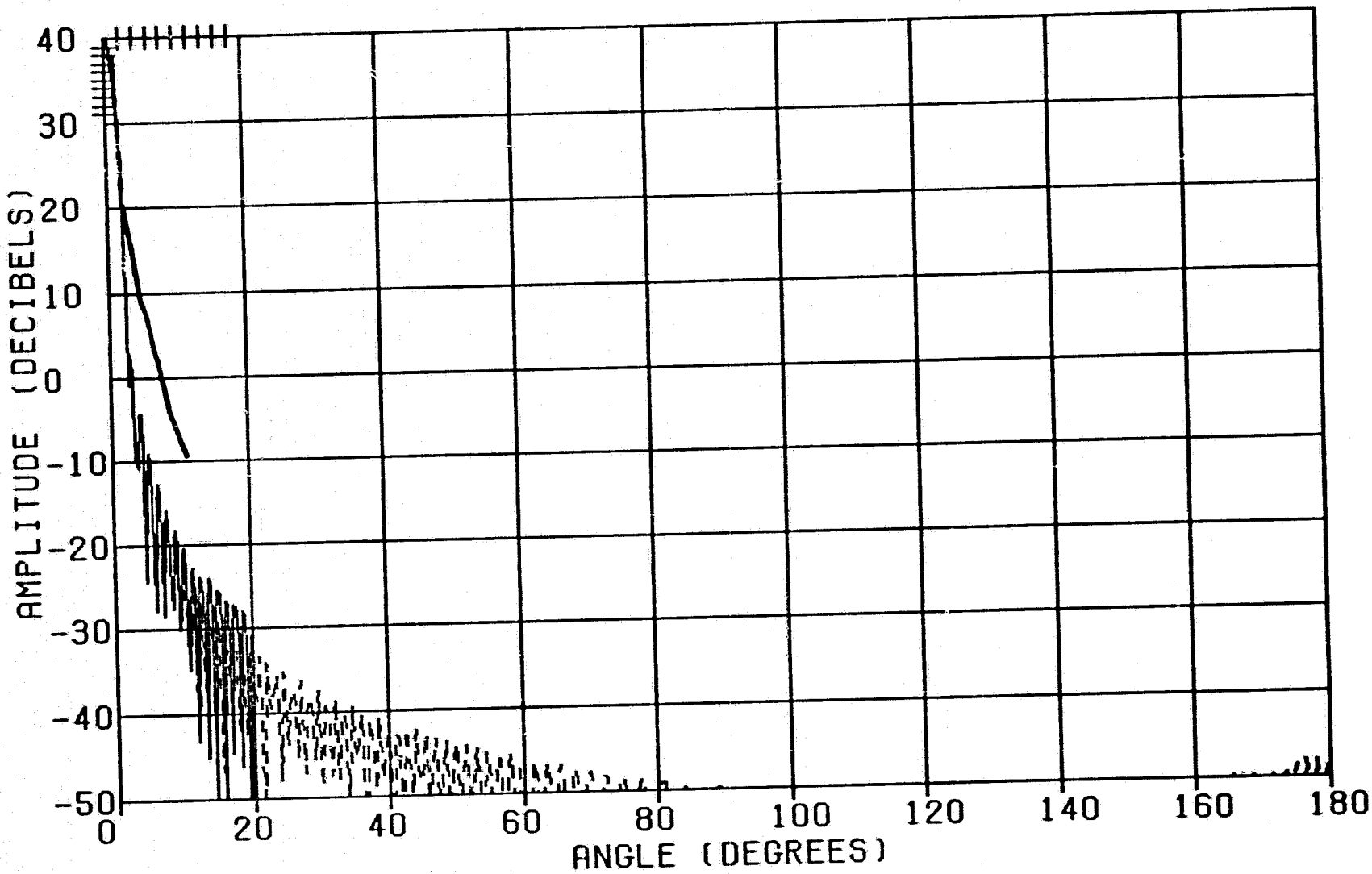

FOCAL LENGTH = 47.244. FEED ANGLE = 28.07. FREQ = 12.0 B
GPAT+GTD PATTERN PHI = 135.0, PRINCIPAL (4 LAMBDA)
GPAT(SOLID), GTD(DASHED)

FIGURE 2-4C-4 FAR FIELD PATTERN FOR 4 λ HORN WITH f/D=0.5 Ø = 135°

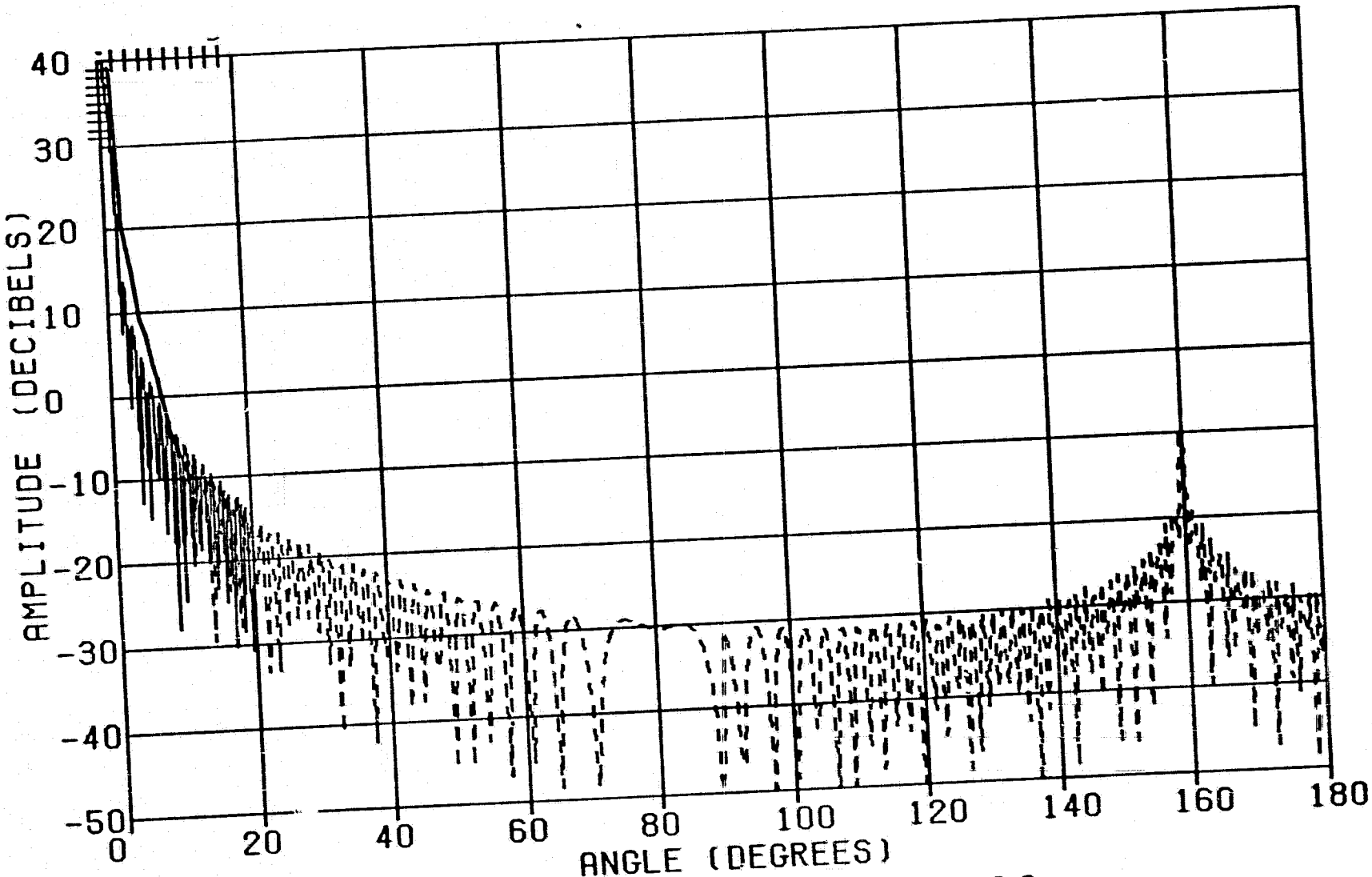

FOCAL LENGTH = 66.141. FEED ANGLE = 20.25. FREQ = 12.0 G
GPAT+GTD PATTERN PHI = 0.0. PRINCIPAL (4 LAMBDA)
GPAT(SOLID). GTD(DASHED)

FIGURE 2-4D-1 FAR FIELD PATTERN FOR 4 λ HORN WITH f/D=0.7 $\phi = 0^{\circ}$

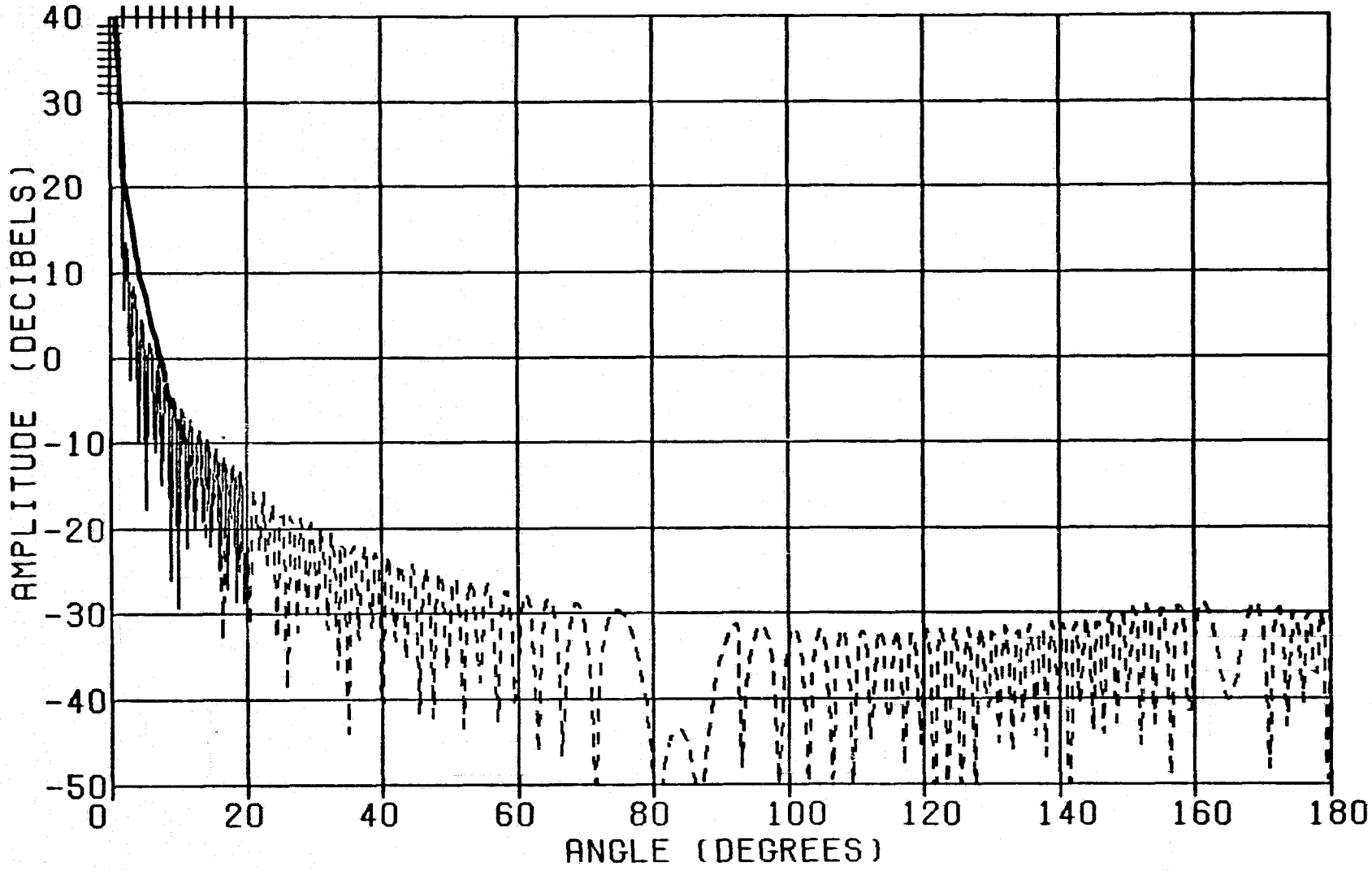

FOCAL LENGTH = 66.141. FEED ANGLE = 20.25. FREQ = 12.0 G
GPAT+GTD PATTERN PHI = 45.0. PRINCIPAL (4 LAMBDA)
GPAT(SOLID). GTD(DASHED)

FIGURE 2-4D-2 FAR FIELD PATTERN FOR 4 λ HORN WITH f/D=0.7 ϕ = 45°

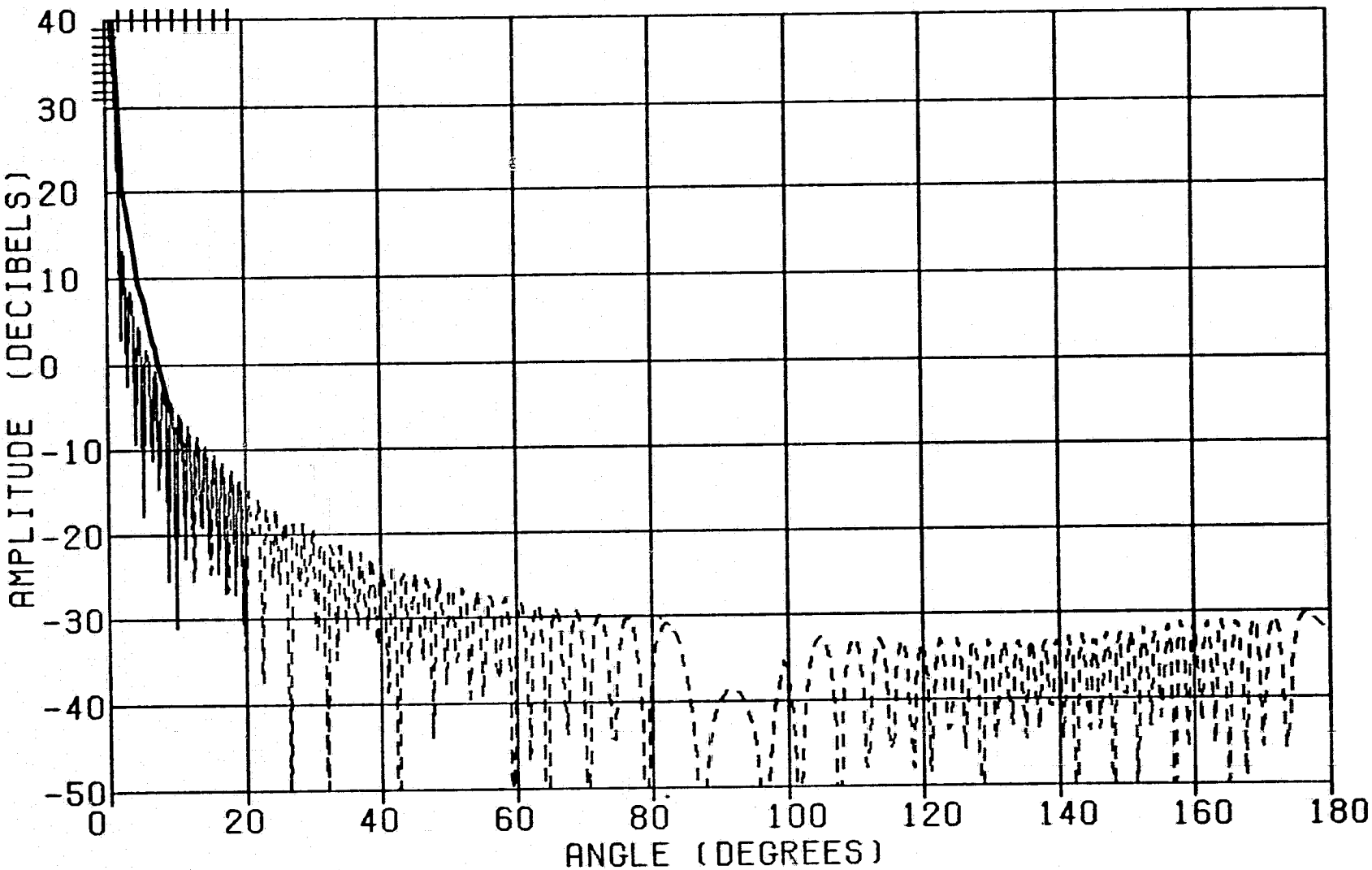

FOCAL LENGTH = 66.141, FEED ANGLE = 20.25, FREQ = 12.0 G
GPAT+GTD PATTERN PHI = 90.0, PRINCIPAL (4 LAMBDA)
GPAT(SOLID), GTD(DASHED)

FIGURE 2-4D-3 FAR FIELD PATTERN FOR 4 λ HORN WITH f/D=0.7 Ø = 90°

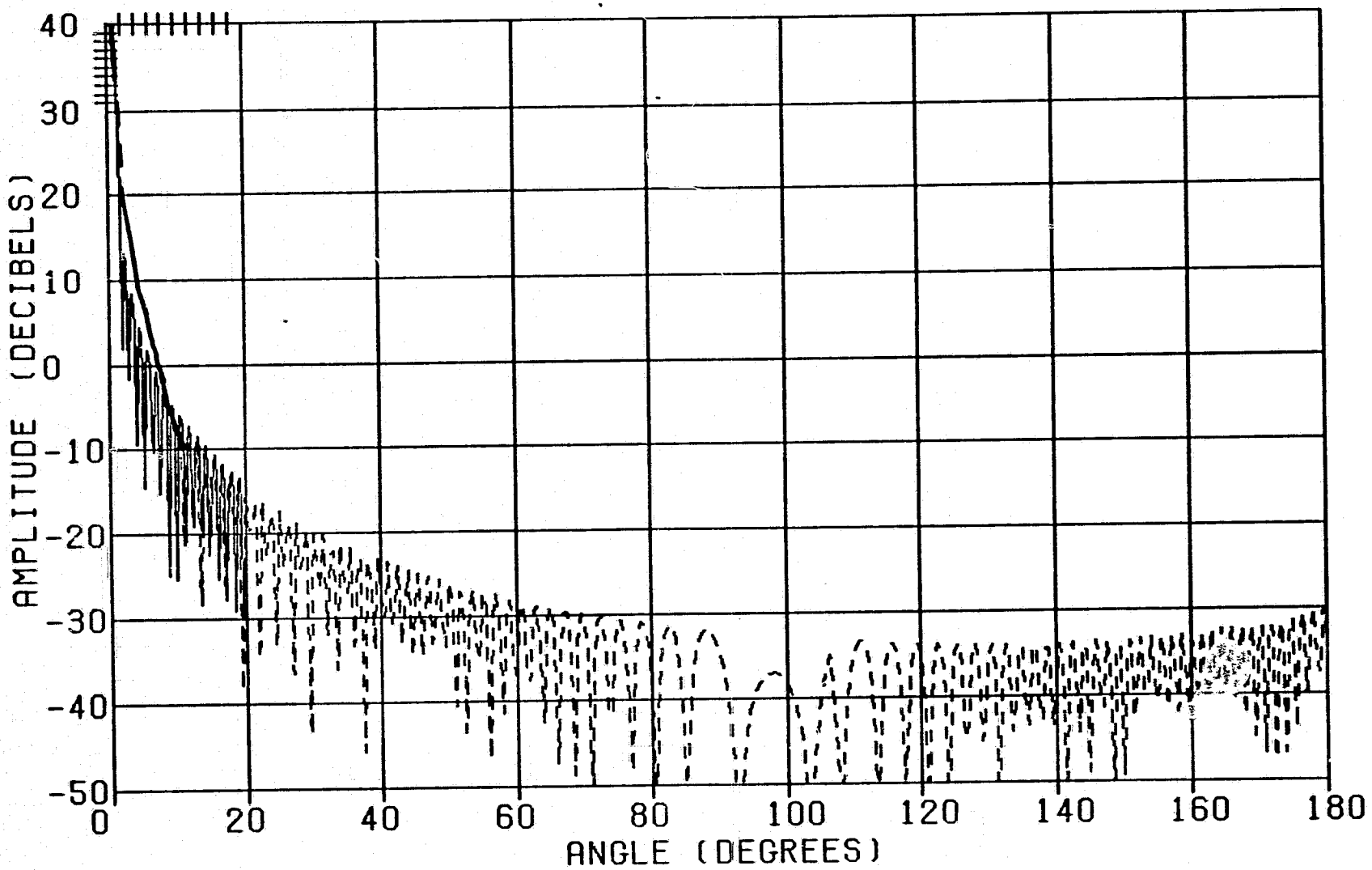

FOCAL LENGTH = 66.141, FEED ANGLE = 20.25, FREQ = 12.0 G
GPAT+GTD PATTERN PHI = 135.0, PRINCIPAL (4 LAMBDA)
GPAT(SOLID), GTD(DASHED)

FIGURE 2-4D-4 FAR FIELD PATTERN FOR 4 λ HORN WITH f/D=0.7 Ø = 135°

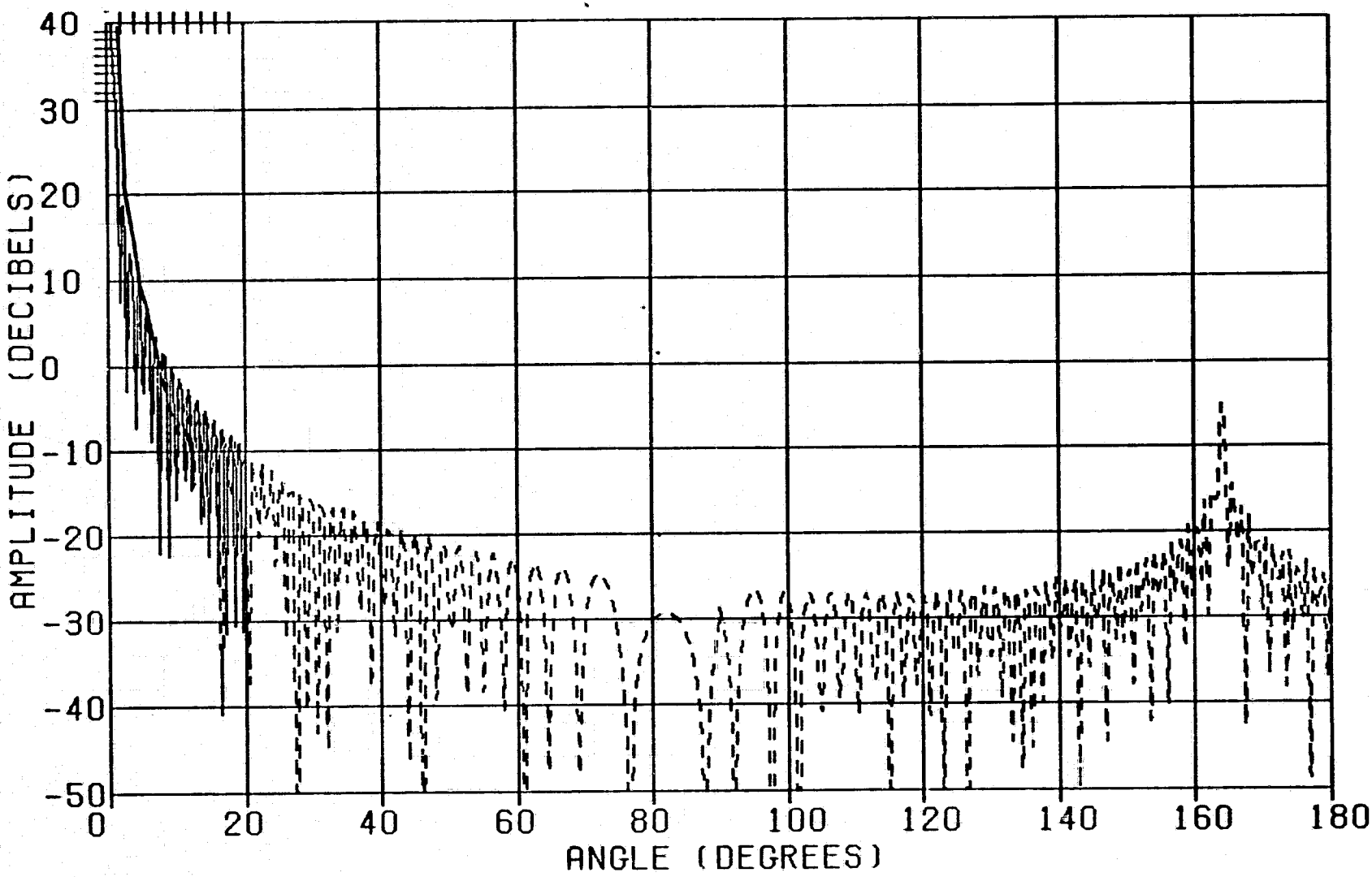

FOCAL LENGTH = 85.039, FEED ANGLE = 15.81, FREQ = 12.0 G
GPAT+GTD PATTERN PHI = 0.0, PRINCIPAL (4 LAMBDA)
GPAT(SOLID), GTD(DASHED)

FIGURE 2-4E-1 FAR FIELD PATTERN FOR 4 λ HORN WITH f/D=0.9 Ø = 0°

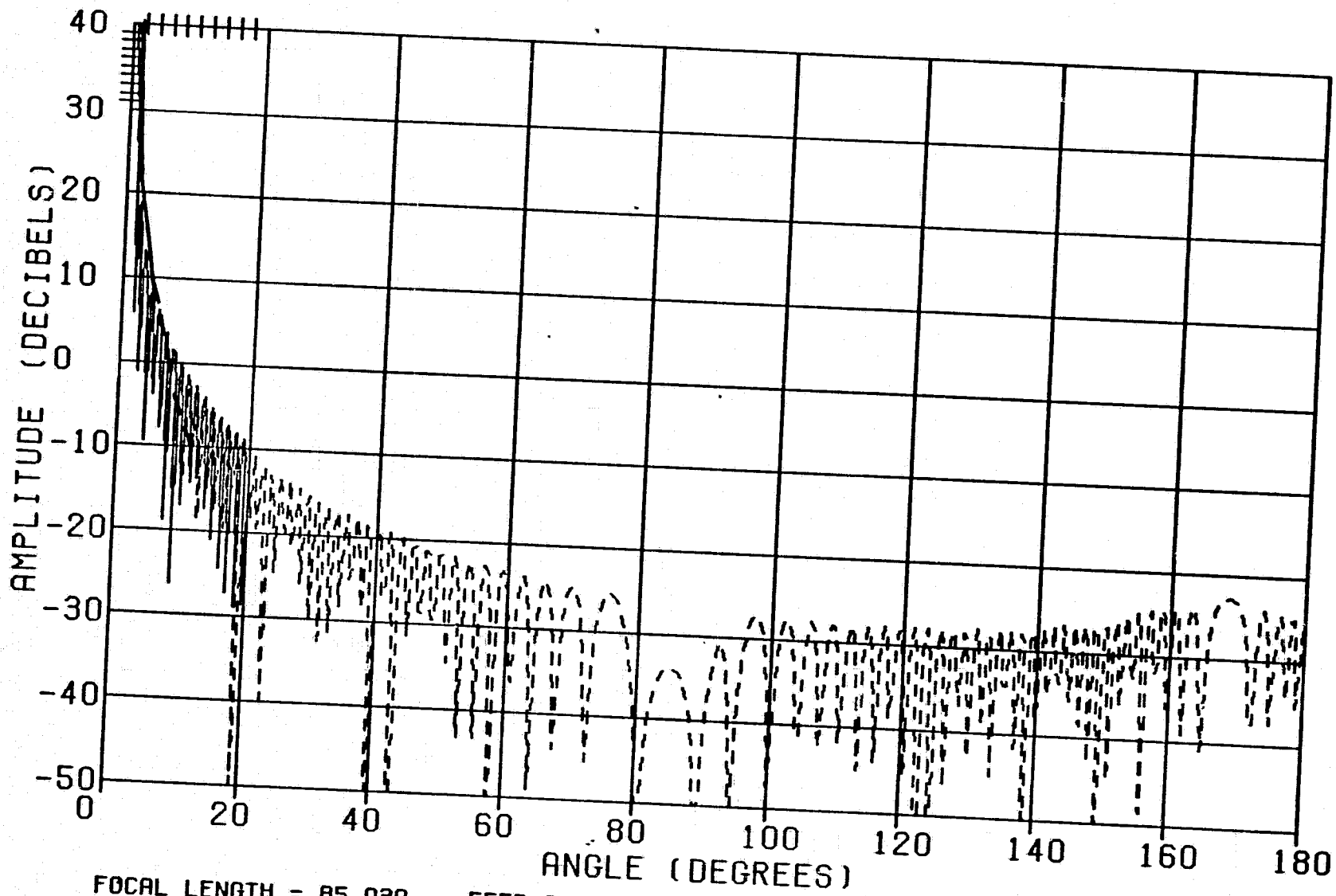

FIGURE 2-4E-2 FAR FIELD PATTERN FOR 4 λ HORN WITH f/D=0.9 Ø = 45°

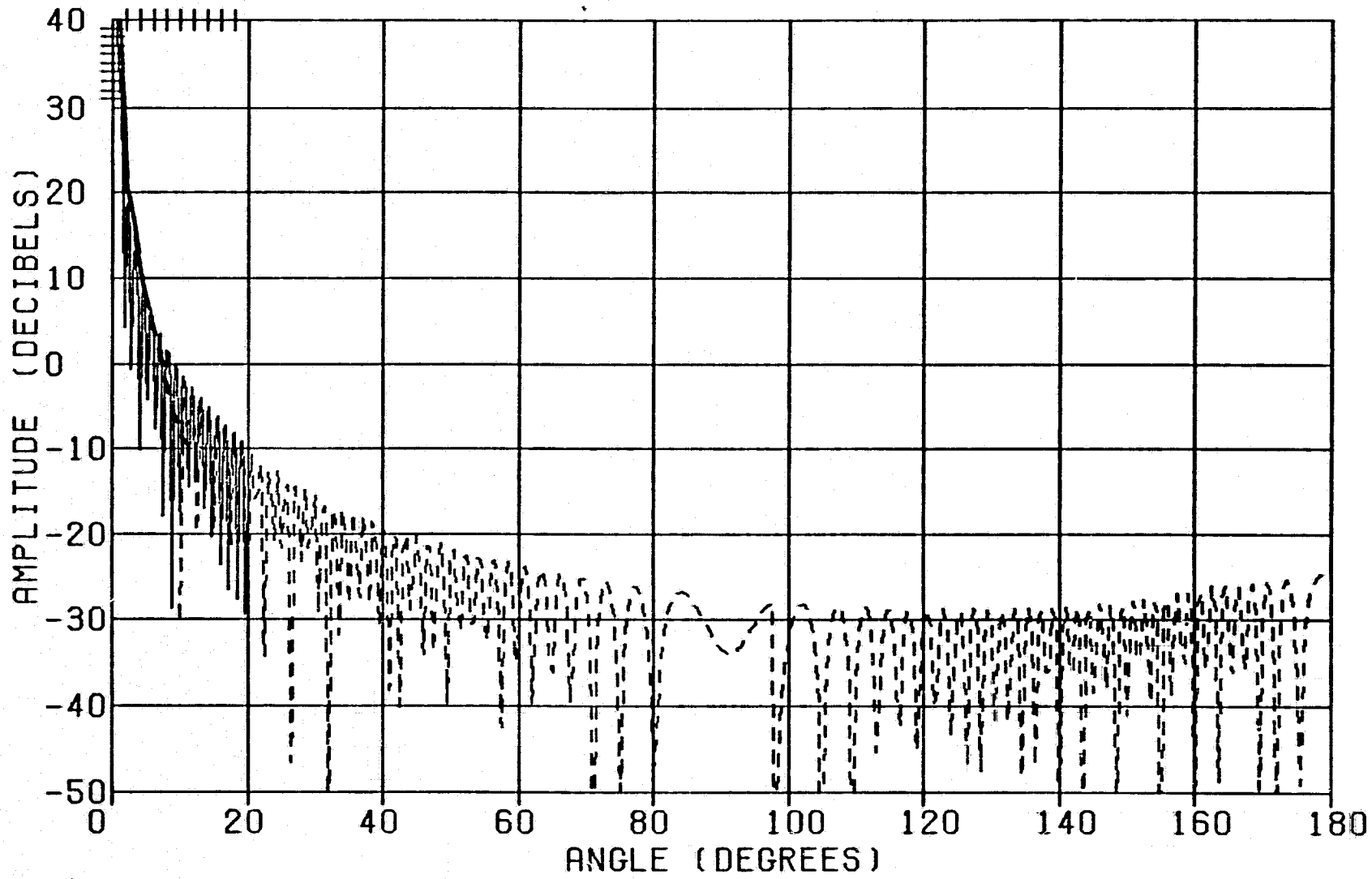

FOCAL LENGTH = 85.039. FEED ANGLE = 15.81. FREQ = 12.0 G
GPAT+GTD PATTERN PHI = 90.0, PRINCIPAL (4 LAMBDA)
GPAT(SOLID), GTD(DASHED)

FIGURE 2-4E-3 FAR FIELD PATTERN FOR 4 λ HORN WITH f/D=0.9 Ø = 90°

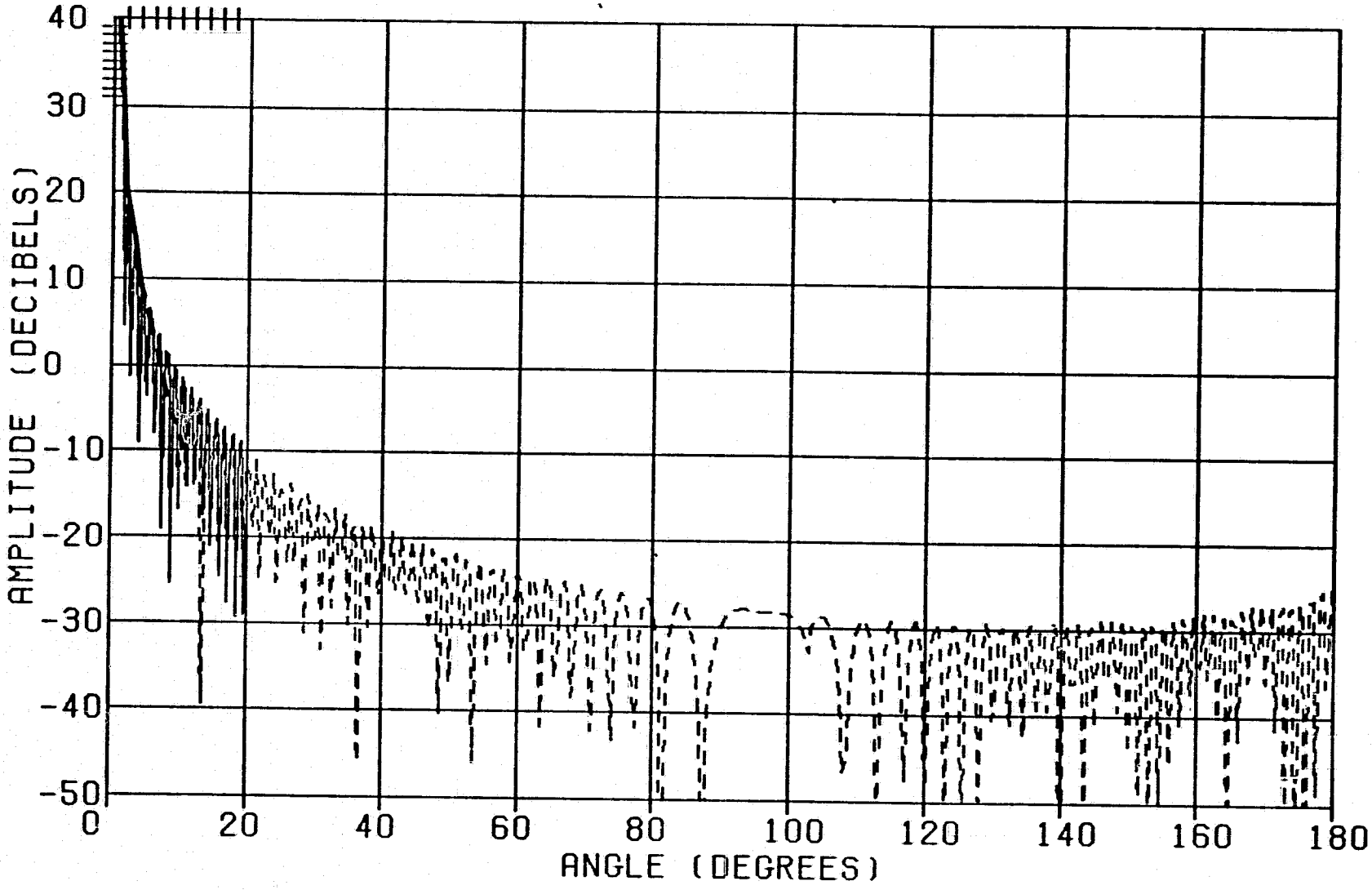

FOCAL LENGTH = 85.039. FEED ANGLE = 15.81. FREQ = 12.0 G
GPAT+GTD PATTERN PHI = 135.0. PRINCIPAL (4 LAMBDA)
GPAT(SOLID). GTD(DASHED)

FIGURE 2-4E-4 FAR FIELD PATTERN FOR 4 λ HORN WITH f/D=0.9 Ø = 135°

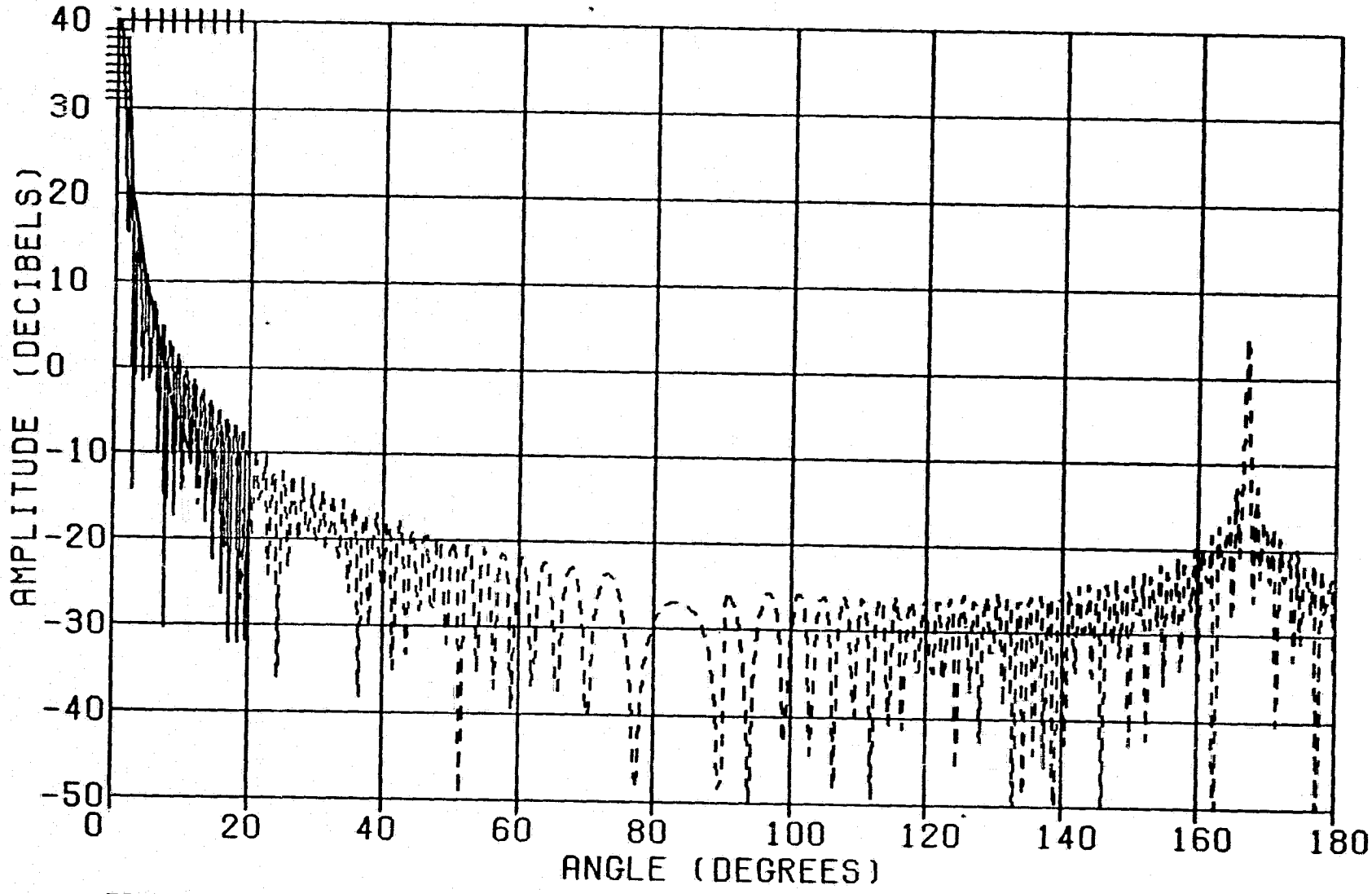

FOCAL LENGTH = 103.936. FEED ANGLE = 12.97. FREQ = 12.0
GPAT+GTD PATTERN PHI = 0.0, PRINCIPAL (4 LAMBDA)
GPAT(SOLID), GTD(DASHED)

FIGURE 2-4F-1 FAR FIELD PATTERN FOR 4 λ HORN WITH f/D=1.1 $\phi = 0^{\circ}$

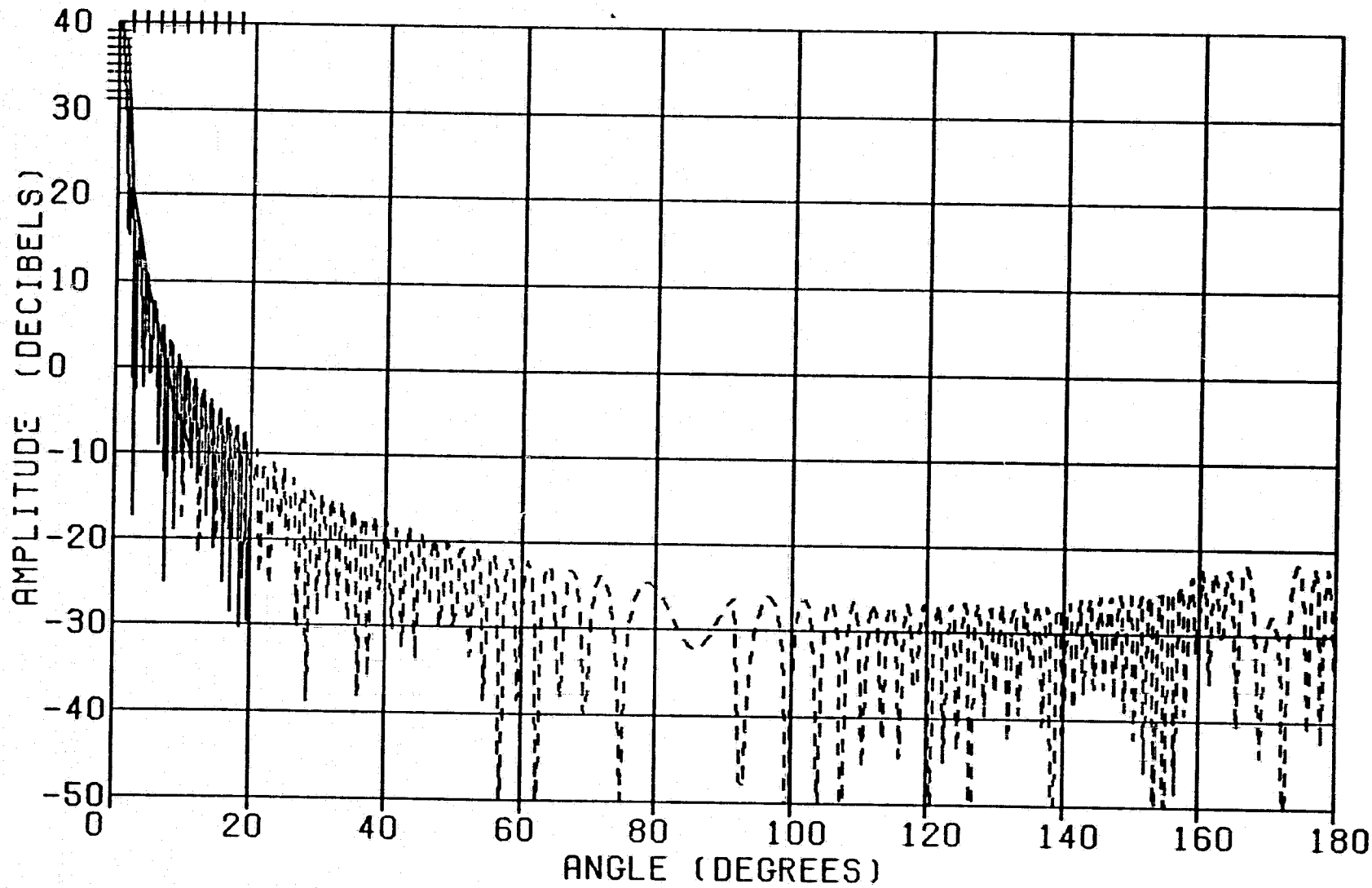

FIGURE 2-4F-2 FAR FIELD PATTERN FOR 4 λ HORN WITH f/D=1.1 ϕ = 45°

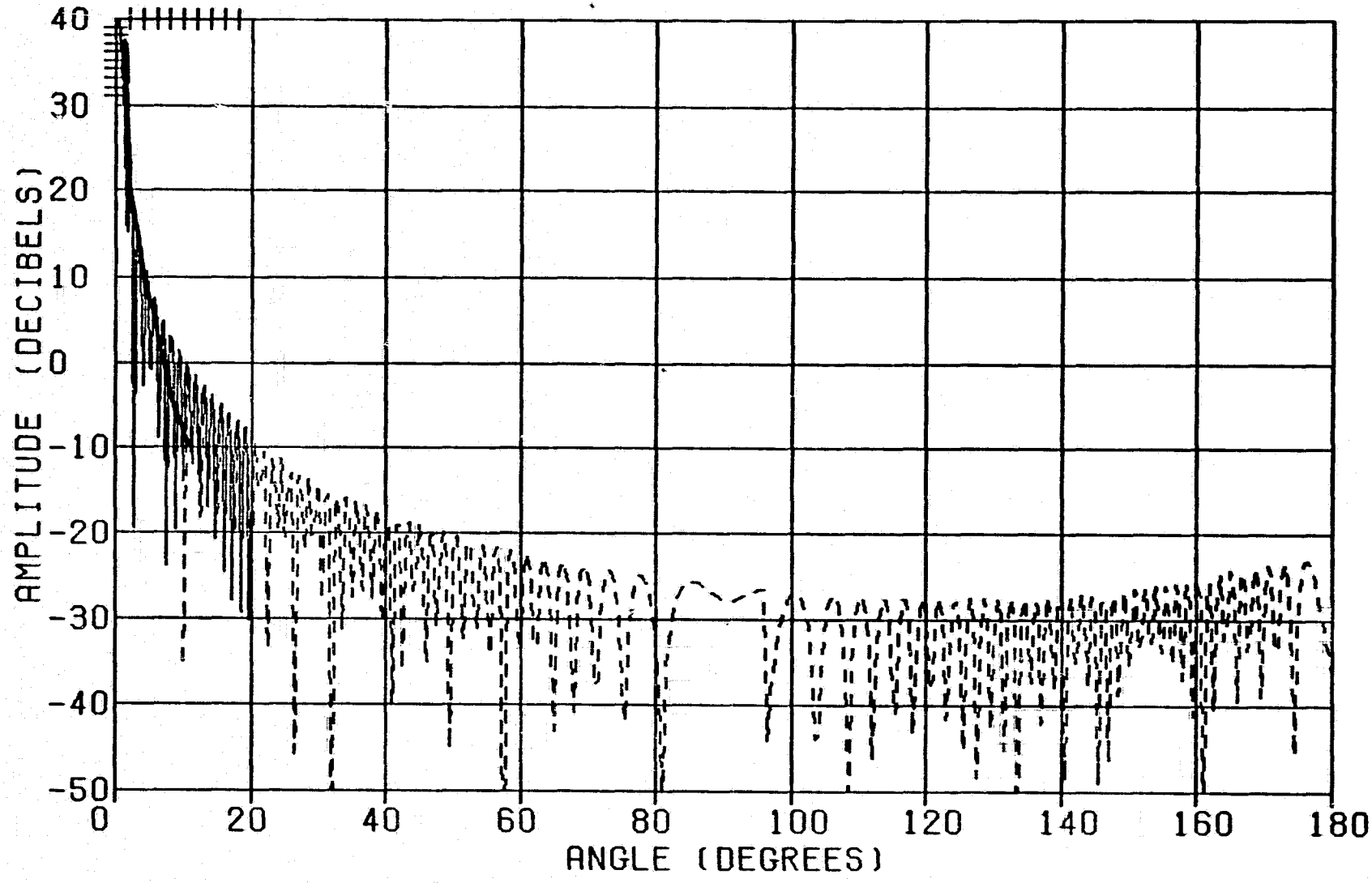

FIGURE 2-4F-3 FAR FIELD PATTERN FOR 4 λ HORN WITH f/D=1.1 Ø = 90°

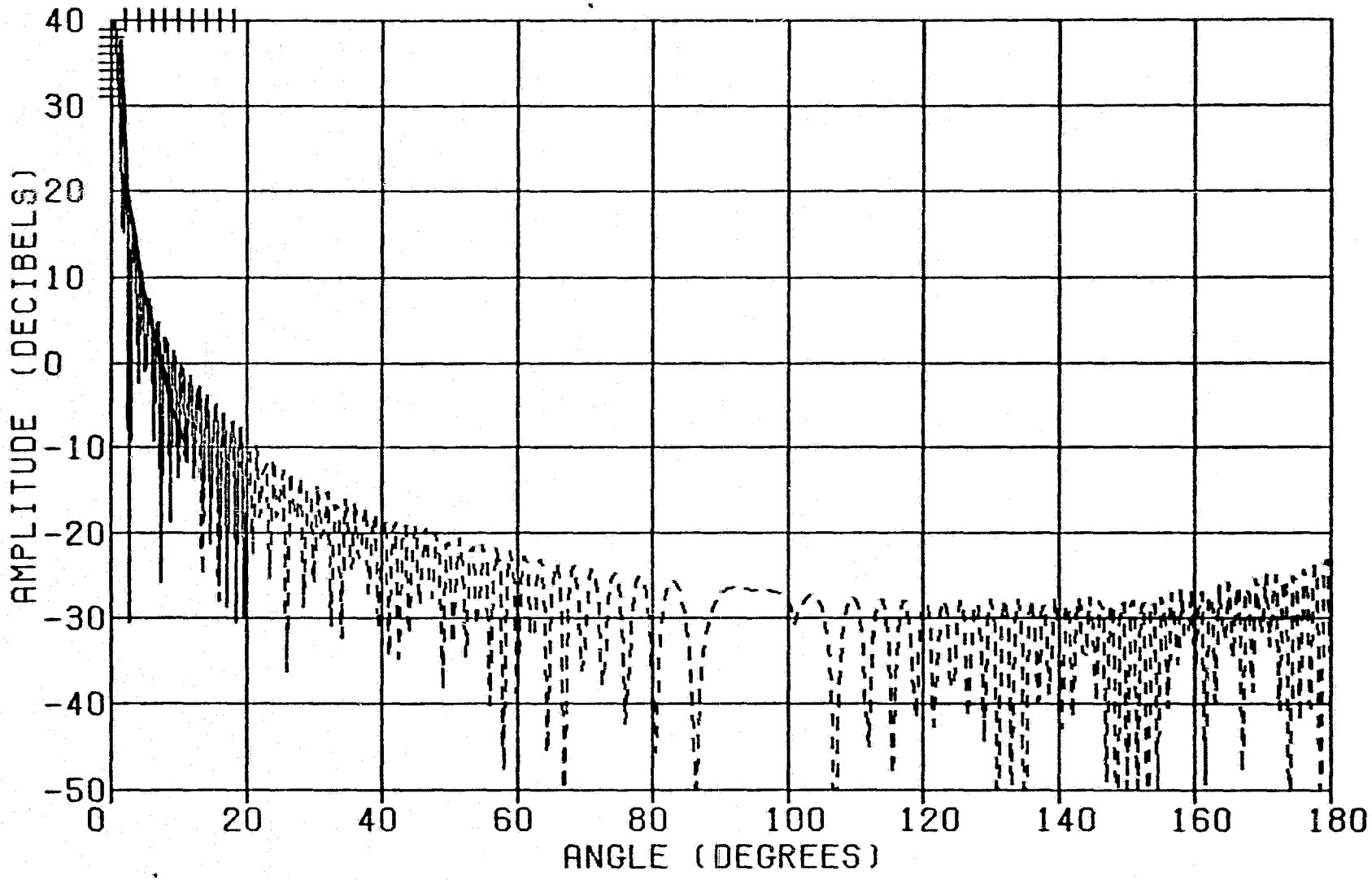

FOCAL LENGTH = 103.936, FEED ANGLE = 12.97, FREQ = 12.0
GPAT+GTD PATTERN PHI = 135.0, PRINCIPAL (4 LAMBDA)
GPAT(SOLID), GTD(DASHED)

FIGURE 2-4F-4 FAR FIELD PATTERN FOR 4 λ HORN WITH f/D=1.1 Ø = 135°

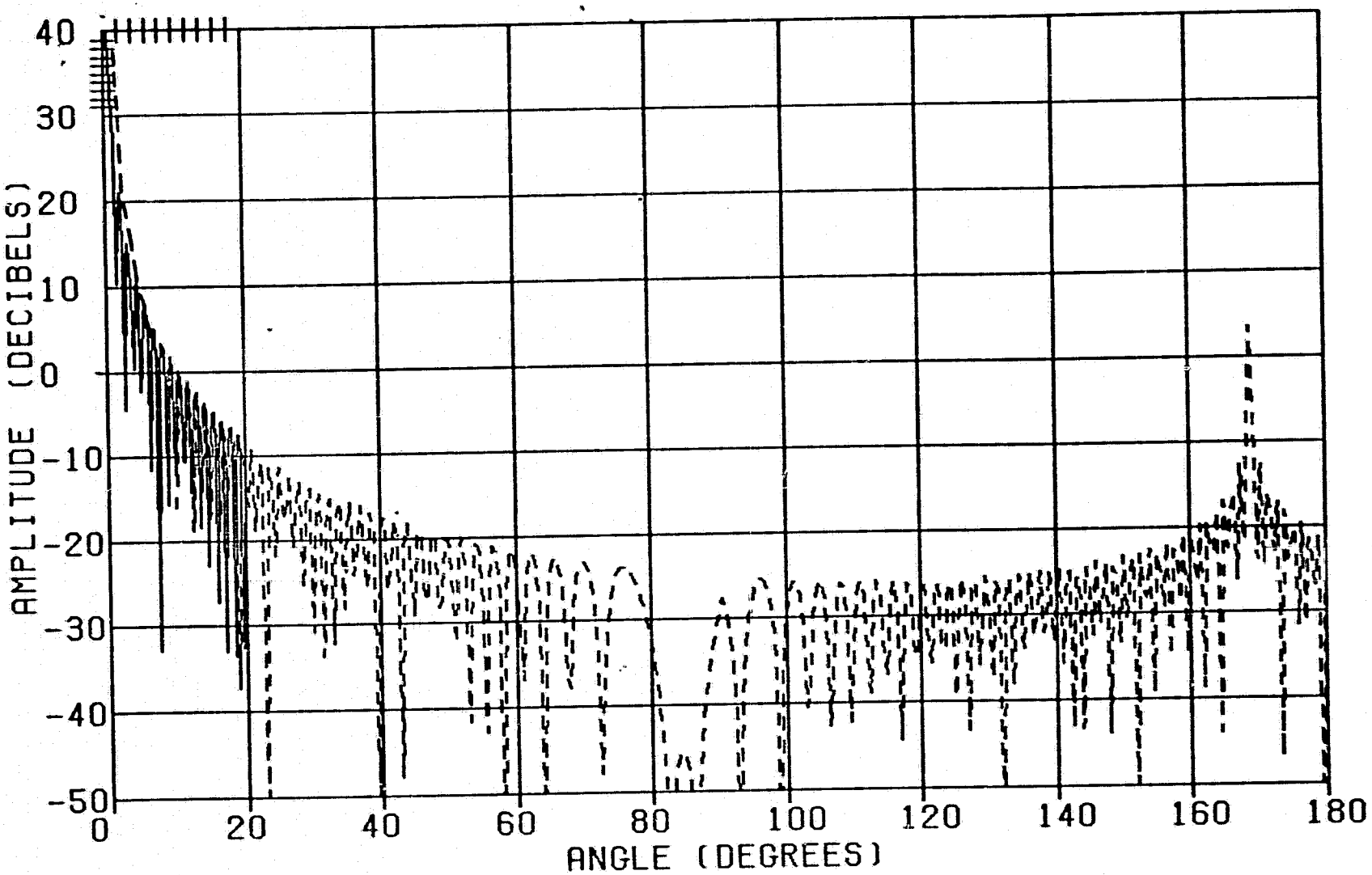

FOCAL LENGTH = 122.83, FEED ANGLE = 10.98, FREQ = 12.0 G
GPAT+GTD PATTERN PHI = 0.0, PRINCIPAL (4 LAMBDA)
GPAT(SOLID), GTD(DASHED)

FIGURE 2-4G-1 FAR FIELD PATTERN FOR 4 λ HORN WITH f/D=1.3 Ø = 0°

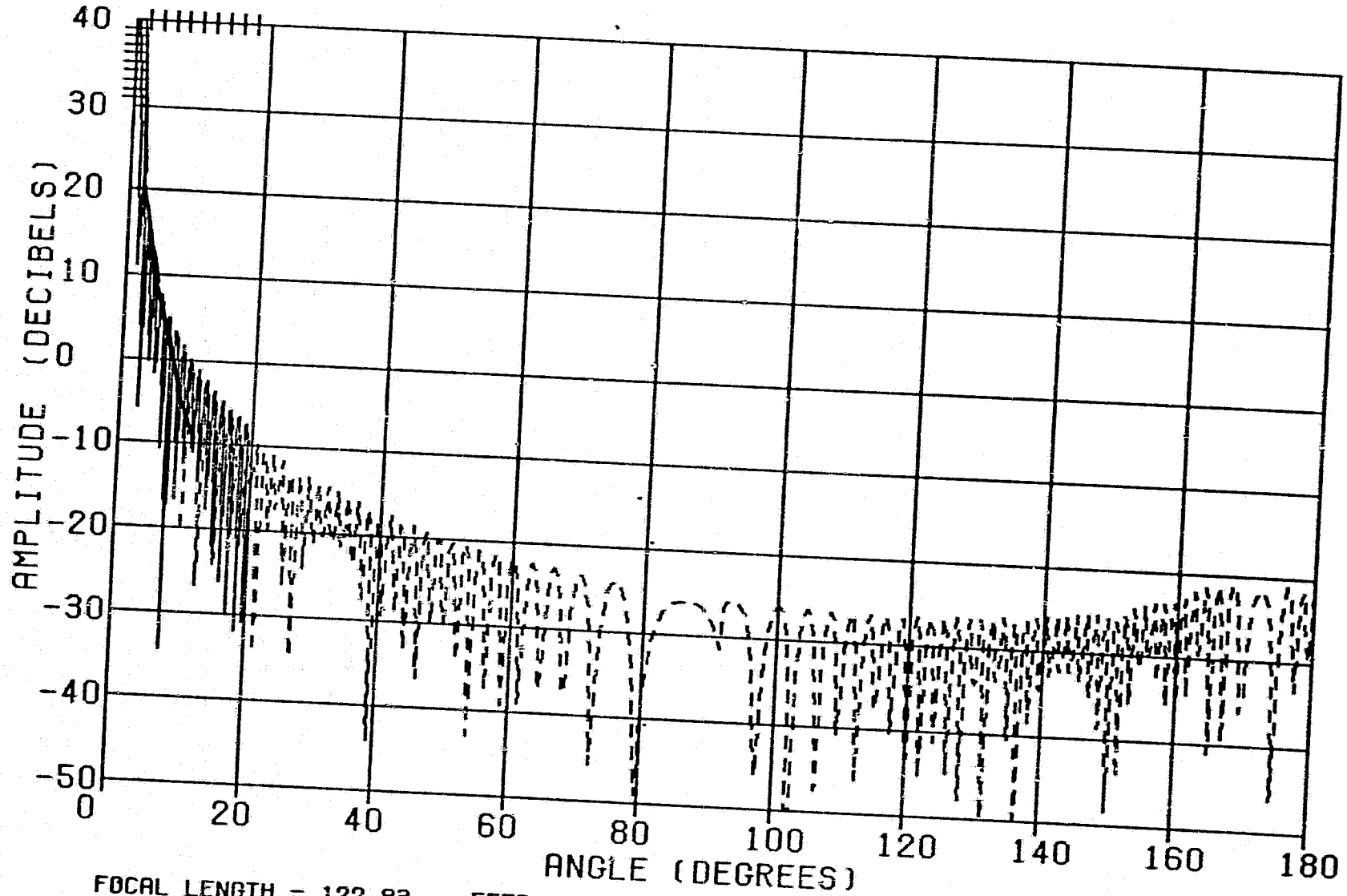

FIGURE 2-4G-2 FAR FIELD PATTERN FOR 4 λ HORN WITH f/D=1.3 Ø = 45°

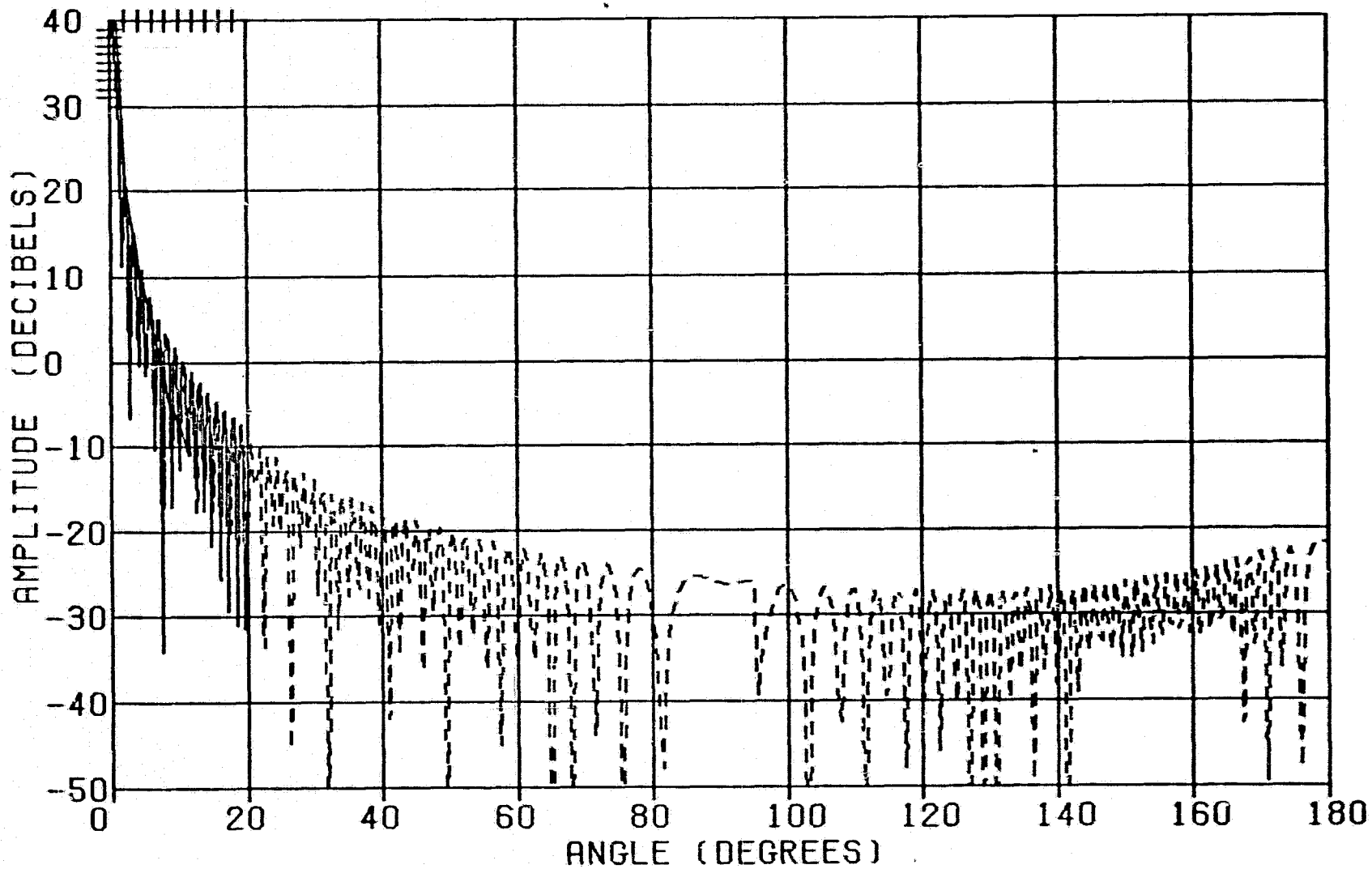

FOCAL LENGTH = 122.83, FEED ANGLE = 10.98, FREQ = 12.0 G
GPAT+GTD PATTERN PHI = 90.0, PRINCIPAL (4 LAMBDA)
GPAT(SOLID), GTD(DASHED)

FIGURE 2-4G-2 FAR FIELD PATTERN FOR 4 λ HORN WITH f/D=1.3 Ø = 90°

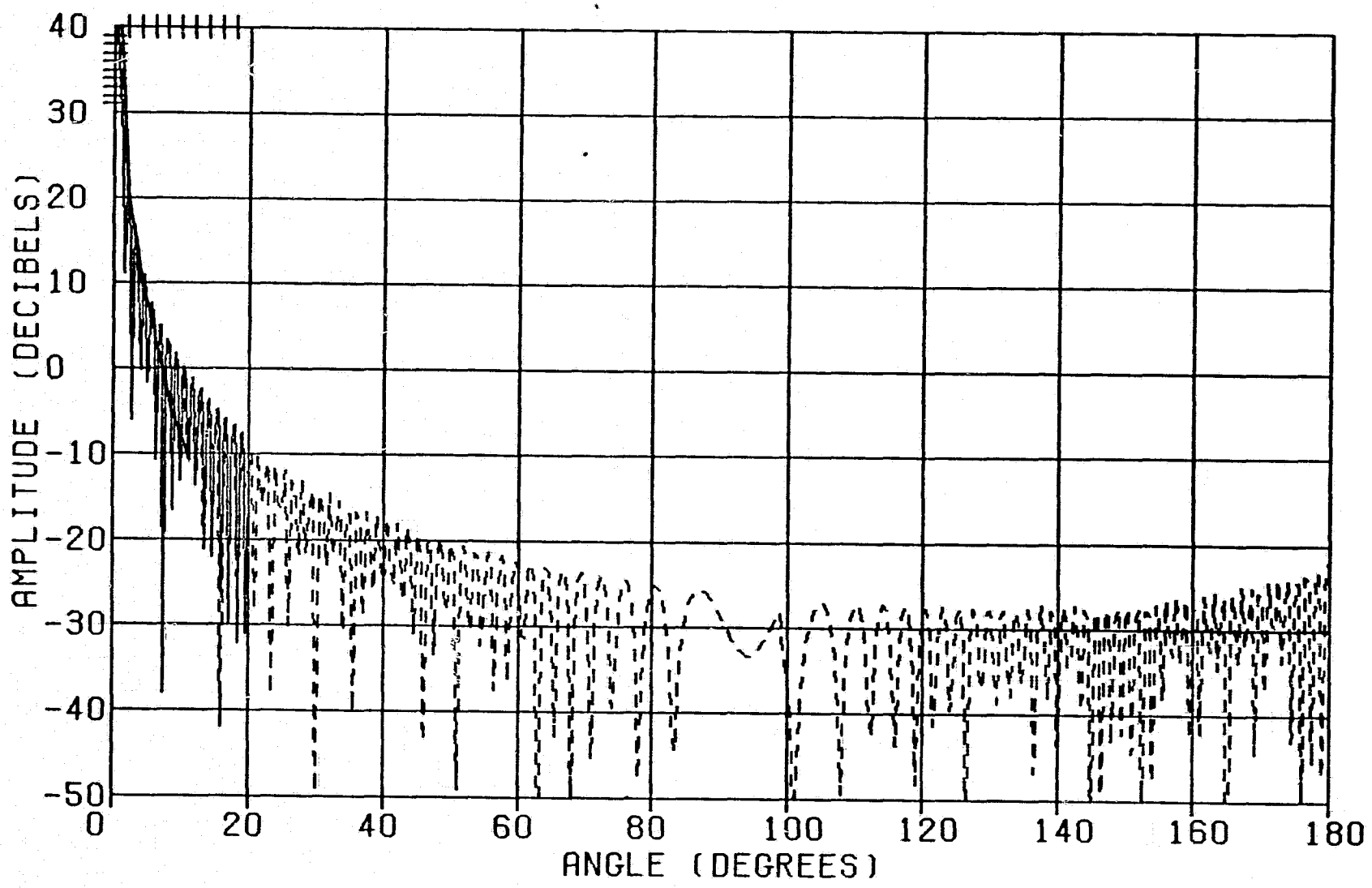

FIGURE 2-4G-4 FAR FIELD PATTERN FOR 4 λ HORN WITH f/D=1.3 ϕ = 135°

2.4 The 3 λ Horn

For f/D > 0.5, the n=2 Chebyshev envelope is a very tight fit for the first 5 sidelobes down to a region of +10 dBi. Below this region to 0 dBi, the envelope is met only for f/D's below 0.5 but larger than 0.3. As the f/D decreases, the edge illumination taper is so severe that the effective aperture area has decreased significantly, thus broadening the main beam and reducing the gain. Sidelobes beyond 20° off-axis are determined principally by the GTD analysis. In this region, there is great variation of sidelobe level as a function of Ø. For f/D = 0.7 (2-3D), the patterns are respectable in the Ø = 45°, 90°, 135° and 270° planes, but exceed our 0 dBi reference level in the 0° and 180° planes. (Only the 0°, 45°, 90° and 135° planes are actually calculated; we assume that the patterns use symmetric about the Ø = 0, 180° axis.) The patterns are slightly better for f/D = 0.5, but even here the 0 dBi plateau is exceeded in the Ø = 0, 180° plane.

In terms of adjacent satellite interference, this minor deviation may be entirely acceptable if the Ø = 90°, 270° plane is aligned with the plane of the orbital arc. In this case, the pattern not only meets the n=2 Chebyshev envelope for the near-in lobes, but also meets a more stringent -10 dBi plateau everywhere [2-3C, Ø = 90°]. Thus, a 3λ 30° flare angle corrugated horn appears to meet the spirit and the letter of the development goals in the Ø = 90°-270° plane for an f/D = 0.5.

For f/D's < 0.5, the far-out sidelobes are very close to the 0 dBi plateau, but the main beam broadening causes the patterns to fall for the near-in sidelobes (θ < 20°).

2.5 The 4λ Horn

Because of the superior primary pattern, the far-field patterns for the 4λ horn exhibit much better far-out sidelobe behavior ($\theta > 20°$). For large f/D, the patterns fail the envelope in the $\theta = 10°$ region near the 0 dBi plateau. In order to meet the envelope in this region, the f/D must be less than 0.7. The f/D = 0.7 (2-4D) group meets the main envelope and the 0 dBi plateau for all θ, and in fact almost meets a -10 dBi plateau. For f/D = 0.5, the entire envelope is met easily, but the on-axis gain requirement is about 1 dB too low.

For lower f/D's, the beam broadening causes the patterns to exceed the envelope in the θ range from 2-20°. The far-out sidelobes are, of course, extremely low.

This data set confirms all the previous work [1] and graphically demonstrates the well-known principle of under-illumination to attain a specified sidelobe level. The important fact to note here is that a very large diameter (4λ) horn with an outstanding primary radiation pattern was also necessary; just under-illuminating the reflector is not a sufficient condition for success.

2.6 Corrugated Feed Horn Design

The results described above indicate that the least f/D which meets the sidelobe criteria is in the vicinity of 0.5. For the two horn sizes used, neither quite meets all three constraints exactly. That is, the 3λ horn meets the gain and near-in sidelobe constraints, but does not meet the plateau region constraints of 0 dBi in one principal plane (0, 180°). The 4λ horn meets the sidelobe constraints but just misses the gain requirements. Examination of a plot of the two feed horn patterns in the region near the edge of the reflector ($\theta \geq 28°$ for f/D = 0.5) indicates the

reasons. For the 3λ horn, edge illumination taper and the far-out sidelobes are too high; for the 4λ horn, the edge taper is too low, so the gain suffers. Since the spillover is -30 dBi or better, the far-out sidelobes in the 4λ case meet the 0 dBi plateau.

These results indicate that a compromise of a 3.5λ horn might meet all three constraints simultaneously in a reflector system with an f/D = 0.5. The process of designing an optimum corrugated feed horn for this symmetric feed pattern case now could be undertaken. The full scale optimization is beyond the scope of this current effort, but we will describe the alternatives and the process for the sake of completeness.

The two basic variables we have at our disposal are the length of the horn and the flare angle. In the case of the two horns used for the baseline analysis, the flare angle is constant at 30° and the length is varied so the aperture size ranges from 3λ to 4λ. By application of the exact formulas [5] or the approximate formulas [6] for far-field radiation patterns of corrugated horns, one may vary the flare angle and the aperture size (or horn length) and determine the best combination which meets the nominal 25 dB edge illumination taper and still maintains the desired wide angle sidelobe levels. As mentioned, a 3.5λ aperture with a 30° flare angle is probably adequate.

Other parameters of interest include the corrugation slot depth and width, and the thickness of a slot wall. Experience has shown that the number of corrugations should be about 10 per wavelength and that the slot width should be much larger than the slot wall thickness. In addition, the slot depth should be about λ/4 at the lowest frequency of interest. This condition is necessary to achieve the anisotropic impedance boundary necessary to launch the TM_{11} wave and establish the hybrid mode HE_{11} of propagation which results in the axially symmetric far field amplitude and frequency independent taper. The basic parameters for such a horn are shown in Figure 2-6.

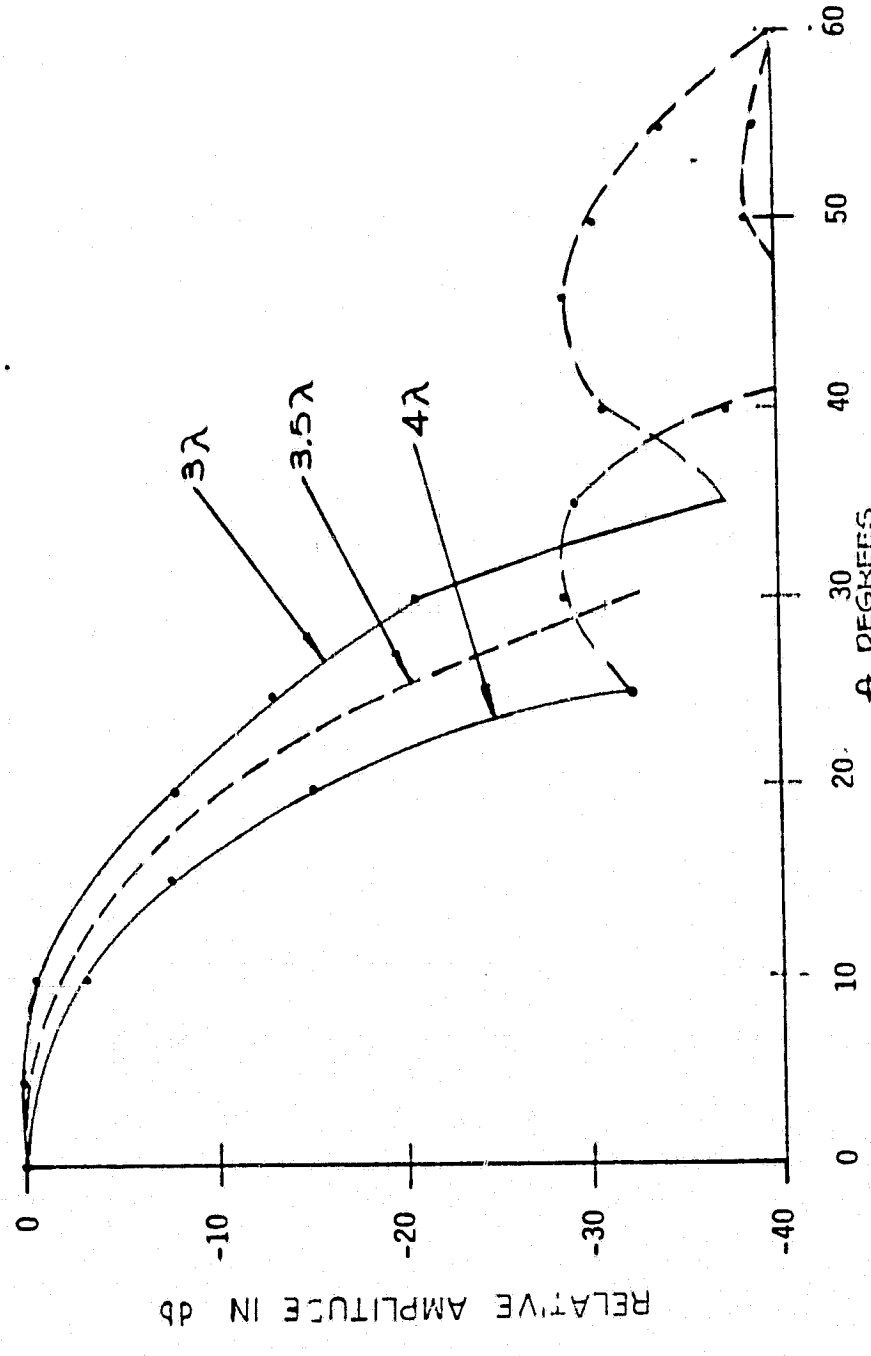

Figure 2-5 3λ and 4λ Feed Horn Far Field Pattern

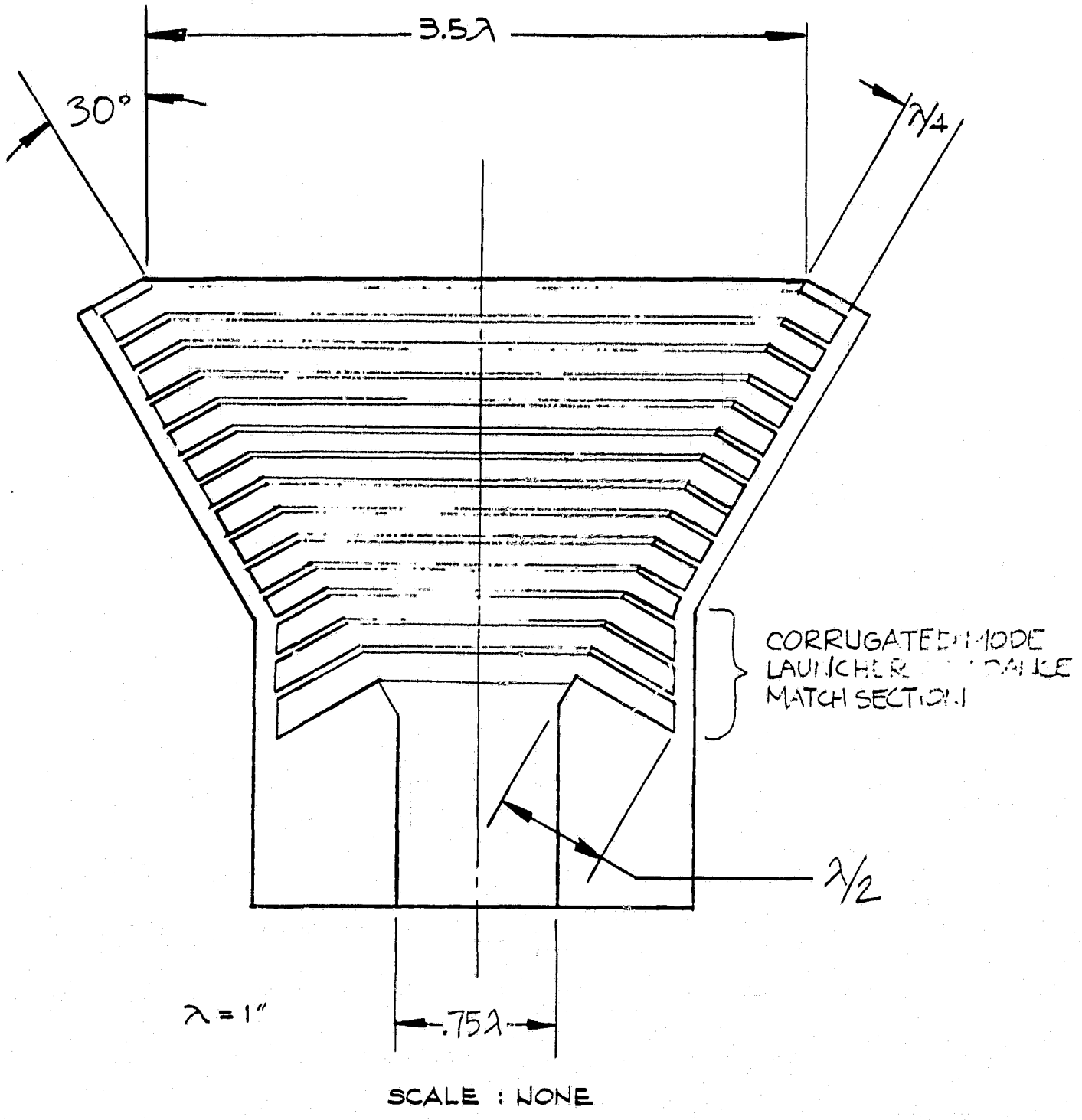

FIGURE 2-6 Cross section: Corrugated horn design for a low side lobe antenna.

2.7 Modified Corrugated Horn

The basic corrugated horn configuration is not die-castable because one cannot remove a core from the conical section. Other types of casting such as investment casting could be used to fabricate a corrugated horn. However, the large quantity mass production requirements of 10,000 units per year demand that the lowest cost fabrication process be used, and that is die-casting. By making the corrugated slots or fins parallel to the boresight axis as shown in Figure 2-7 instead of perpendicular to wall, a die-cast feed could be obtained. If the average slot depth (as measured from the midpoint of the slot along the wall) is made to be $\lambda/4$, then the same anisotropic impedance boundary will occur, and the hybrid mode will be launched. The need for 1°-2° draft angles in the slots to permit the mold to be pulled out of the piece may have some effect on the bandwidth. The entire design requires careful analysis and experimental verification is necessary for complete validation of the concepts.

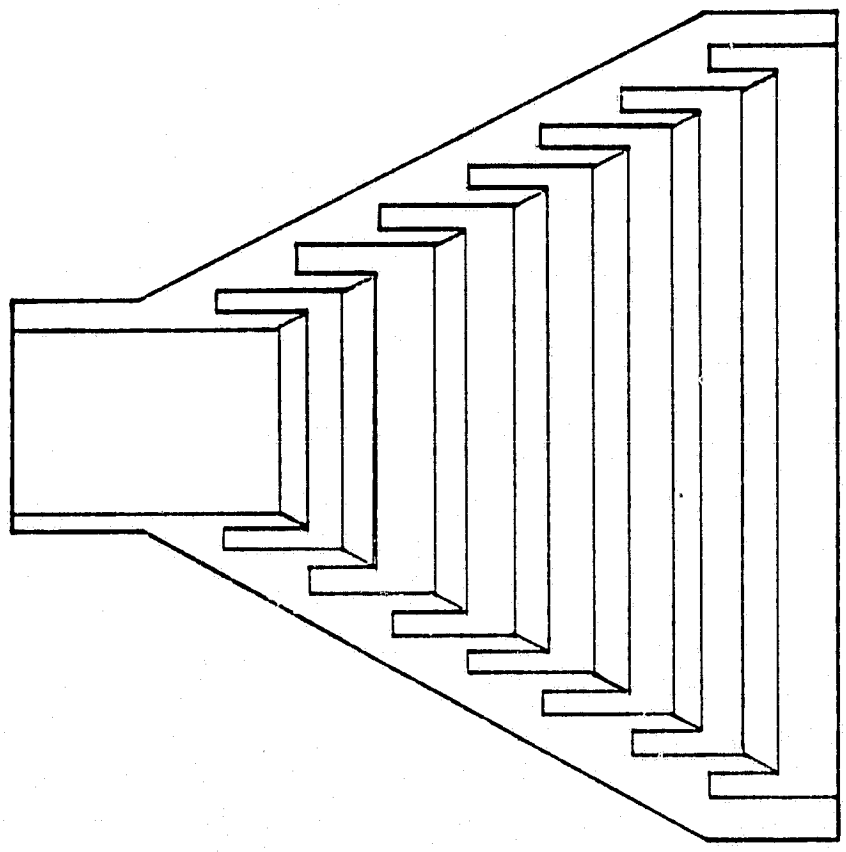

Figure 2-7 Die-castable Corrugated Horn

3.0 THE SEVEN-HORN CLUSTER ARRAY

3.1 Rationale

It is evident from inspection of Figure 2-2 that the optimum f/D is in the range of 0.4 - 0.6 for feed horns with aperture from 3λ to 4λ. We already know from the geometry of the offset fed configuration that some asymmetry in the illumination function is required to perfectly match for an ideal far-field pattern. One approach to determining this asymmetry is to synthesize the feed function with a multi-element clustered array of small aperture feed horns. In the previous section, the use of the HE_{11} hybrid mode provided only one real degree of freedom, i.e., one primary beam shape and a corresponding edge taper and spillover level. Through the use of a seven-horn array, we obtain more degrees of freedom and therefore expect to obtain a better illumination function and a better approximation to the desired far-field pattern.

3.2 Geometry and Method

Referring to Figure 3-1, an offset reflector is illuminated by a cluster array type of feed. Each feed element illuminates the reflector and generates a component beam in the far-field of the reflector. These component beams are displaced by some small angle $[\theta_n, \phi_n]$ about the principal axis of the antenna boresight. If each component beam is assigned with a proper excitation both in amplitude and phase, the resultant beam, i.e., the sum of these component beams, can approximate the desired Chebyshev pattern. To obtain an optimum set of feeding coefficients, it may be necessary to iterate the summing process a few times. It can be done by least-mean-square method, minimax method, or just by cut-and-try.

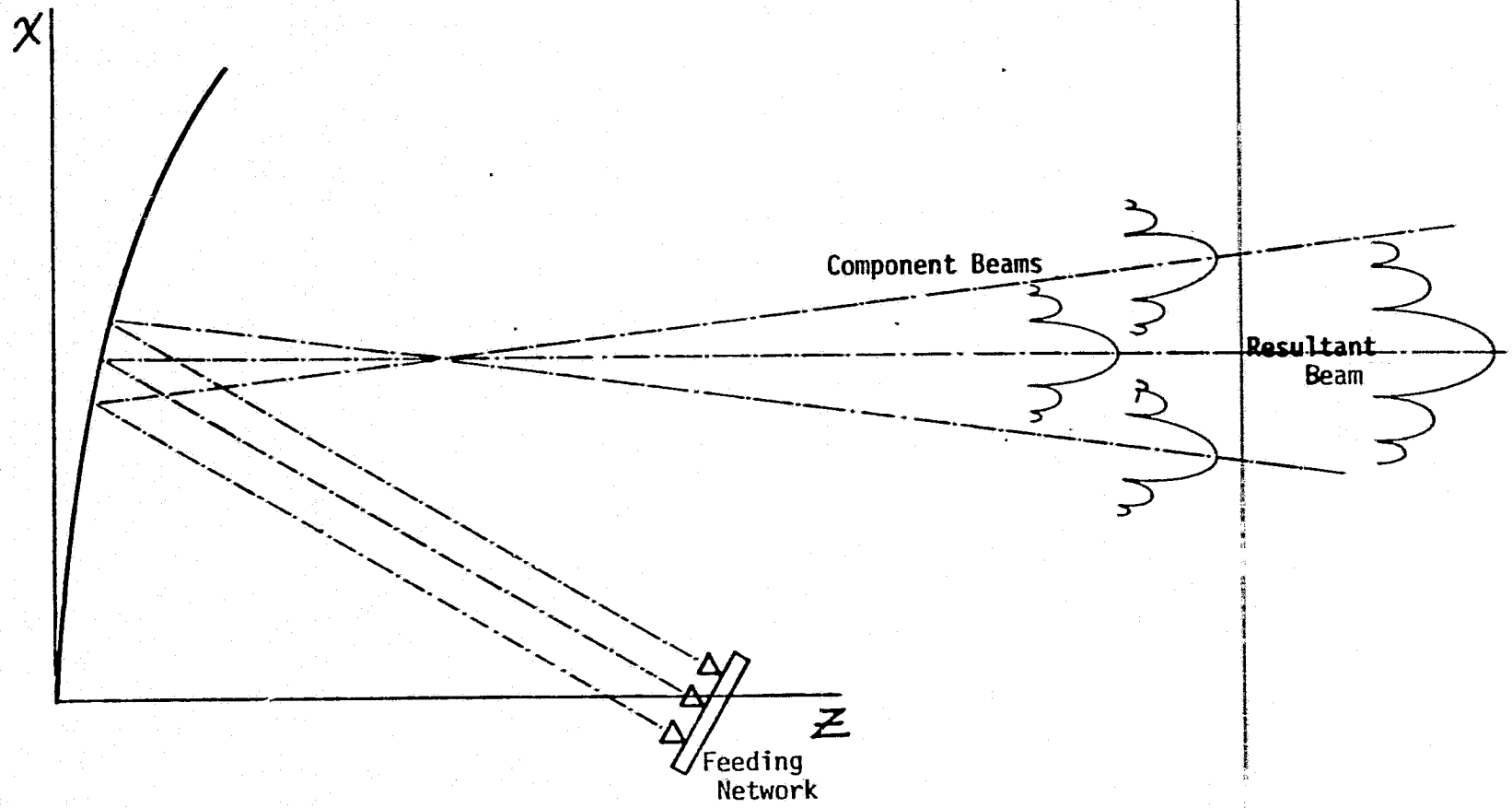

Figure 3-1. Geometry of the cluster array of small feeds staggered about the focal point.

To obtain a low sidelobe far-field pattern, an array feed of 7 horns in a cluster is the simplest form that also gives good flexibility as shown in Figure 3-2. The center horn will radiate the largest percentage of power while the surrounding six horns will radiate a low power to shape the main beam and sidelobe pattern of the center horn. If the parent reflector has a moderate f/D > 0.4 and the feed horns are not very large (1.02 x 1.0λ), the seven component beams will have very similar shapes. Besides, each feed horn will produce a taper of 3∿4 dB at the reflector edge, thus deviating very slightly from a uniform illumination. For these reasons, we may assume all the component beams have a far-field pattern function of $J_1(\theta_n')/\theta_n'$, where θ_n' is the angle measured from the beam center for each deflected beam, as shown in Figure 3-3. In this figure, the need for and the definition of the coordinate transformation is described. Thus, the resultant beam can be expressed as:

$$R(\theta,\phi) = \sum_{n=1}^{7} A_n \frac{J_1(\theta_n,\phi)}{\theta_n}$$

where A_n's are the complex weighting factors (feeding coefficients) for each beam. The only mathematically tedious part of this process is in determining the beam shifting factors and in automating the corresponding translations to relate the off-focus beam shift angle to the on-focus reference system. This translation must be made for each of the six off-focus horns. It involves the calculation of a series of intermediate transformations described by Rahmat-Samii [9]. The beam deflection that occurs as the feed element moves has been derived for an offset fed antenna. We used a beam deflection factor (BDF) = 5°/λ.

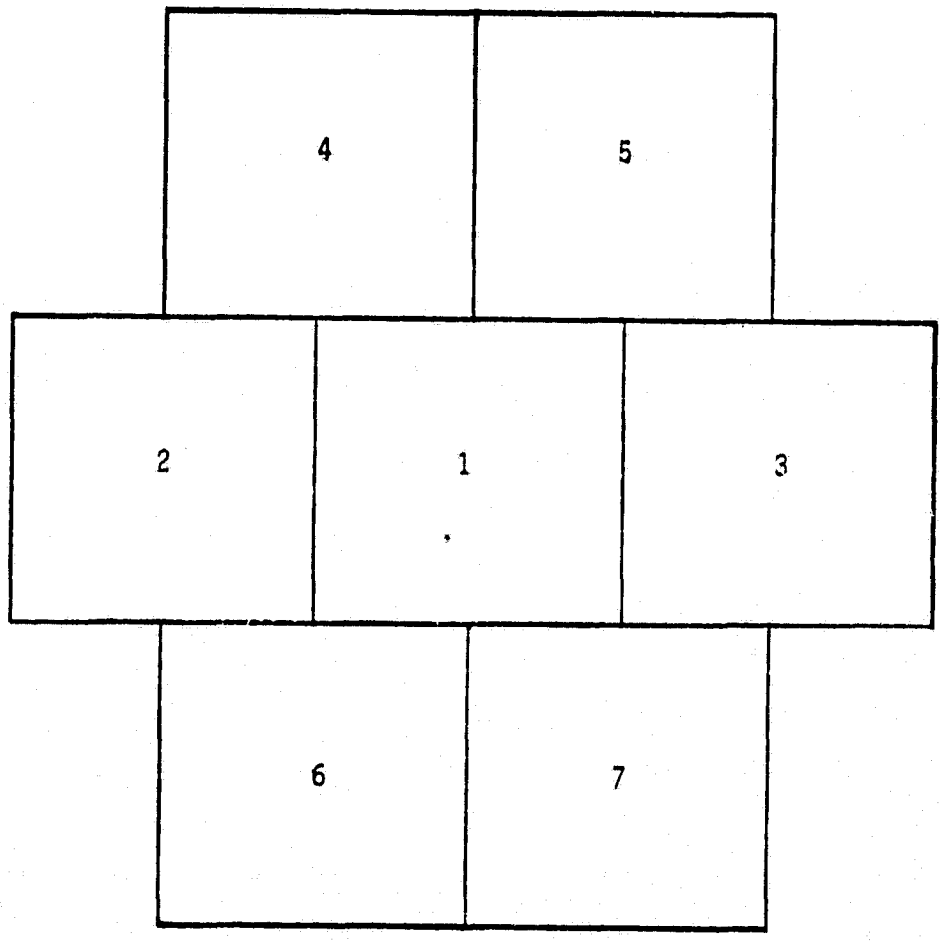

Figure 3-2. 7-Element Array of 1λ Square Horns

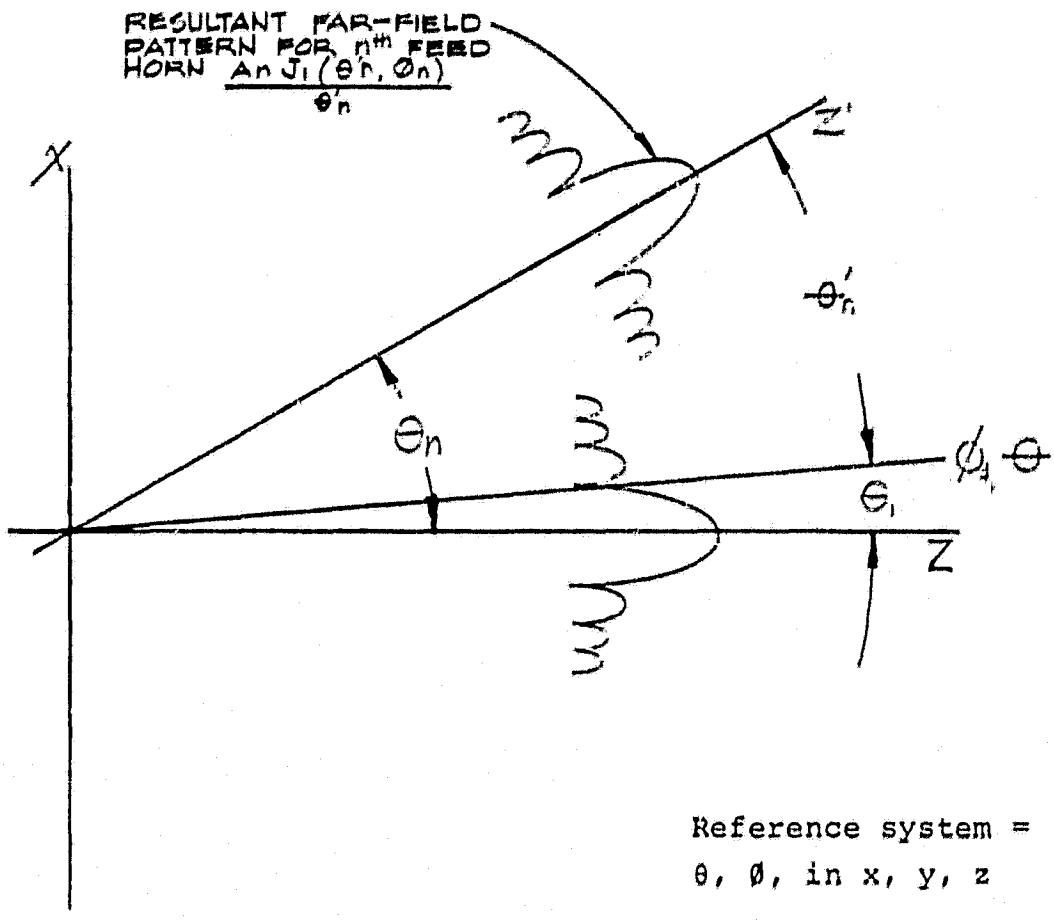

Reference system = θ, ϕ, in x, y, z

Beam shifted system = θ', ϕ' in x', y', z'

In the θ_1, ϕ_1 direction, the Resultant Field RF (θ_1, ϕ_1) =

$$A_1 \frac{J_1(\theta_1, \phi_1)}{\theta_1} + \sum_{n=2}^{7} A_n \frac{J_1(\theta'_n, \phi'_n)}{\theta'_n}$$

where $\theta'_n, \phi'_n = T[\theta_1, \theta_n, \phi_1, \phi_n]$, the coordinate transformation which takes account of θ_n, ϕ_n the beam deflection factors that cause the coordinate system shift. In the figure, θ'_n is the n<u>th</u> feed element contribution in the θ_1, ϕ_1 direction.

Figure 3-3. DESCRIPTION OF THE SUPERPOSITION PROCESS FOR FAR-FIELD SUMMATION SHOWING THE ADDITION OF TWO BEAMS IN THE θ_1, ϕ_1 DIRECTION.

3.3 The Resultant Pattern and Excitation Coefficients

An optimum design of feed array and their excitation coefficients are shown in Figure 3-4. The reason why we use a 1λ size square horn is to achieve a VSWR < 1.20. If higher VSWR is allowed, the feed horn can be made smaller. The radiation pattern is shown in Figure 3-5. For comparison, an ideal Chebyshev pattern of order 2 (Ripple = 0.01 dB, half power angle = 0.7°) is superimposed on this pattern. As can be seen, this design can approximate the desired Chebyshev pattern to -30 dB sidelobe level and beyond.

The feed coefficients can be realized by a feed network power splitter which provides the required unequal power levels to the feed horns. There are two kinds of feeding networks namely, waveguide type and stripline type. Waveguide type will have low loss while stripline type will have lower cost. For compromising in loss and cost, air stripline may be considered. A schematic design is shown in Figure 3-6. The loss of this network is estimated at 0.35 dB.

3.4 Air Stripline Feeding Network

A dielectric supported air stripline is shown in cross section in Figure 3-6 and consists of two parallel center conductors attached to a thin dielectric support substrate. Ground planes, which are of aluminum construction parallel to the center conductors, complete the balanced transmission line for the TEM-mode propagation. By making the dielectric substrate thickness small with respect to the stripline height, most of the fields will be concentrated in the air-filled region, thereby minimizing the dissipation loss due to the dielectric material.

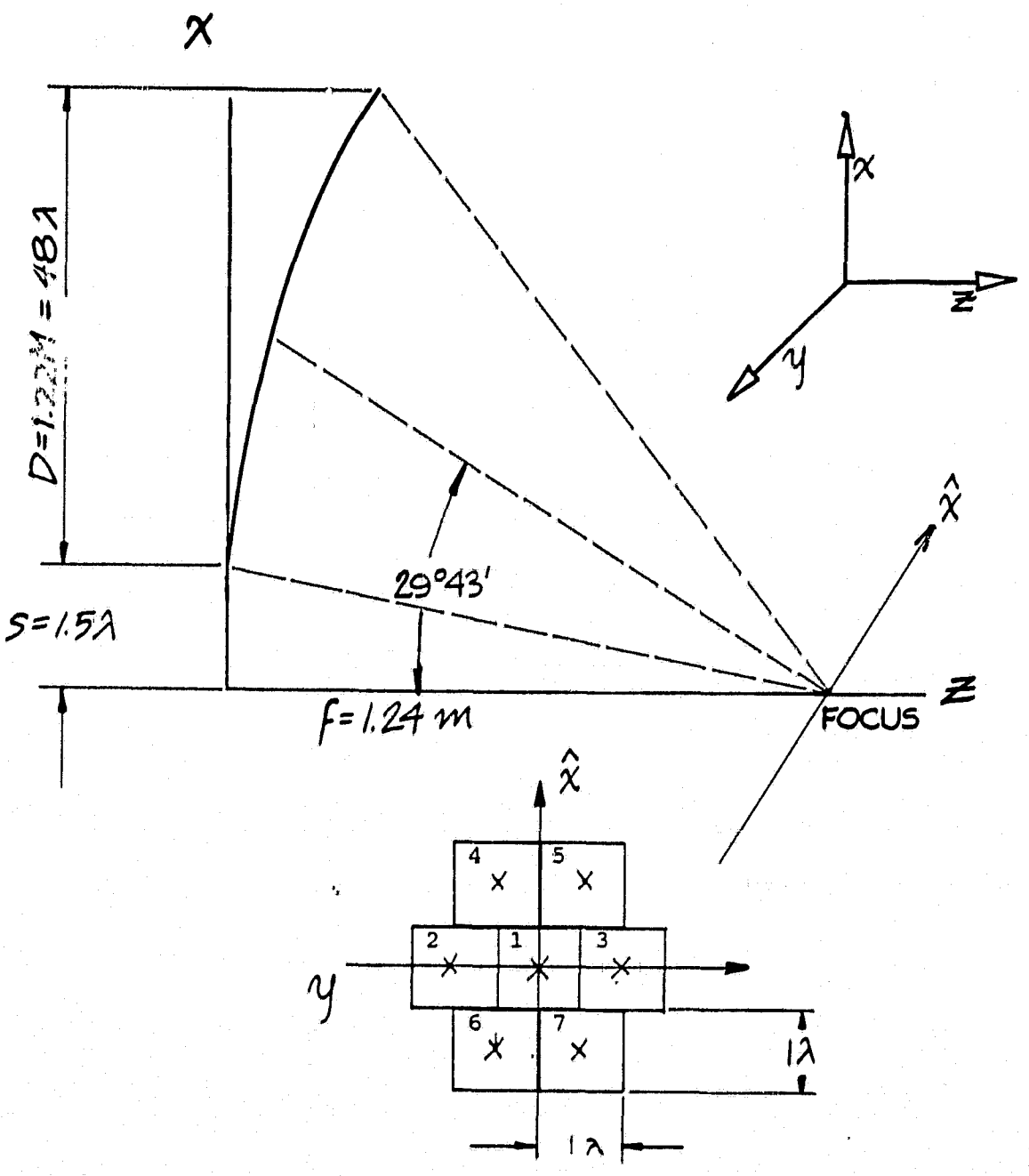

Element Number	Fed Coordinates x	y	z	Excitation Coefficient MAG	Phase
1	0	0	0	0.937	25.14°
2	0	1	0	0.141	28.70°
3	0	-1	0	0.165	28.64°
4	1	½	0	0.141	39.60°
5	1	-½	0	0.135	39.50°
6	-1	½	0	0.130	64.30°
7	-1	-½	0	0.141	79.30°

Figure 3-4. 7-Element Feed and Excitation for an Offset Reflection Design Which meets an n=2 Chebyshev Envelope

C-2

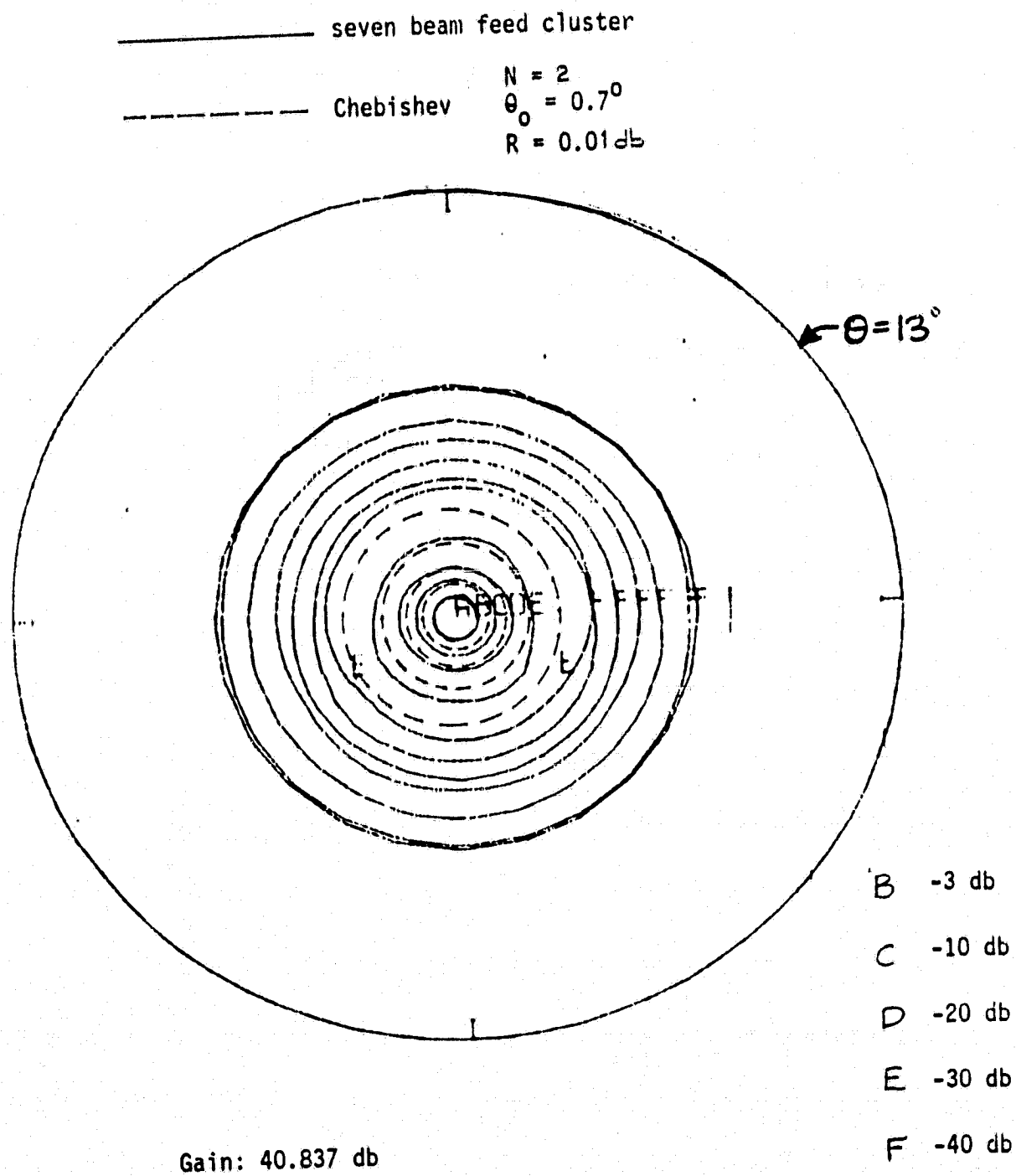

Figure 3-5. Radiation pattern of best approximated Chebychev pattern.

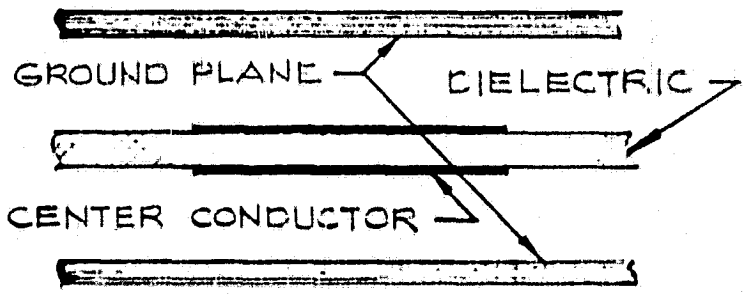

Figure 3-6. Air Stripline Cross Section View.

Gish & Graham [8] had employed a variational method to calculate the characteristic impedance and phase velocity from which the design information using this category of stripline is derived. Note that only a small portion of the field lines will pass through the dielectric substrate due to fringing. Thus, the attenuation in air stripline is due primarily to the conductor losses. For 50 ohm copper plated ground plane line the loss is 0.1 dB/ft at 4 GHz and 0.3 dB/ft at 12 GHz.

The next step is to design a 7-way power division network to properly excite the seven-feed cluster feed array. There are various kinds of couplers and hybrids which can be used. For the application, circular ring hybrids and a side coupler hybrid were selected for simplicity. A model network (scale 3 times) is shown in Figure 3-7.

Figure 3-8 shows a series of far field patterns in various ϕ planes for the 7-element cluster array. The n=2 Chebishev model requires that sidelobes be less than 0 dBi at 6° off axis, and these patterns meet that requirement. This is more clearly illustrated in Fig. 3-9, an expanded scale version of Fig. 3-8. Figure 3-10 shows the calculated far field pattern for the individual feed elements.

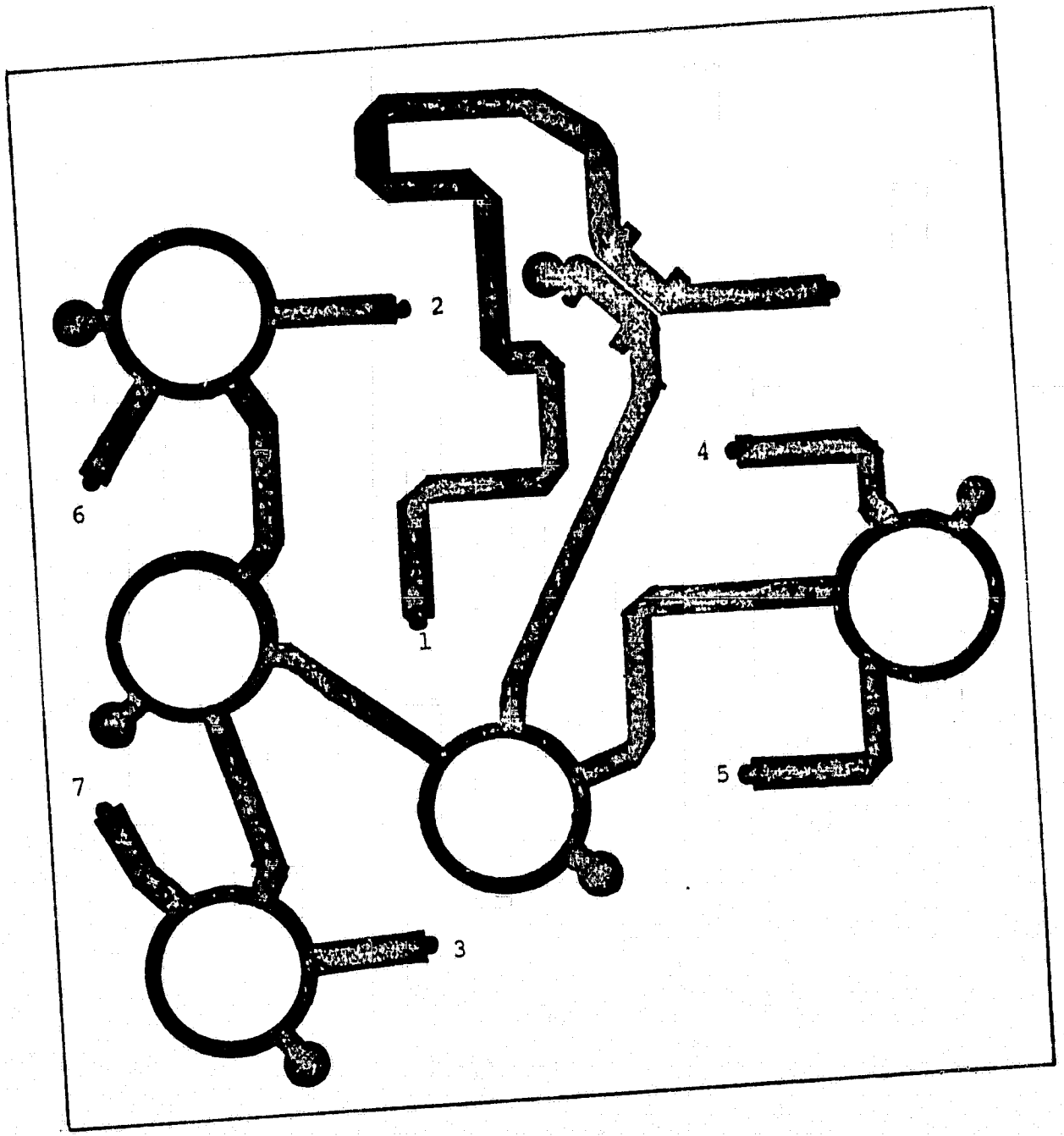

Figure 3-7. Typical feed splitter network for a 7-element cluster feed.

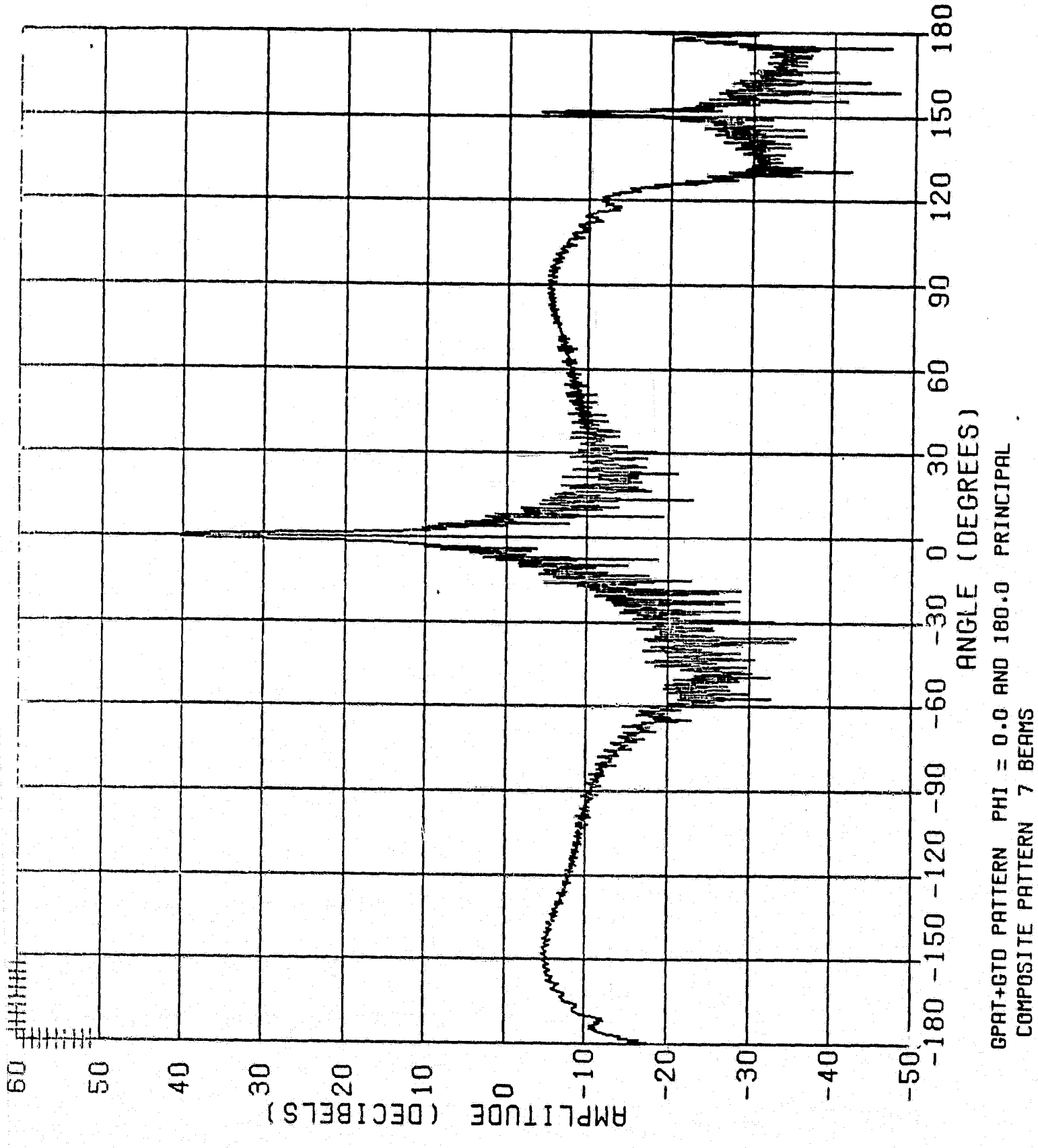

Figure 3-8A Far Field Pattern for 7-Element Array Feed

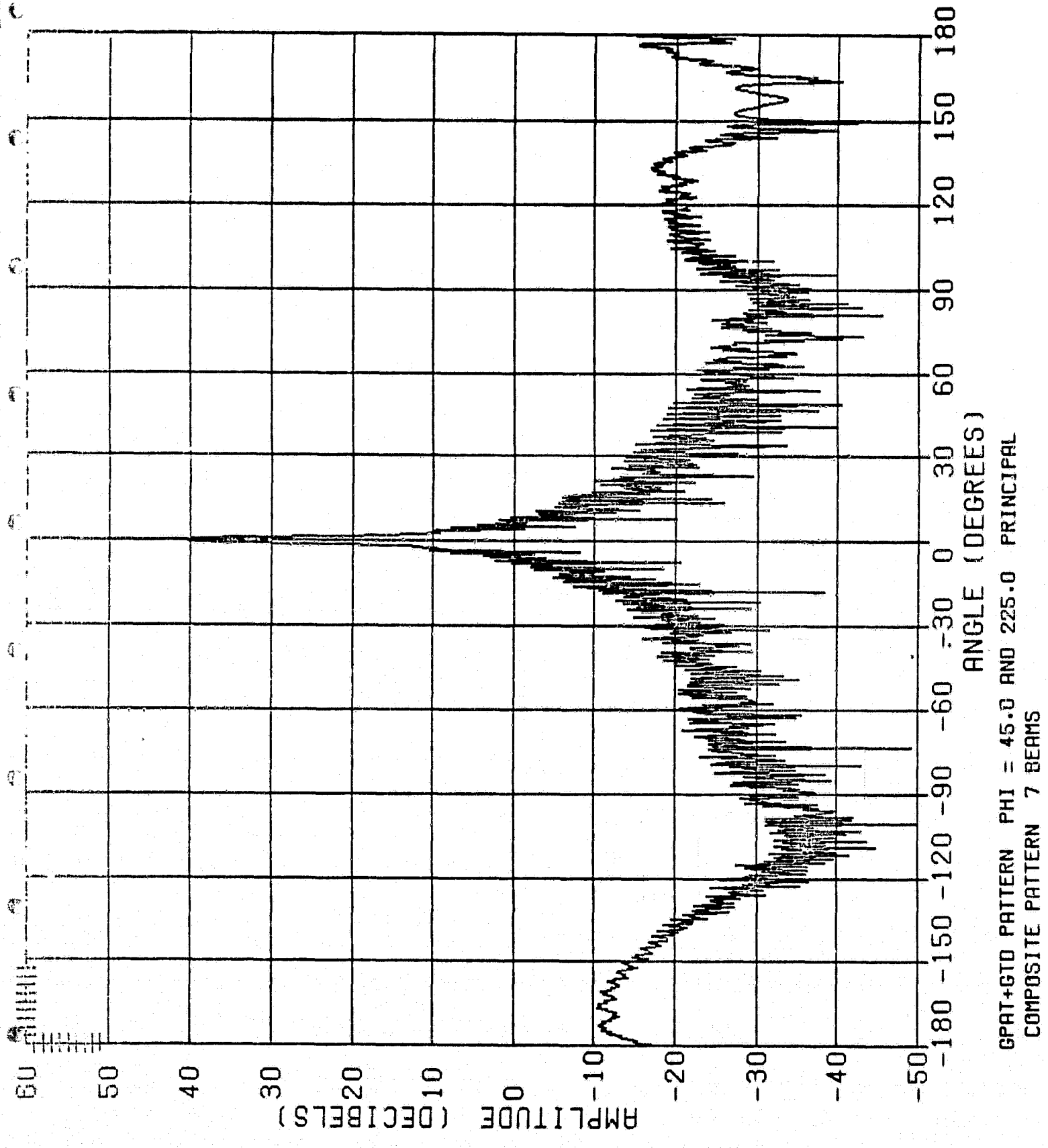

Figure 3-8B Far Field Pattern for 7-Element Array Feed

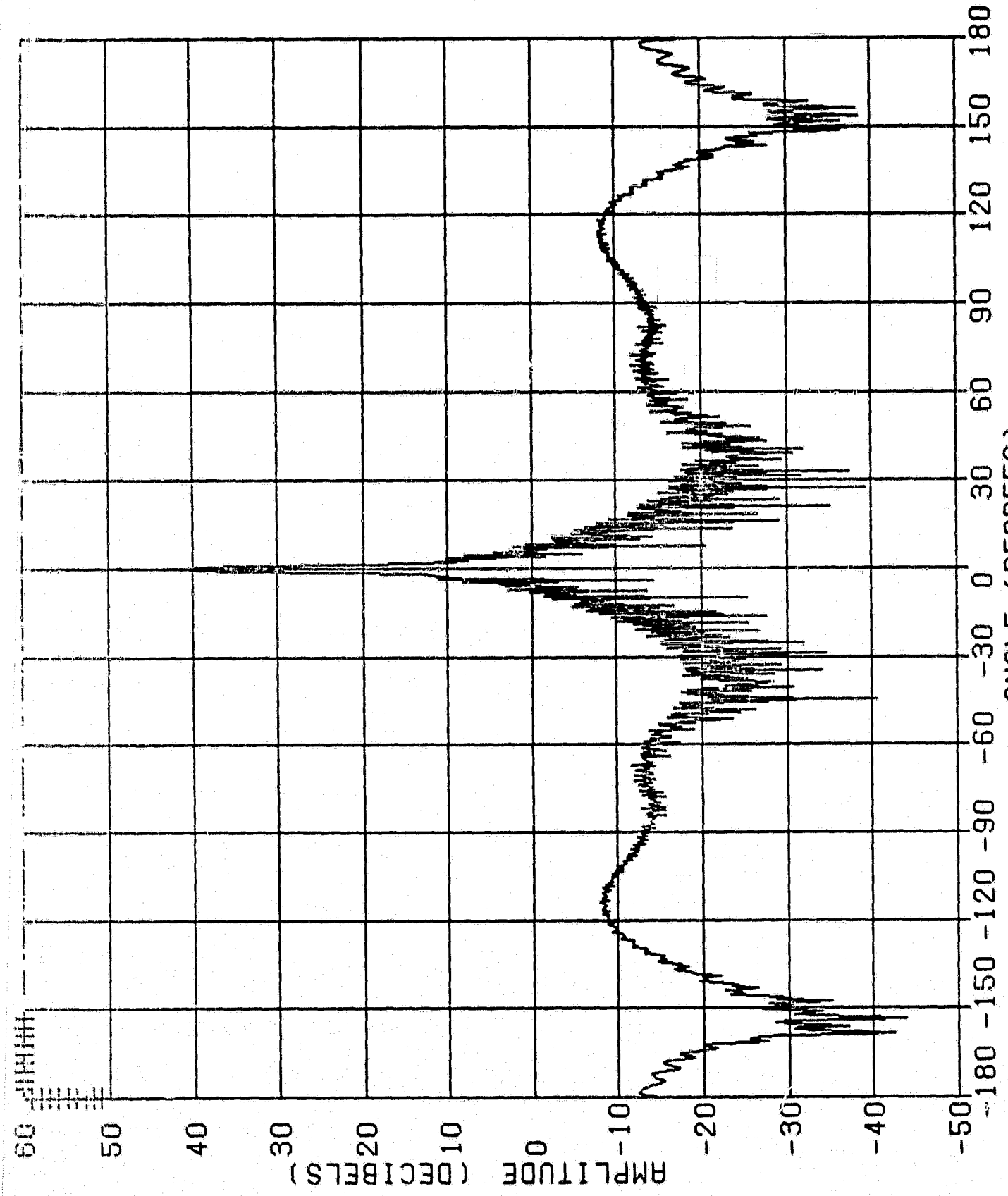

Figure 3-8C Far Field Pattern for 7-Element Array Feed

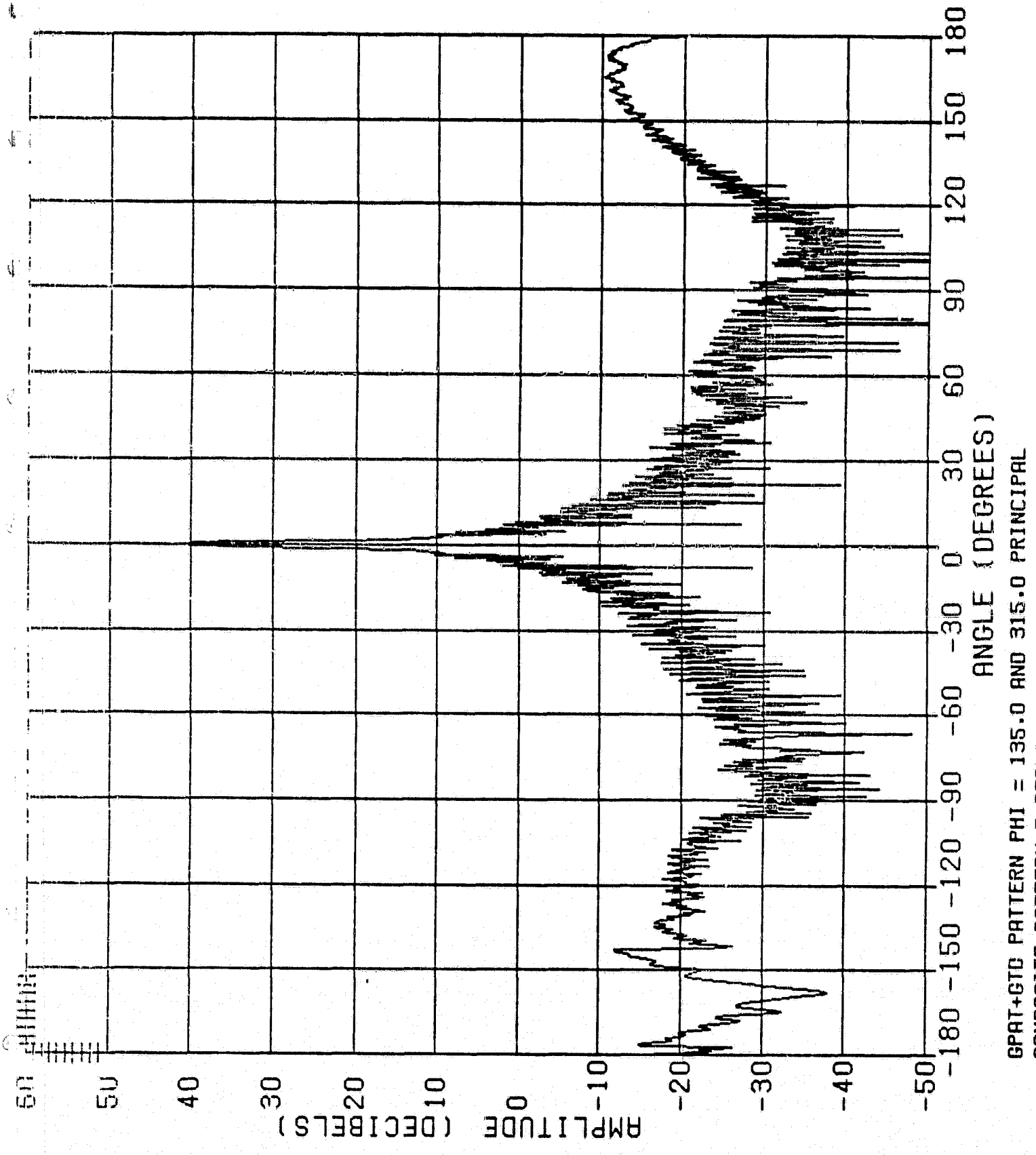

Figure 3-8D Far Field Pattern for 7-Element Array Feed

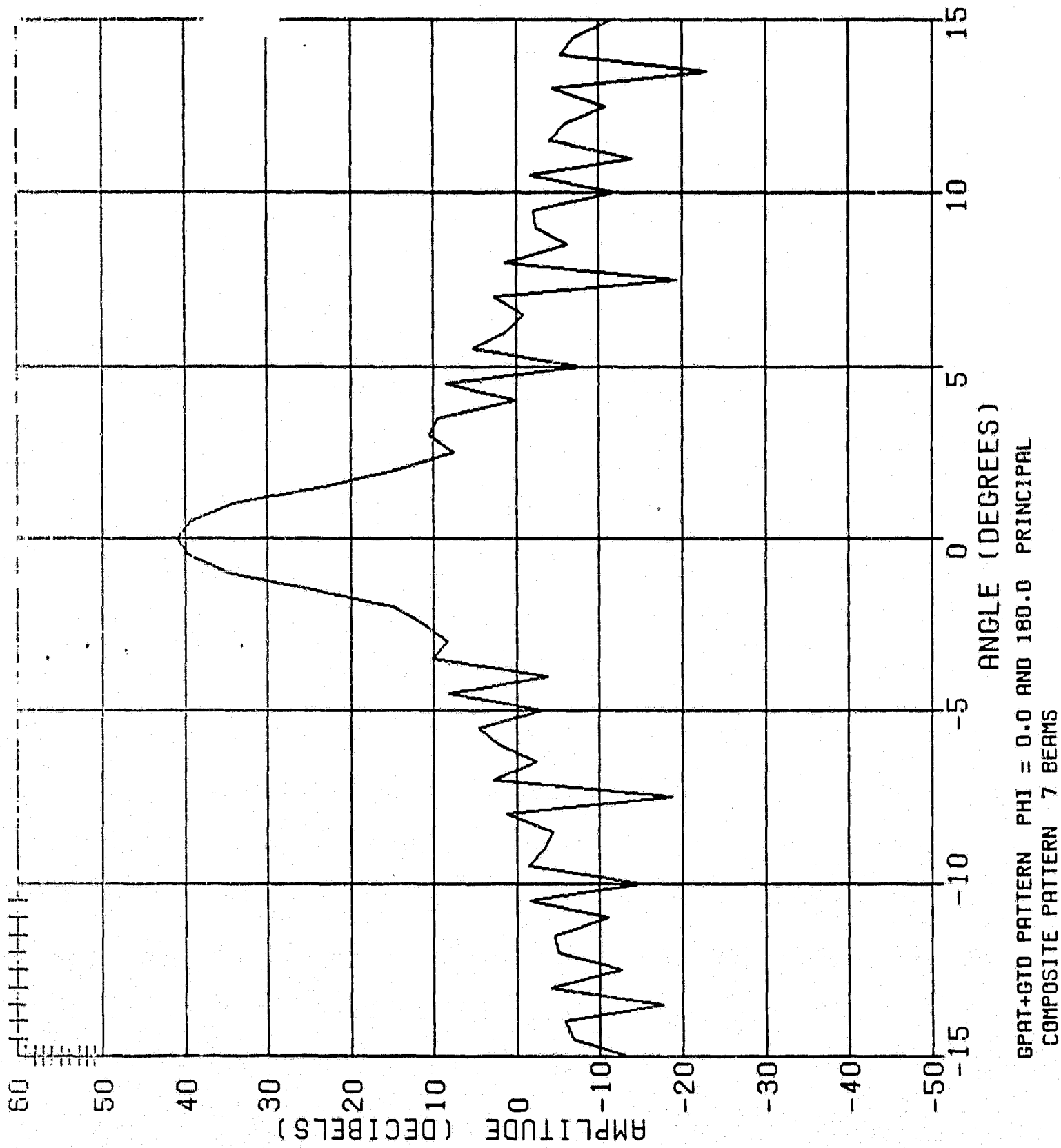

Figure 3-9A Expanded Far Field Pattern for 7-Element Array Feed

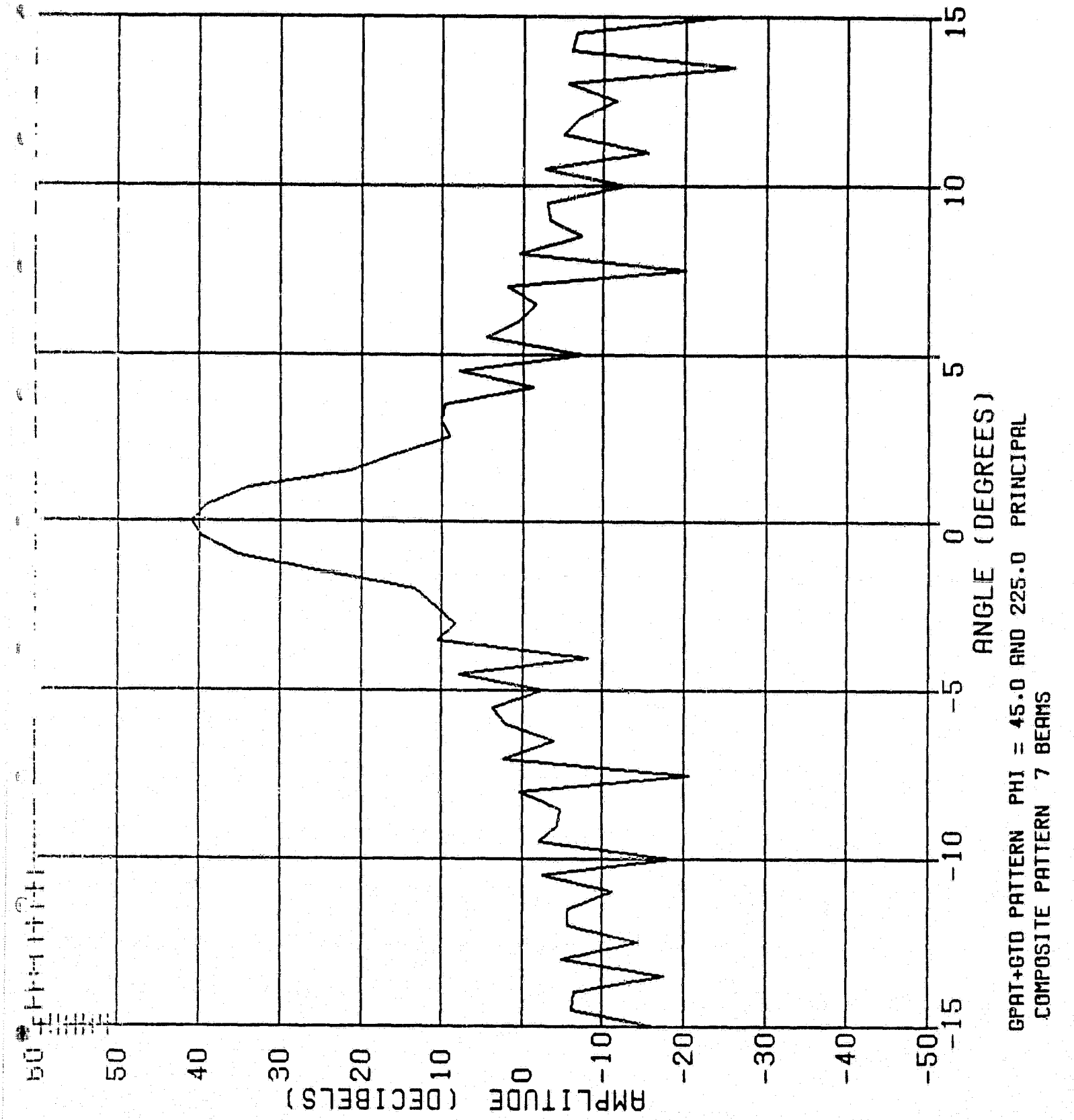

Figure 3-9B Expanded Far Field Pattern for 7-Element Array Feed

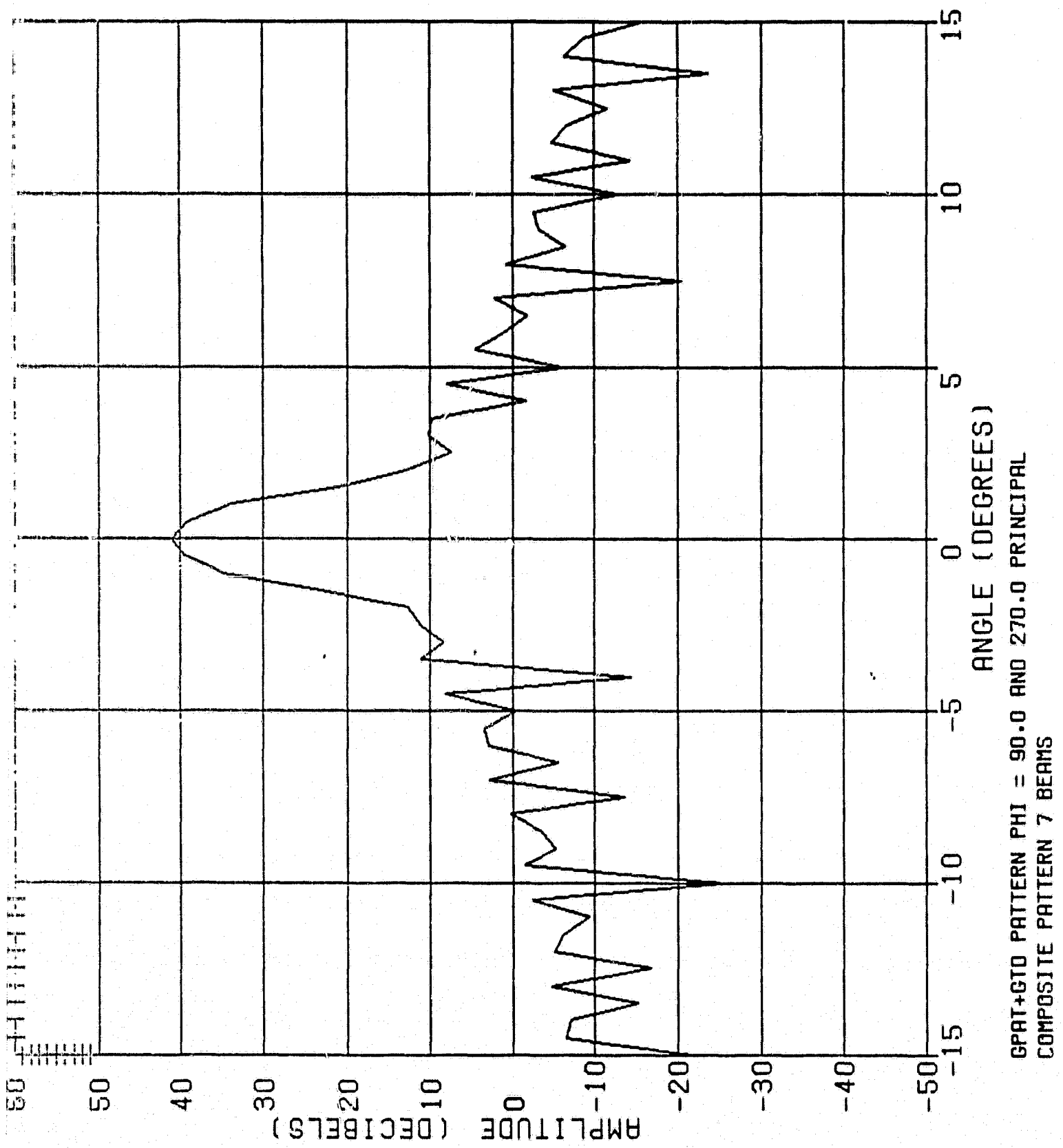

Figure 3-9C Expanded Far Field Pattern for 7-Element Array Feed

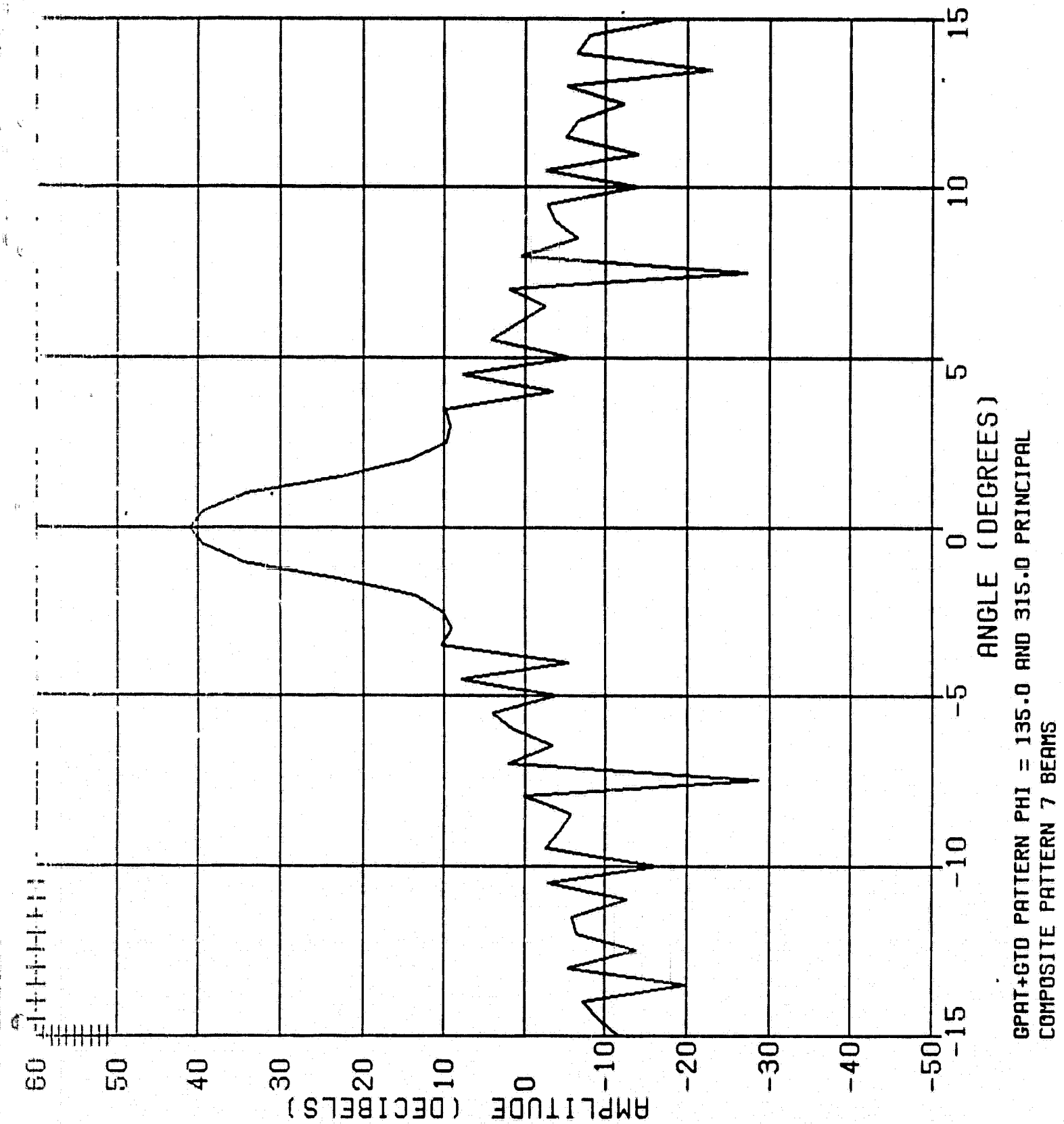

Figure 3-9D Expanded Far Field Pattern for 7-Element Array Feed

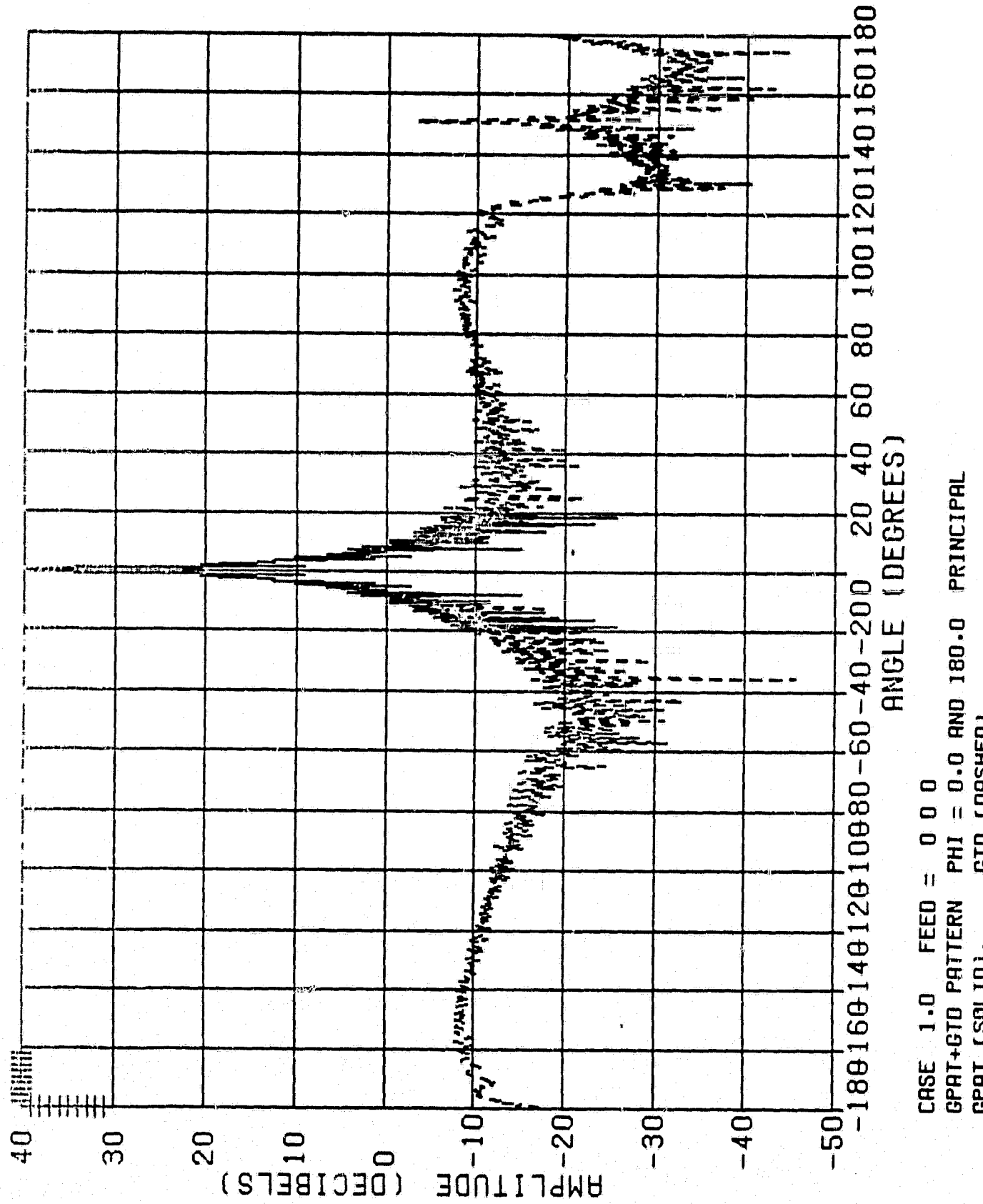

Figure 3-10A Far Field Pattern for Individual Feed Elements. as shown.

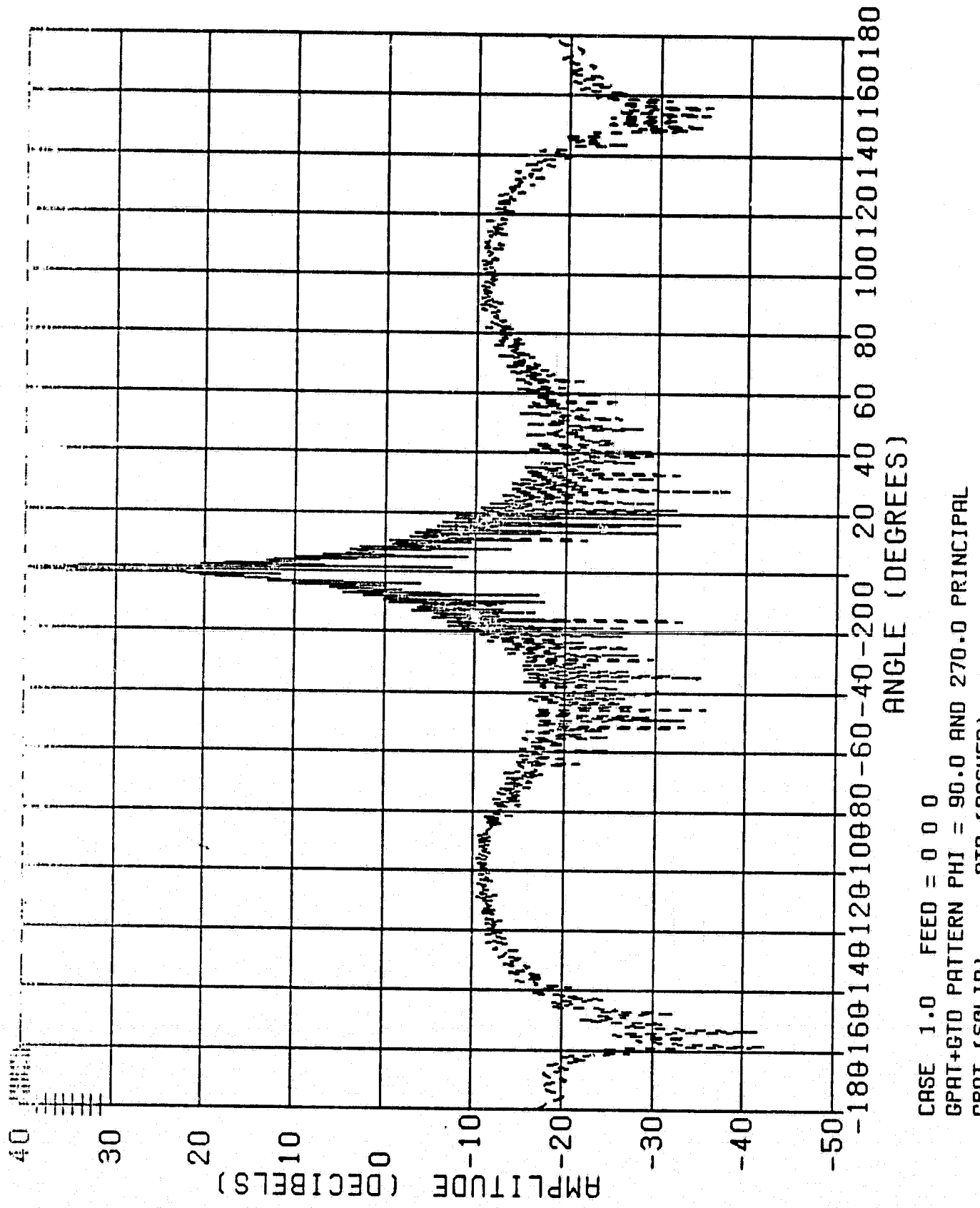

Figure 3-10B Far Field Pattern for Individual Feed Elements, as shown.

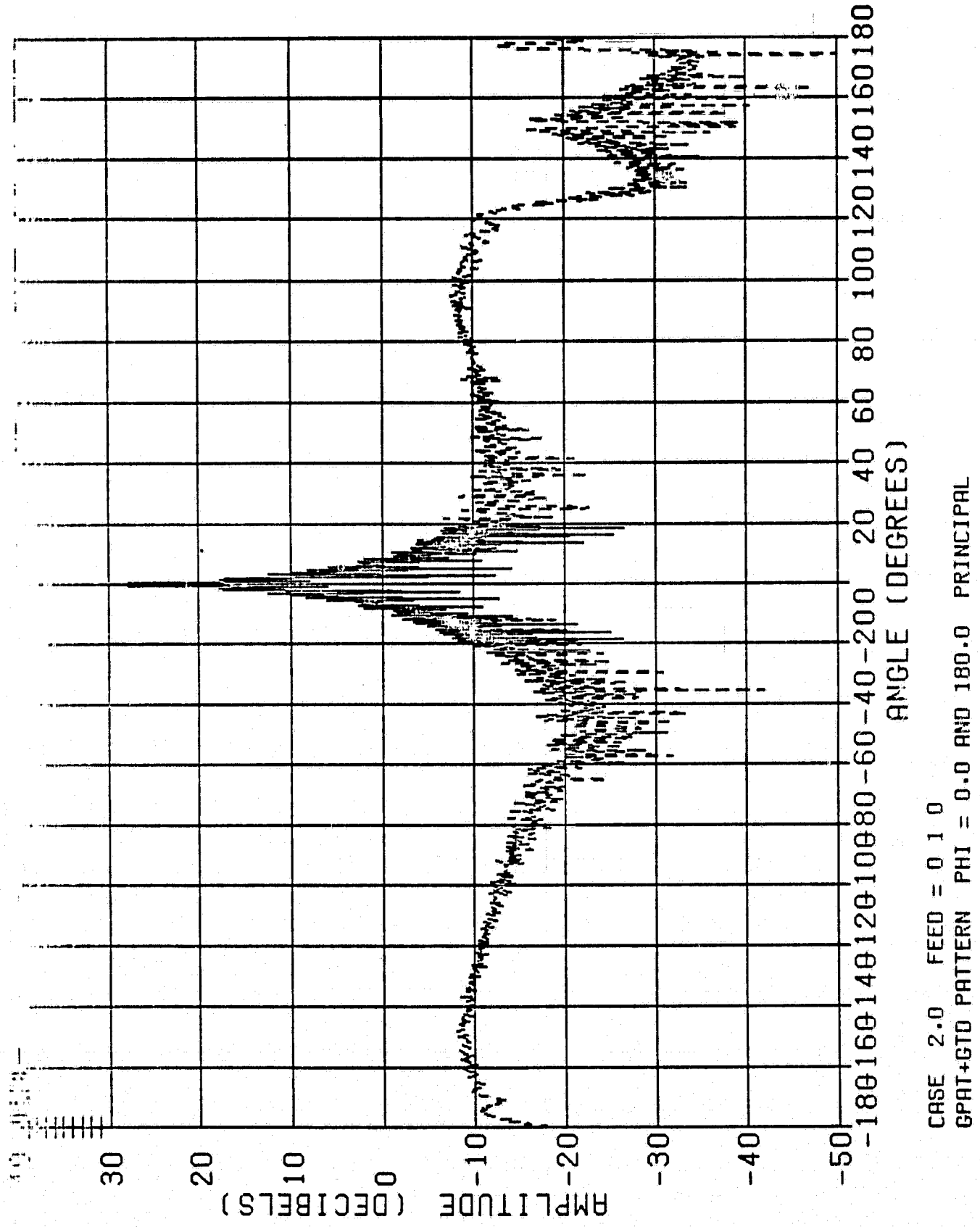

Fig. 3-10C Far Field Pattern for Individual Feed Elements, as shown.

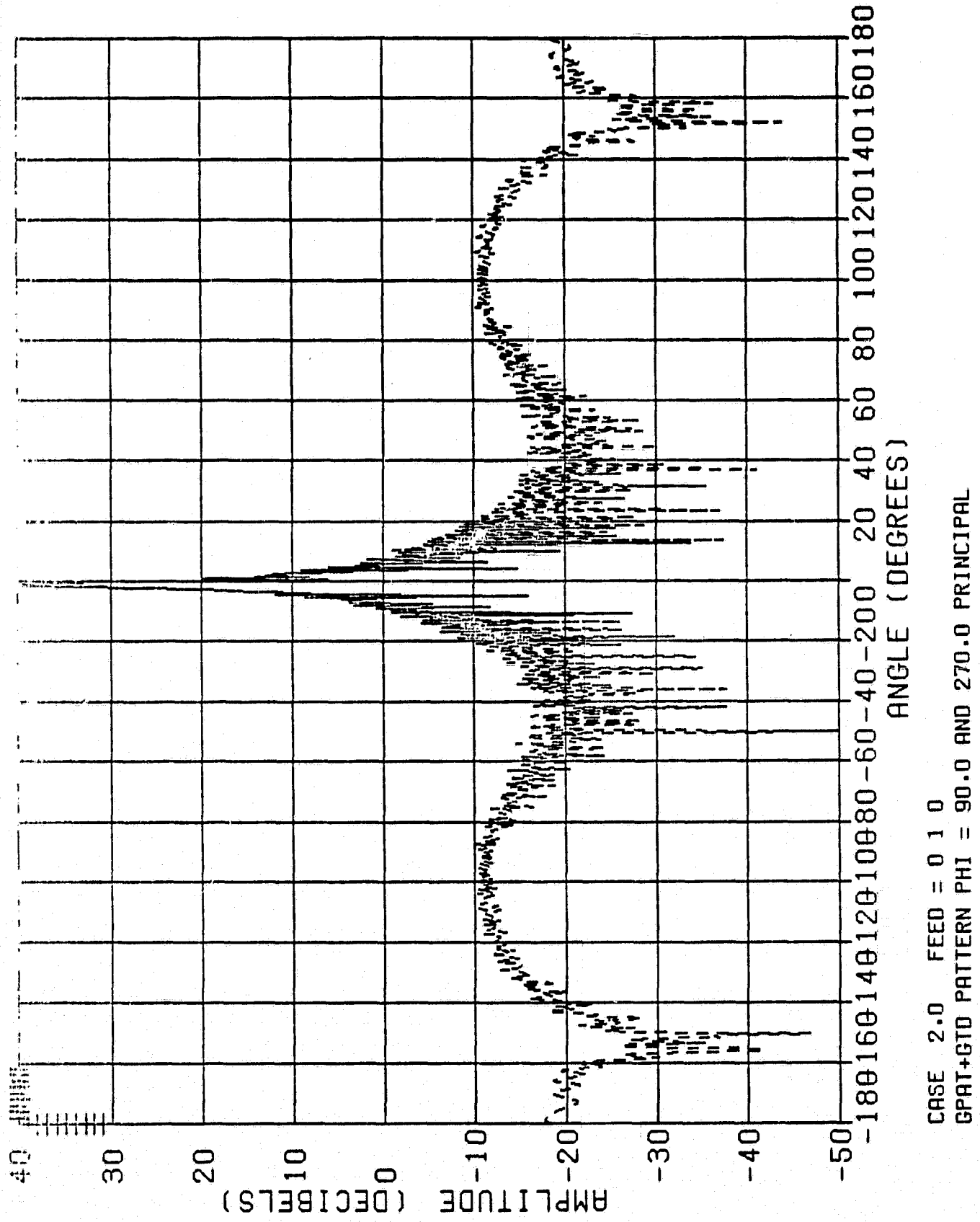

Figure 3-10D Far Field Pattern for Individual Feed Elements, as shown.

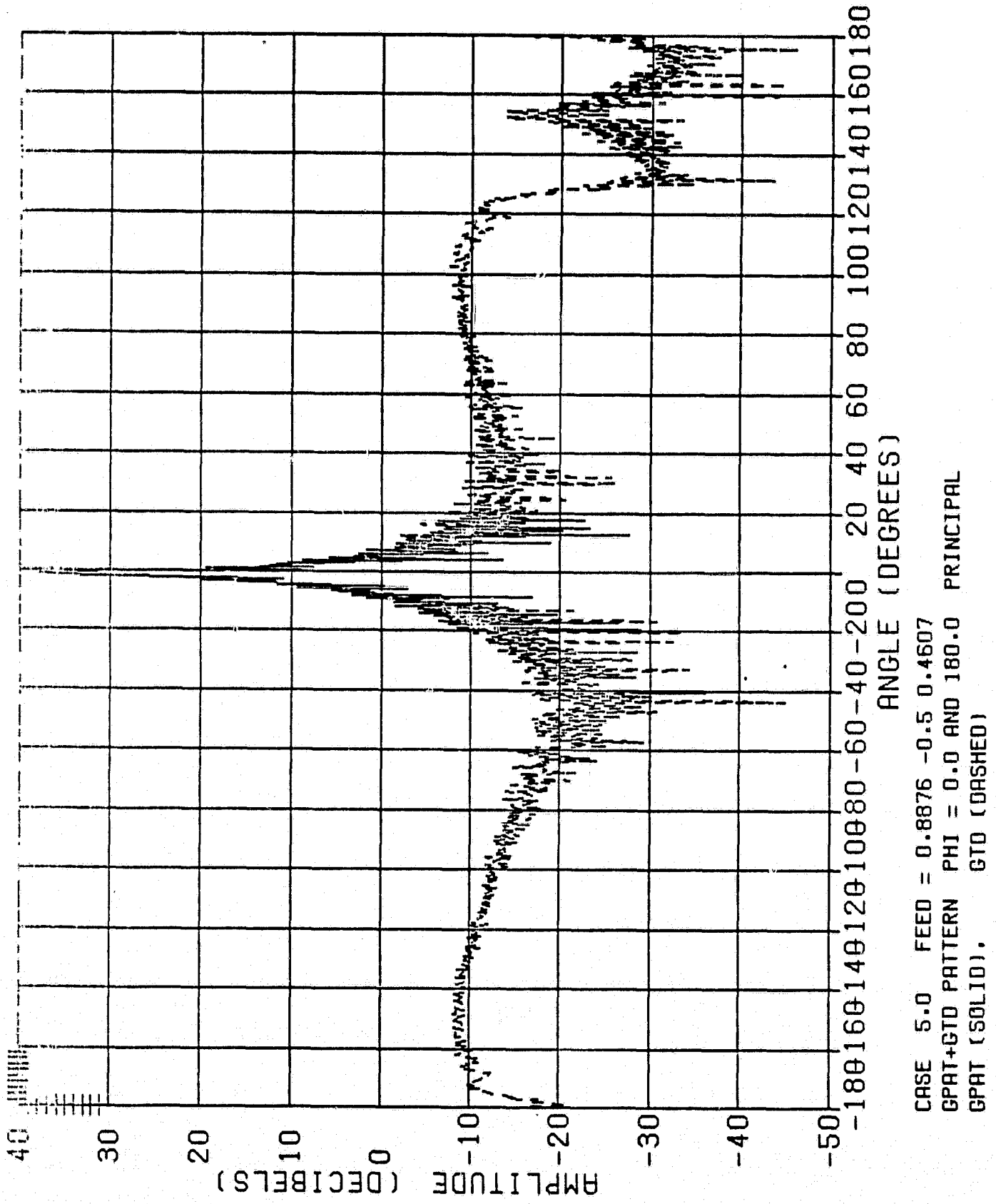

Figure 3-10E Far Field Pattern for Individual Feed Elements, as shown.

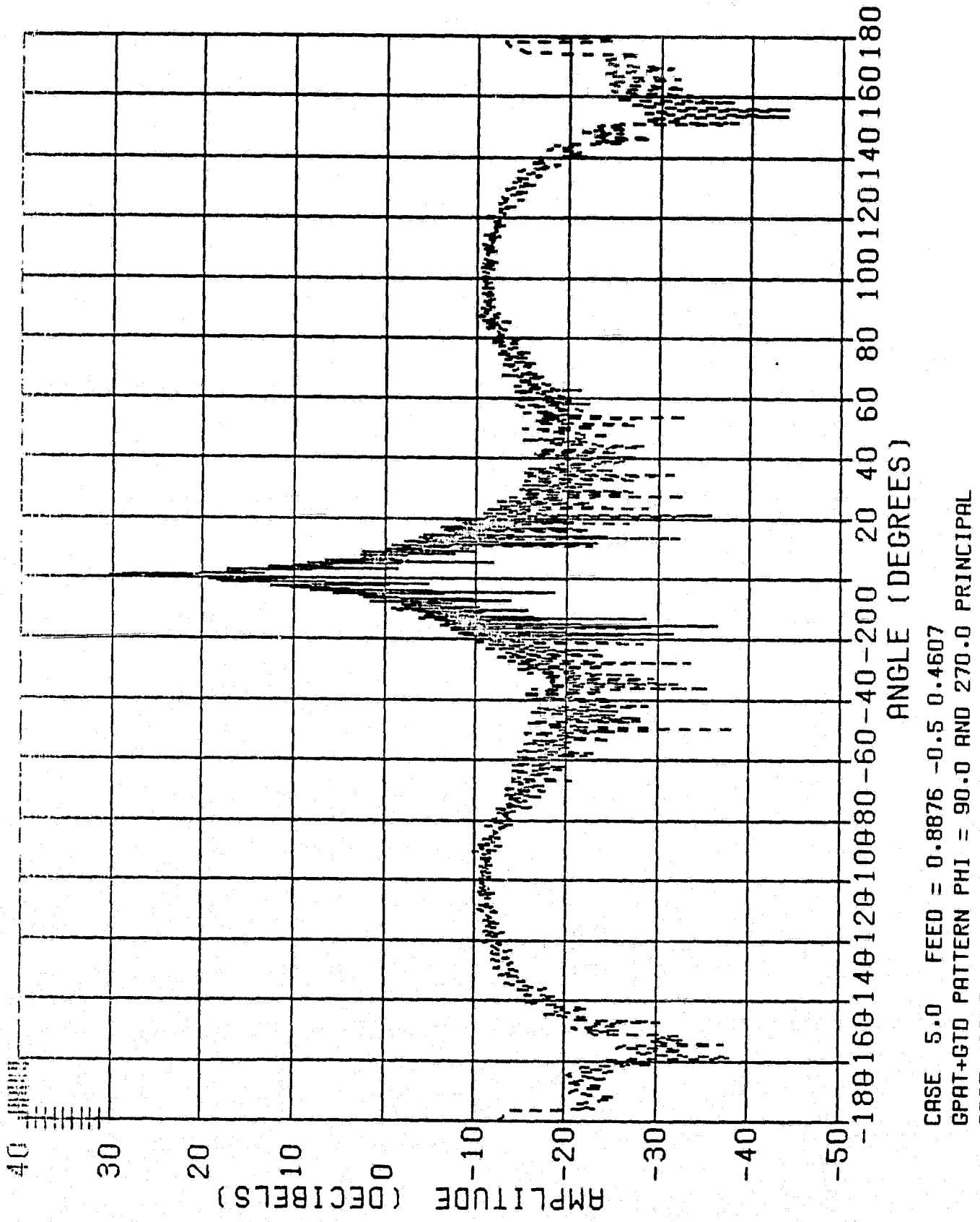

Figure 3-10F Far Field Pattern for Individual Feed Elements, as shown.

4.0 MULTIMODE HORN FEED SYNTHESIS

The concept of pattern synthesis by the introduction of additional modes in a single horn has been developed [9, 10, 11] but the problem of matching a given arbitrary pattern with a number of modes in a single horn is quite difficult. In this section we present a method for estimating the necessary focal field distribution based on an extension of the cluster array method. We then address the possibility of realizing this focal field distribution with a rectangular corrugated feed.

4.1 Focal Plane Field Synthesis

The objective of this section is to derive a focal field distribution corresponding to a desired Chebychev function. In a strict analytical approach, Bem [12], Valentino and Toulios [13] conducted some analytical work on deriving the focal plane field of an offset reflector antenna. In their analysis they assumed an incident field (plane wave) induces a current on the reflector surface. This current then produces an electric field in the focal plane region. Although this is a straight forward process, the double integral involves integrating the induced current on the surface to obtain the focal region field. The process is extremely lengthy so that the use of numerical techniques to carry out this integral is beyond reach even with modern high speed computers. Thus, the following assumptions were generally made in order to obtain a closed form analytical solution.

(1) The incident plane wave is uniform in amplitude and phase.

(2) The distances from any point on the reflector surface to a point on the focal plane where the electric field intensity is calculated are equal.

In the first assumption, if the plane wave has a Chebyshev pattern instead of a uniform pattern, an analytical closed form will not be possible even with their (Valentino, Toulios and Bem) much simplified approach.

In the second assumption, it is only a good approximation for a long focal length ($F/D >> 1$) and/or a small size reflector ($D < 10\lambda$). Thus, our results will only be approximate, especially in those regions away from the focus and at a wide scan angle.

Because of the difficulty involved in a strict analytical technique, we have adopted a "synthesis" approach. In fact, the process involved in this technique has already been discussed in the previous section where a seven square waveguide feed cluster was proposed as an alternate approach to obtain low sidelobes. For that design we chose the square guide size of 1λ (wave length). Since our objective here is to obtain a focal field distribution corresponding to a Chebyshev far-field pattern, a 19 element feed array is used. Each element is a square 0.6λ in size. The reason to use a larger array and smaller feed spacing is to acquire better sampling of a wider area around the focal plane.

4.2 Calculation of Focal Plane Field Using The 19-Element Feed Cluster Concept

Here we show the feeding coefficient of a 19-feed reflector antenna such that the resulting secondary pattern can best approximate a given Chebychev pattern. These patterns were derived in the same way as in the previous section. The feeding coefficients so obtained are for a truncated focal field distribution, or a piece-wise linear representation. The reflector and feed array geometry used in this process is shown in Figure 4-1. The 3 dB beam contour of all the 19 component beams are plotted in Figure 4-2. As shown, each component beam is 3° in shape and the beam-to-beam separation is about 1.5°.

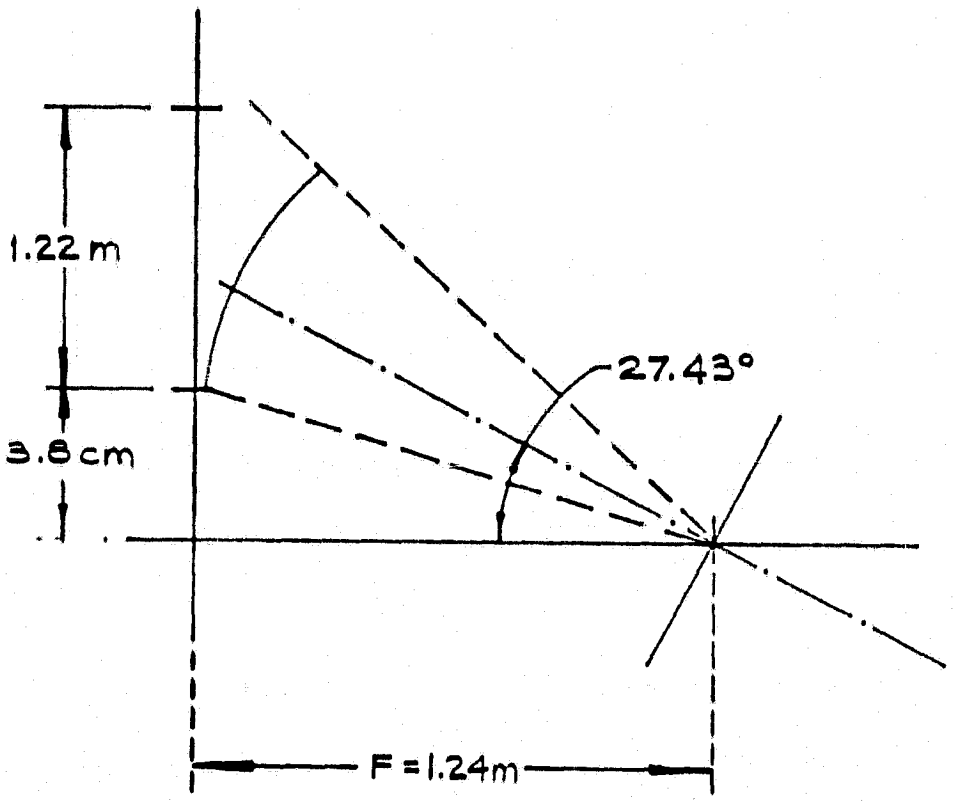

Figure 4-1. Reflector and Feed Array Geometry

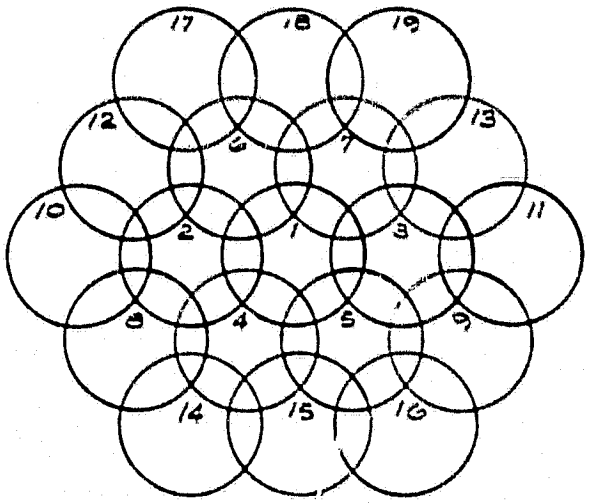

Figure 4-2. 3 dB Contour of 19 Component Beams

One major difference with a nineteen element approximation is that we can perform the coefficient matching so that in the region of the main beam we obtain a much narrower beam width to at least the -30 dB levels and conform to an n = 3 Chebyshev envelope.

The ideal Chebyshev pattern for the ripple size, R = 0.5 dB, the half power beam width, θ_0 = 1° and order n = 3, is illustrated in Figure 4-3. Figure 4-3 is the far field pattern which will be used to compare with the reflector pattern as generated by the 19-element feed.

The feeding coefficients are then changed such that the far field pattern will best approximate the ideal Chebyshev pattern as shown in Figure 4-3. The result is shown in Figure 4-4. The feeding coefficients of the feed array are shown in Table 4-1, and in Figure 4-5. The elliptical equal electric field strength contour which represents the truncated and best approximated focal field distribution can be constructed from the feeding coefficients.

We do not propose that a nineteen element array actually be used, because the cost would be prohibitive in this application. What is needed is a simple feed which approximates the elliptical contour of the focal field distribution.

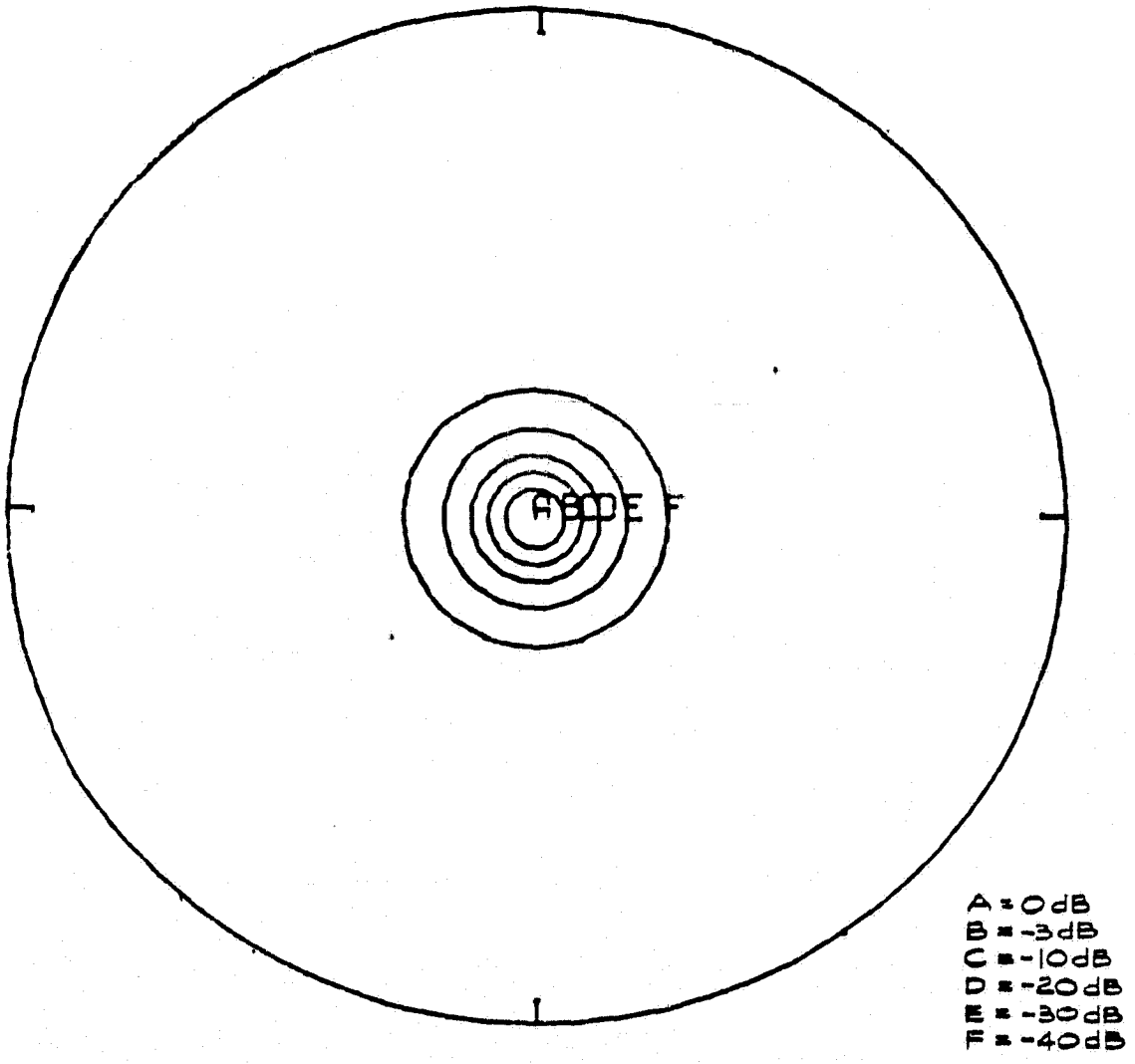

Figure 4-3. Ideal Chebyshev Radiation Contour
R = 0.5 dB
n = 3

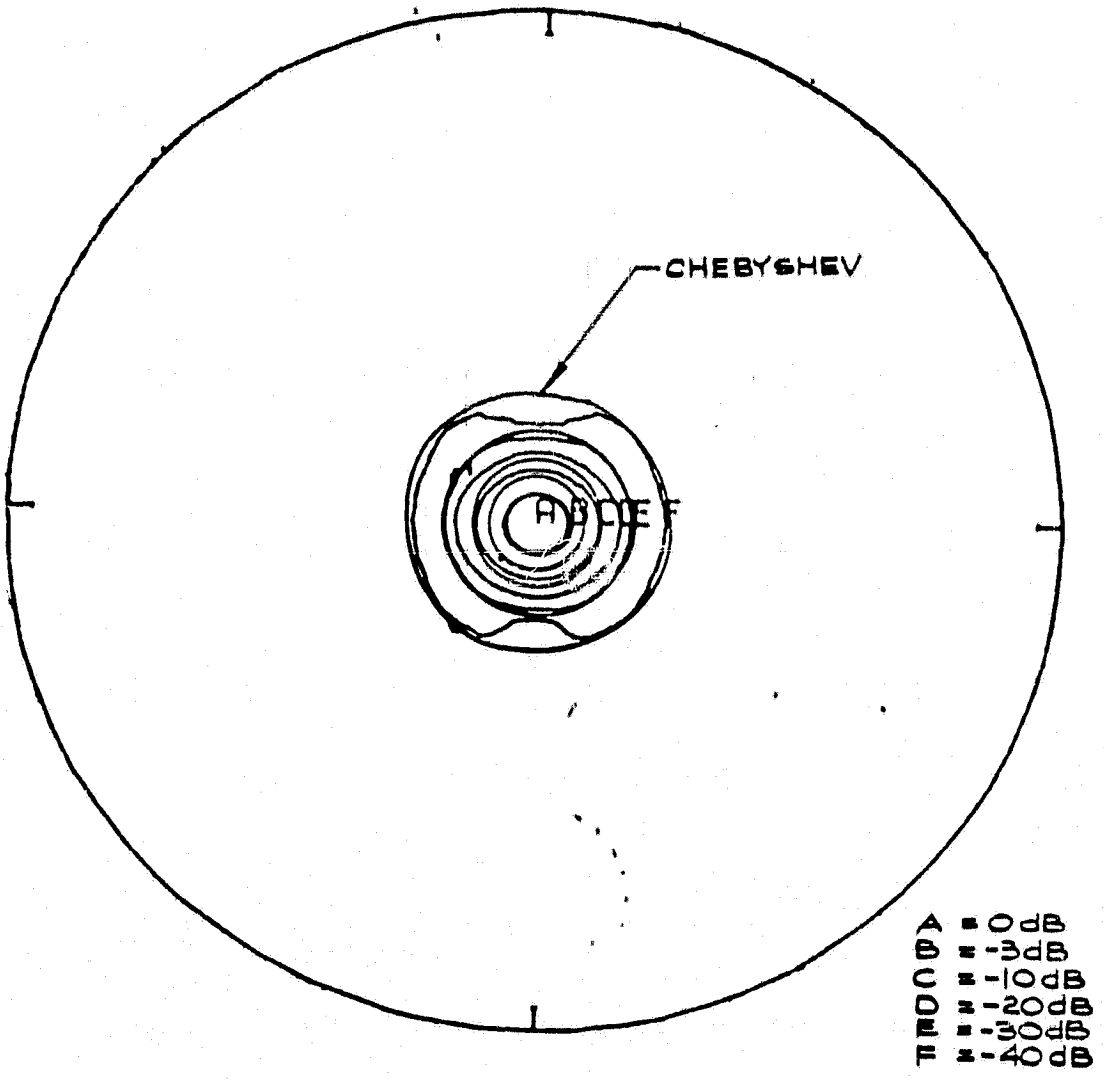

Figure 4-4. 19-element reflection pattern for best approximation to the Chebyshev of Figure 4-3.

Table 4-1. FEEDING COEFFICIENTS FOR THE 19-ELEMENT ARRAY

Feed File: $a/\lambda = 0.6$

Feed	$\hat{x}^1$	$\hat{y}^1$	x	y	z
1	0	0	0	0	0
2	0	0.6	0	-0.6	0
3	0	-0.6	0	-0.6	0
4	0.6	0.3	0.5326	-0.3	0.2764
5	0.6	-0.3	0.5326	0.3	0.2764
6	0.6	0.3	-0.5326	-0.3	-0.2764
7	-0.6	-0.3	-0.5326	0.3	-0.2764
8	0.6	0.9	0.5326	-0.9	0.2764
9	0.6	-0.9	0.5326	0.9	0.2764
10	0	1.2	0	-1.2	0
11	0	-1.2	0	1.2	0
12	-0.6	0.9	-0.5326	-0.9	-0.2764
13	-0.6	-0.9	-0.5326	0.9	-0.2764
14	1.2	0.6	1.0651	-0.6	0.5528
15	1.2	0	1.0651	0	0.5528
16	1.2	-0.6	1.0651	0.6	0.5528
17	-1.2	0.6	-1.0651	-0.6	-0.5528
18	-1.2	0	-1.0651	0	-0.5528
19	-1.2	-0.6	-1.0651	0.6	-0.5528

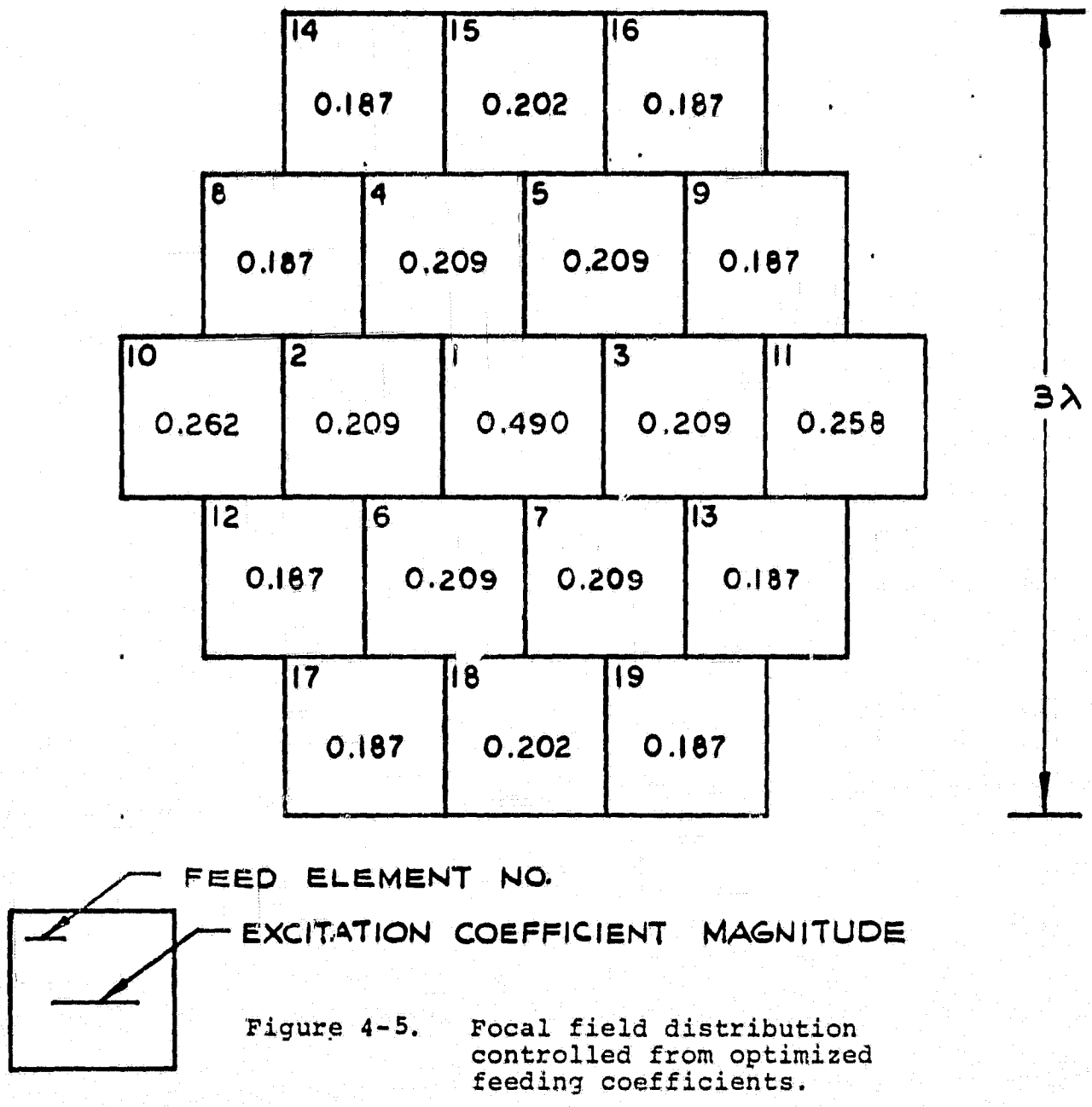

Figure 4-5. Focal field distribution controlled from optimized feeding coefficients.

4.3 Realizing the Focal Field Distribution With A Rectangular Multimode Horn

A multi-element array type feed is more expensive and probably more lossy than this broadcasting satellite application warrants. We therefore examine the possibility of using a single aperture type of feed in a qualitative manner.

Rudge and Adtia [9, 10, 11] have proposed the use of higher order modes in a waveguide to synthesize (or match) the focal plane field for a uniform incident plane wave. There are two sets of higher modes employed. One set is used to shape the principal polarization distribution and the other set is used to match the cross polarization component. The higher order modes can be generated and propagated by a discontinuity, such as step, iris, etc., in an over-sized waveguide. For a rectangular guide, the incident, dominant mode (TE_{10} mode) is an odd mode. Because we are only interested in principal polarization, the use of a symmetrical discontinuity is sufficient. However, for a multi-mode horn, proper phasing of all the propagating modes will narrow the bandwidth. A corrugated structure is much more wideband and therefore is more desirable. Because the equal power contour of the focal field distribution for a Chebyshev far-field pattern exhibits an elliptical shape, the use of a rectangular corrugated horn propagating only the dominant hybrid mode (HE_{11}) can produce the required focal field distribution. A first cut at the design of such a horn is shown in Figure 4-6. The exact details of a suitable design are left for future work.

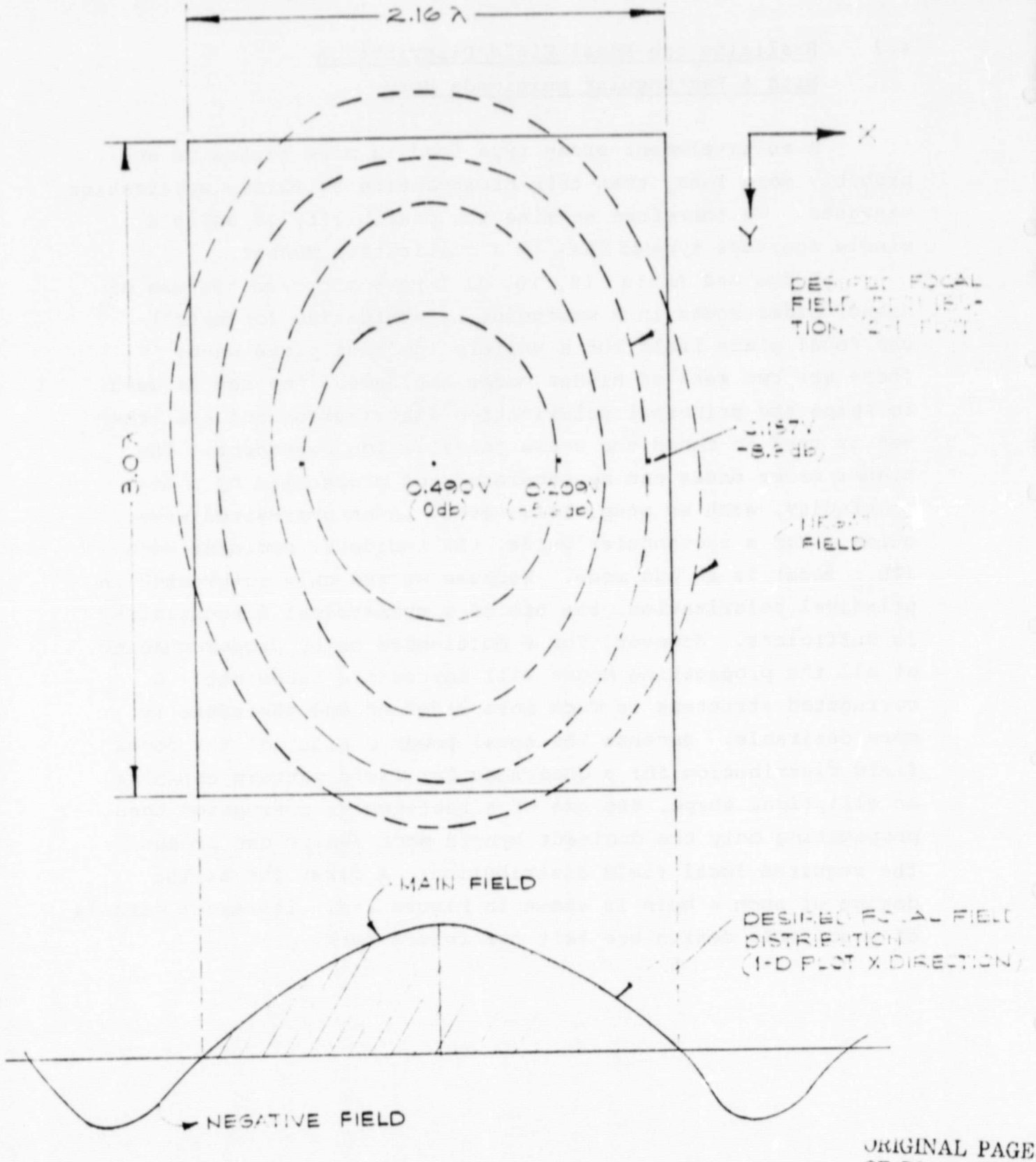

Figure 4-6A. A determination of a rectangular corrugated waveguide aperture size.

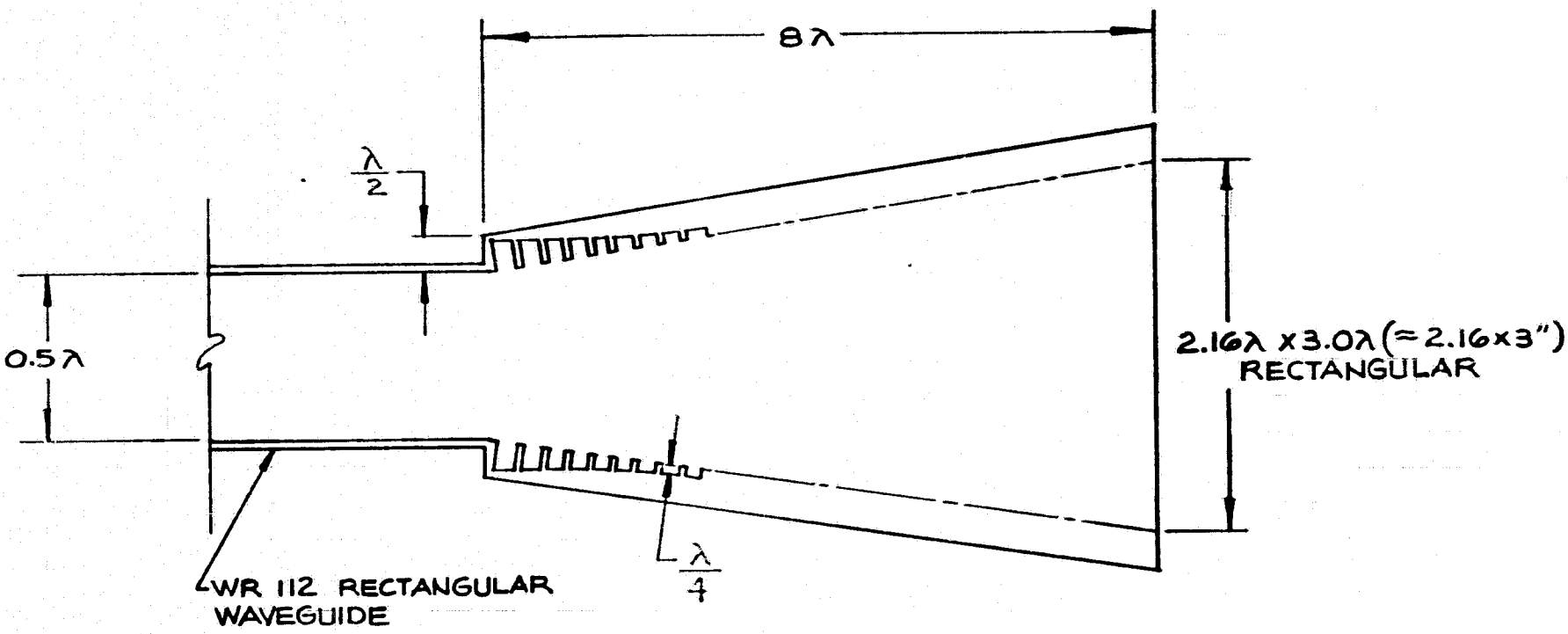

Figure 4-6B. A rectangular corrugated horn for approximating a focal field distribution corresponding to a Chebyshev far-field pattern.

5.0 MECHANICAL DESIGN AND BUDGETARY COST ESTIMATE

5.1 Objectives

The objectives of this section are to prepare a mechanical design and a budgetary cost analysis for the 1.22m offset-fed antenna with the geometric parameters developed in Section 2. We will consider the mechanical and structural requirements necessary to accommodate the following constraints or goals for a broadcast satellite applications.

a. Minimum shipping volume
b. Ease of shipping, assembly, and maximum live load stability
c. Minimum instruction for assembly
d. Ease of adjustability for finding satellite and adjusting polarization
e. Minimum deflections for maximum signal integrity
f. Minimum costs
g. Resistance to deleterious environmental effects

The budgetary cost estimates herein are based on amorization of tooling costs over 10,000 units. It is likely that more than one supplier would enter the marketplace, and so 10,000 units/year is a conservative, low estimator for production quantities. Six alternative configurations were developed and evaluated for cost and performance. The recommended design has the following features.

a. Shipping Volume/Weight: Rough container volume is 5 ft. x 5 ft. x 1 ft. The estimated weight based on sheetmetal design is approximately 130 lbs. for a steel dish design, and 90 lbs. for an aluminum dish design.
b. The design permits assembly without the need for special tools or skilled labor. Adjustments for feed rotation and alignment are straightforward.
c. The component surfaces are all galvanized except for the feed and the dish face which will be painted to reduce heat reflection.

d. Allowable dish surface deviation -

.010 inch RMS design,
.020 inch RMS maximum

e. For additional performance specification, see Section 6.

5.2 Summary of Salient Mechanical Parameter Calculations

Wind load is the primary design constraint. We have assumed a nominal beam deflection of less than 0.15° and calculated the various parameters based on the methods described in the Andrew Bulletin 1015, "Wind Forces and Loads Produced by Parabolic Antennas." We have also assumed a maximum wind load of 80 mph.

F_a = Axial Force

F_s = Force Perpendicular To Axis

M = Twisting Moment

Applicable Formulas:

$$C_a = \frac{Fa}{AV^2},$$

$$C_s = \frac{Fs}{AV^2}$$

$$C_m = \frac{M}{DAV^2}$$

C = Coefficient

A = Frontal Area (Ft^2)

V = Wind Velocity (MPH)

D = Antenna Diameter (ft.)

$A = \frac{\pi}{4} (4 \text{ ft})^2 = 12.57 \text{ Ft}^2$, D = 4 ft., V = 80 MPH

Therefore, $F_a = 80448\ C_a$, $F_s = 80448\ C_s$

$M = 321792\ C_m$

Table 5-1. MAXIMUM THRUST DUE TO WIND LOAD FOR VARIOUS ANGLES OF ATTACK

α = angle measured from boresight axis

Angle α	Fa	Fs	M	V
0	+322#	0	0	80 MPH
45	+342#	+16#	- 48 Ft-lb	80 MPH
56	+353#	+40#	- 71 Ft-lb	80 MPH
90	- 20#	+68#	+110 Ft-lb	80 MPH
125	-101#	+97#	+121 Ft-lb	80 MPH
180	-217#	0	0	80 MPH

Using the Gaussian Model* for main beam shape and allowing 1.4 dB of loss due to deflection of the antenna at 40 MPH, we find that $\theta_{40\ MPH} = 0.153°$. Over 49 inches that is .128 inches of deflection. This deflection is for both the dish and the feed supports.

To maintain signal quality within the allowable tolerance requires analysis in the following steps:

1. Check deflection in the feed mount beams (item 3, drawing 11401-001) due to wind, ice, and dead weight loadings.
2. Check the rigidity of the joint of the feed mount beams and the dish frame.
3. Check the rigidity of the dish to stay on target with the satellite when undergoing dynamic wind loadings.

The design as it is (see attached drawing package 11401-001 through -012) has addressed checks one and two carefully but made more liberal assumptions on the third check because of the complexity of the analysis (curved plate with a circumference ring in a twisting mode) and because the mounting requirements are not clearly defined as yet but are critical in the analysis. It is expected that small changes in the mounting requirements will have no effect on the manufactured cost. Substantial changes such as a chimney mount, large base plates, etc., would probably incur additional cost because of more parts. Therefore, furthe analysis on the support structure is unwarranted until mounting methods have been determined.

---

* Main beam gain = $-12\ (\theta/\theta_{3\ dB})^2$ dB; an approximation good to $\theta = 1.5\theta_{3\ dB}$, where $\theta_{3\ dB}$ is the full 3 dB beam width.

5.3 Mechanical Design

Figure 5-1 shows an isometric view of the recommended mechanical design. Structural integrity of the antenna surface is maintained by the use of the two large but inexpensive channels. Adjustments can easily be made in aiming the antenna over a ±30° range in azimuth and a 10°-70° range in elevation. For mounting conditions other than on an ideal flat surface, more complicated mounting equipment is necessary. A chimney mount is feasible for this size antenna. The feed polarization may be easily adjusted by rotation of same in the retaining collar. Assembly is straightforward.

5.4 Cost Estimates

Table 5-2 summarizes the components in this design, the unit costs, the tooling costs, and the amortized costs.

A 1.22m offset fed microwave antenna can be designed in a kit form at a manufactured cost of $130.28/unit based on amortizing tooling cost 10,000 units.

Other factors affecting cost and designs are the esthetics and type of mount; i.e. roof, chimney, ground. However, it can be seen from the estimates that small changes in supports or tooling do not add much to the overall cost of the antenna. Each additional $10,000 of tooling adds only $1.00 to the unit; four more adjustment rods adds only $3.24, and one more base adds only $6.57. These costs are prime costs only. To estimate a sales price, the cost for program management, procurement and other manufacturing overhead functions must be included. Also, the typical markup to cover corporate operation like sales, marketing, administration, engineering, and a profit must be included. A factor of 3 to 4 times the prime cost is probably a realistic estimator. Thus, the sale price for an ultra high performance offset fed 1.22m antenna could be in the range of $400 to $500 in 1980 dollars.

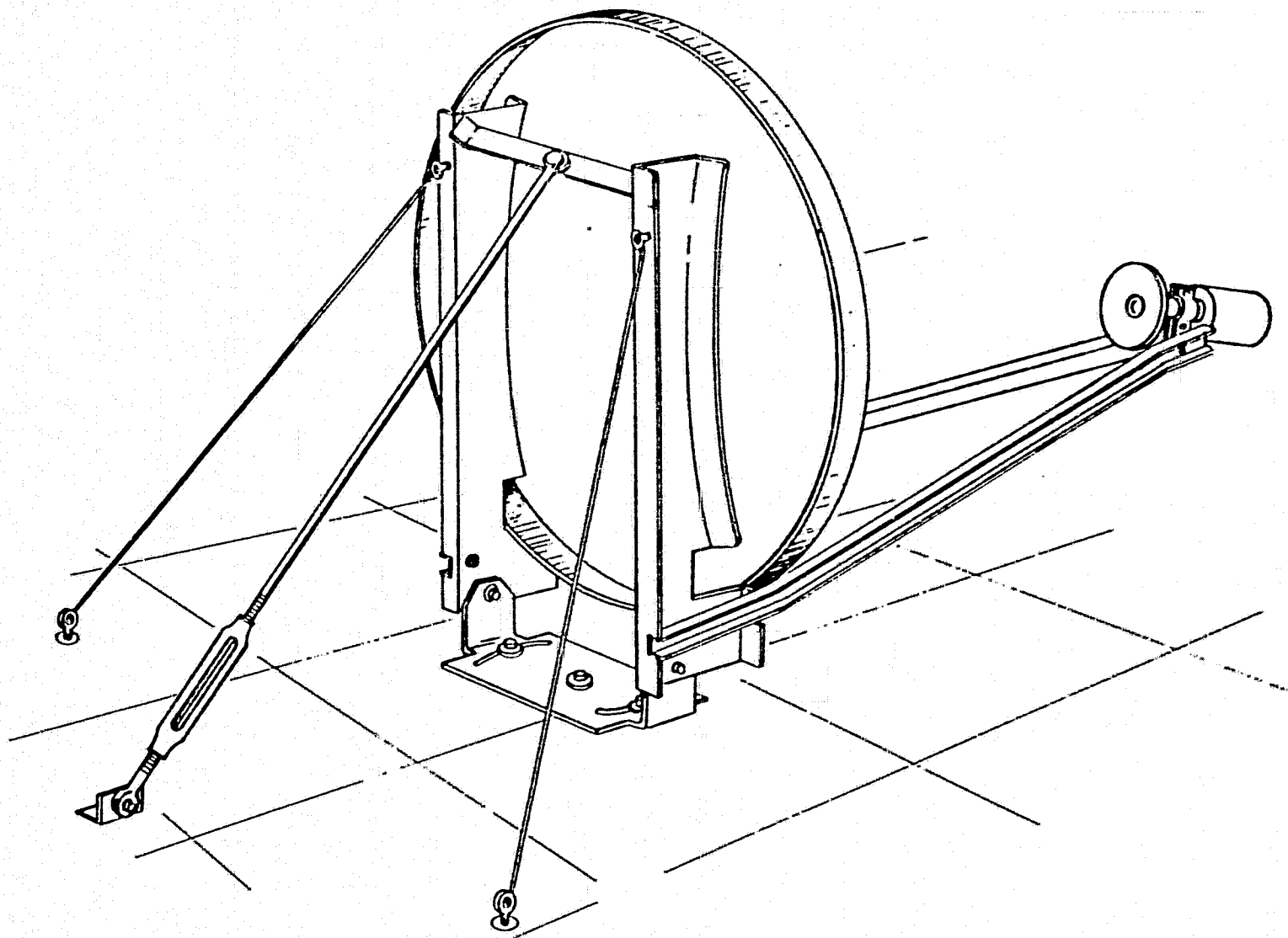

Figure 5-1. 1.22m, 12 GHz Offset Fed Antenna

Table 5-2. 1.22m OFFSET FED ANTENNA MANUFACTURING COSTS

Item/Part Number	Description	Qty	Tooling	Cost/Unit (w/o tooling)
1 11401-002	Pivot Strap	1	$ 1,500	$ 1.45
2 11401-003	Anchor angle	1	$ 1,000	$ 0.63
3 11401-004	Beam, feed mount	2	$ 5,000	$ 10.22
4 11401-005	Mounting plate, feed	1	$ 6,800	$ 1.35
5 11401-006	Clamp	1	$ 7,500	$ 0.06
6 11401-007	Adjustment rod	1		$ 0.81
7 11401-008-01	Frame, dish, RF	1	$ 25,000	$ 4.67
8 11401-008-02	Frame, dish, RH	1	$ 25,000	$ 4.67
9 11401-009	Base	1	$ 15,000	$ 6.57
10 11401-010	Feed, horn	1	$ 10,000	$ 7.00
11 11401-011	Feed, transition	1	$ 10,000	$ 3.00
12 11401-012	Antenna dish	1	$ 70,000	$ 40.91
13	Feed, electronic	1		
14	Bolt, eye, 3/8 x 6-1/2" long	1		$ 0.78
15 #2995T16	Turnbuckle	1		$ 0.77
16	Bolt	10		$ 0.15
17	Bolt	2		$ 0.03
18	Nut	12		$ 0.07
19	Washer	12		$ 0.06
	Labor-assembly & Packaging			$ 12.00
	Packaging		$ 9,000	$ 5.00
	Paperwork & Labels, etc.			$ 1.00
	Spotwelding subassembly		$ 38,000	$ 2.08
	Estimated one-time engineering cost for final design, documentation, and vendor interface		$ 30,000	
TOTAL			$268,800	$103.28

Amortized over 1 year (10,000 units)

$$\text{Manufactured cost} = \frac{\$268,800}{10,000 \text{ units}} + \$103.28/\text{unit} = \$130.16/\text{unit}$$

6.0 SPECIFICATIONS FOR A 1.22m OFFSET-FED ANTENNA

This section describes the specifications developed for the broadcasting satellite application with consumer-oriented performance goals.

6.1 GENERAL

Specifications in Section 2.0 (Environmental) below shall apply to the antenna reflector, its feed, and mount. Each item shall be considered under the following conditions:

6.1.1 Kitted, prior to assembly, in storage;

6.1.2 During transportation;

6.1.3 Assembled and operating day or night;

6.1.4 Assembled and surviving extremes.

6.2 ENVIRONMENTAL

6.2.1 Wind Operational

With wind loads below 40 mph, signal loss shall not exceed that of Figure 6-1.

6.2.2 Wind Survival

Reflector shall survive without damage winds to 80 mph without ice or 60 mph with two inches of radial ice.

6.2.3 Survival Temperature

Reflector shall survive temperatures of -40° to +140°F.

6.2.4 Temperature

Reflector shall operate within specification with ambient temperatures of -40° to +110°F.

6.2.5 Ice

Design for ½ inch radial ice on nonradiating surfaces. Reflector heatable from rear.

6.2.6 Snow

Design for six inches of snow on nonradiating surfaces.

6.2.7 Hail

Survive, without damage, hail ½ inch in diameter.

6.2.8 Solar Radiation

Reflector shall survive solar radiation from any angle (during assembly and/or storage) and shall operate within specification under solar radiation from all operational angles.

6.2.9 Earthquake

No survival requirements.

6.2.10 Salt

No corrosion after 5 years in non-coastal locations, 3 years in coastal locations.

6.2.11 Fungus

Shall not be a fungus nutrient.

6.3 PHYSICAL REFERENCE

For reference, the following nonenvironmental specifications apply:

6.3.1 Aperture

1.22m equivalent diameter of projected circular aperture.

6.3.2 F/D Ratio

Focus distance of the reflector parent parabola shall be 0.5 times parent parabola diameter.

6.3.3 Azimuth and Elevation

Azimuth adjustment ±30° around a nominal azimuth direction.
Elevation adjustment = 5° to 70°.
Resolution of pointing indicator: 1° division.

6.2.4 Heat Focusing

When aimed at the sun for five minutes, feed temperature shall not exceed 150°F.

6.3.5 Fire Retardant

All materials used in significant quantities shall be fire retardant.

6.3.6 Operational Life

Operational life shall ve five years minimum.

6.3.7 Feed Weight

Weight of feed and integrally associated equipment will not exceed 10 pounds.

6.4 ELECTRICAL PERFORMANCE PARAMETERS

6.4.1 Frequency Band

The receive band shall be 11.7-12.2 GHz.

6.4.2 Gain

The gain at 12.0 GHz shall be a minimum of 41.0 dB (55% efficiency). As a goal, the actual gain target shall be 41.5 dB (60% overall efficiency).

6.4.3 Near-in Sidelobe Levels

The first and second sidelobes shall be 30 dB or more below the on-axis gain level for at least the plane through the equatorial arc. As a goal, the first and second sidelobes for the orthogonal plane shall also be 30 dB or more below the on-axis gain level. The first and second sidelobe level specification for the plane orthogonal to the equatorial arc plane shall be at least 25 dB below the on-axis gain level.

6.4.4 Sidelobe Level Envelope

The sidelobe level envelope for all principal polarization planes shall be given by the second-order (n=2) Chebyshev envelope defined by the following equation:

$$G(k\theta/\theta_0) = G(0) - 10 \log_{10} \left(1 + E^2 C_n^2 (k\theta/\theta_0)\right) \text{ dB}$$

where

$G(\theta)$ = the Chebyshev envelope

$G(0)$ = the on-axis gain of the antenna

θ_0 = ½ of the full 3 dB beamwidth in degrees

E = $(10^{R/10} - 1)^{1/2}$, a parameter

R = the ripple factor borrowed from filter theory, in dB

$C_n(k\theta/\theta_0)$ = $\cosh \left(n \cosh^{-1} (k\theta/\theta_0)\right)$

n = the order of the polynomial, 1, 2, . . .

k = the normalizing constant which matches the envelope to the 3 dB point at the 3 dB beamwidth θ_0

$$= \cosh \left(\frac{\cosh^{-1}(1/E)}{n} \right)$$

This envelope is only significant outside the 3 dB beamwidth, and is valid only to a level of 0 dB-isotropic. This envelope covers all effects due to an imperfect reflector surface, scattering from reflector edge, spillover from the feed horn, and so forth.

As a goal, the antenna shall meet a third order envelope (n=3, Eq.1) in the plane of the equatorial arc to a level of 0 dBi.

6.4.5 Polarization

The polarization shall be linear and vertical to the plane of the equatorial arc.

6.4.6 Crosspolarization Isolation

This on-axis crosspolarization isolation shall be 25 dB. Off-axis crosspolarization shall be a minimum of 20 dB.

6.5 REFERENCE FEED SYSTEM

6.5.1 General

The basic feed system for reference purposes shall consist of a corrugated horn with a total aperture of 3.5 wavelengths.

6.5.2 Far Field Pattern

The feed horn far field pattern shall have at least -25 dB level relative to the on-axis gain at ±28° off-axis for all planes; i.e., it shall be axially symmetric to within ±2 dB at the ±28° points for two orthogonal planes.

6.5.3 Polarization Adjustment

The feed system must be capable of adjustment about the feed horn axis of ±75° from a local vertical sense.

6.5.4 Feed Position Adjustment

The feed system must be capable of ±0.5 inch linear adjustment along the boresight axis of the parent parabola in order to guarantee being positioned at the exact focal point of the reflector system.

6.5.5 Waveguide Flange Interface

The feed system shall have a standard waveguide flange commonly used on WR75 waveguide for an interface.

6.5.6 VSWR

The feed system Voltage Standing Wave Ratio (VSWR) shall be less than 1.25 : 1 over the receive band.

6.5.7 Sidelobes

The feed sidelobes shall be at least 30 dB below the on-axis gain.

6.6 ALTERNATE FEED SYSTEM

6.6.1 7-Element Cluster Array

The alternate feed system shall consist of a 7-element cluster array of 1λ square horns arranged in a pattern depicted in Figure 6-2.

6.6.2 Far Field Pattern

This feed system shall have an excitation magnitude and phase given by the table in Figure 6-2. The feed system shall be driven by power divider network from a common coaxial input port.

11.7 - 12.2 GHz

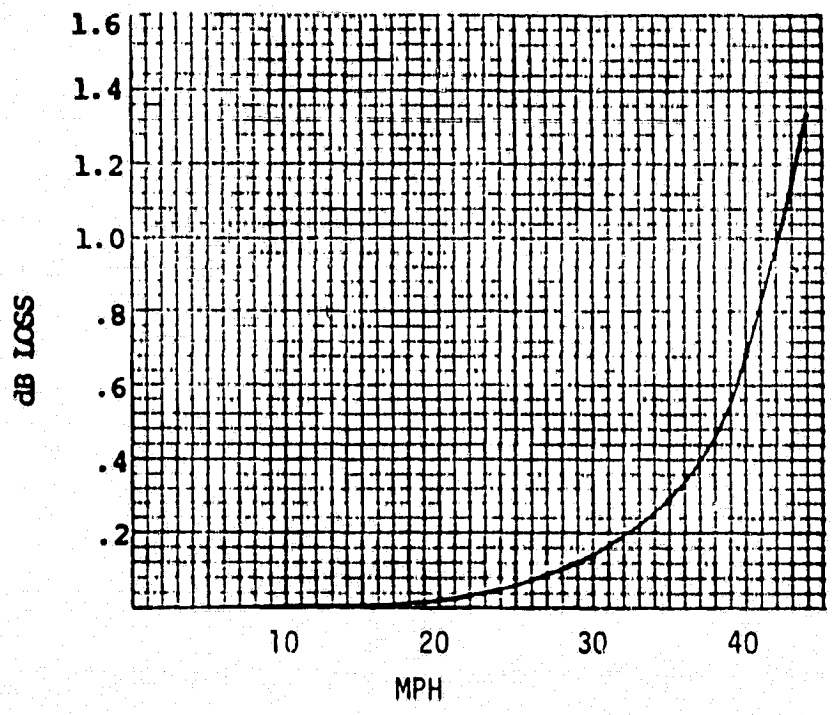

Figure 6-1. Signal Loss Due to Wind Load.

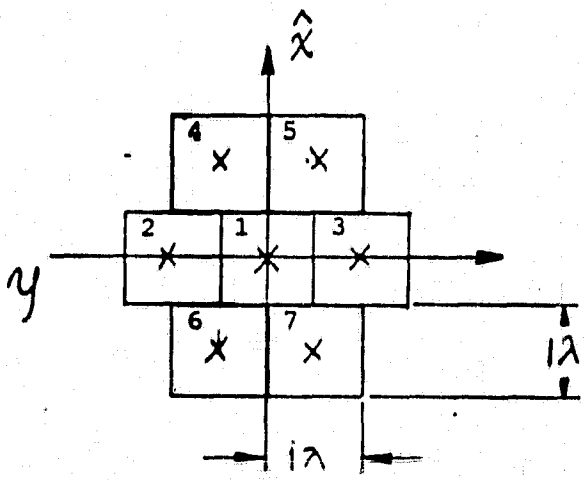

Element Number	Feed Coordinates x	y	z	Excitation Coefficient MAG	Phase
1	0	0	0	0.937	25.14°
2	0	1	0	0.141	28.70°
3	0	-1	0	0.165	28.64°
4	1	½	0	0.141	39.60°
5	1	-½	0	0.135	39.50°
6	-1	½	0	0.130	64.30°
7	-1	-½	0	0.141	79.30°

Figure 6-2. 7-Element Feed and Excitation for an Offset-Fed Antenna Design.

7.0 CONCLUSION AND RECOMMENDATIONS

We have analyzed the range of performance available for the three conflicting parameters of first sidelobe level, gain, and far out sidelobe levels using a corrugated feed horn with an axisymmetric pattern as a baseline point of departure. The results indicate that the very stringent Chebyshev envelope with n = 2 can be met with an f/D = 0.5 and a corrugated horn with flare angle and aperture width of 30° and 3.5λ respectively. The analysis of Section 2 indicates that the sidelobe level design goals can be met in the plane of the equatorial arc, but the gain is unlikely to exceed 41 dB (55%) without additional effort in corrugated feed horn design and optimization on a test range.

Changing from an analysis to a synthesis procedure, in Section 3 we used a seven-element cluster array of 1λ horns and determined the optimum set of amplitude and phase coefficients for obtaining the desired Chebyshev response in the far field. This approach yielded entirely satisfactory results with respect to the sidelobe goals, but suffers from a possible loss in overall efficiency because of feed distribution network insertion loss. Also, the assumptions made concerning the individual far-field patterns of each 1λ horn require experimental validation before any degree of confidence could be placed in the approach. This method is likely to add $20 - $50 to the sale price of the antenna, but it may be worth it in terms of really obtaining -30 dB first sidelobes and a 0 dBi or better plateau for the far-out regions. Again, only experimental verification can provide the level of confidence needed to go forward with a strong statement to the CCIR concerning cost and performance.

Through an extension of the multiple element cluster array concept, we approximated the focal field distribution needed for matching the ideal Chebyshev far-field pattern and found a nearly symmetric ellipticity was required. This ellipticity can be obtained through the use of a rectangular corrugated horn. The parameters for this horn were not derived, but

since the relative focal field intensity is now approximately known, it is possible to pursue this option intelligently.

We designed a low-cost realization of the 1.22m offset fed antenna according to the assumption of man-producibility for a consumer-oriented market. The manufacturing cost in 10,000 units/year production quantities is in the range of $150 per antenna, and a sale price is in the range of $400 - $500.

We developed a performance specification for this application suitable for a procurement and development effort for a prototype.

Recommendations

We recommend fabrication of an electrical analog version of the offset fed antenna to be made in fiberglass using hand lay up and high precision surface fabrication techniques. This will permit verification of performance without any large investment in tooling by NASA, which is inappropriate for a government agency.

We recommend fabrication of a true corrugated feed for use in a baseline reference test setup must as was done analytically in Section 2. We recommend that some additional design and analysis be done on the rectangular corrugated horn and the 7-element cluster array to further substantiate their viability in the present application. After some additional study, the best alternative should be built and tested on a range, just as the axisymmetric corrugated horn should be tested.

Pending the results of these tests, a decision could be made regarding the type of horn for use in a mass-producible model: circular corrugated, rectangular corrugated, or a cluster array.

APPENDIX I

DERIVATION OF FAR-FIELD FEED HORN PATTERNS FROM AN ARBITRARY APERTURE DISTRIBUTION

In previous work [1], a specific aperture distribution in the form of $J_1(u)/u$ was shown to provide a far-field pattern for the main reflector that met the Chebyshev envelope. In this section, we summarize how we transform the aperture illumination function into the required feed horn far-field pattern through a geometric mapping. The process is described completely in the article by Rahmat-Samii [7]. Figure A-1 shows the definition of the two coordinate systems we are relating via the transformation. The aperture coordinate system is a polar coordinate type of system with an origin eminating from the center of the aperture parallel to the axis of the main parabola as shown in Figure A-1 with components given by and ϕ. The feed horn oriented coordinate system is a spherical system with principal components of θ_F and ϕ_F. θ is measured from the principal axis of the feed horn and ϕ is measured from the vertical reference line so marked in Figure A-1.

Two intermediate coordinate systems are necessary to complete the transformation. The second and third coordinate systems are as follows: We have a coordinate system centered at the focus of the parent parabola with main axis along the boresight axis of the parabola which is a cylindrical system with components z, r, ϕ. The fourth coordinate system is one centered in the aperture of the parent parabola which is a spherical system with components ρ, θ_ρ and ϕ_ρ. We have kept track of polarization orientation.

The steps in the transformation process take us from the feed horn centered coordinate system to the parent parabola focus coordinate system in θ_ρ and ϕ_ρ. From there we move to the parent parabola aperture centered coordinate system with components z, r, ϕ and now from there we map from r, ϕ and z into r, ϕ and z via a translation in the aperture plane.

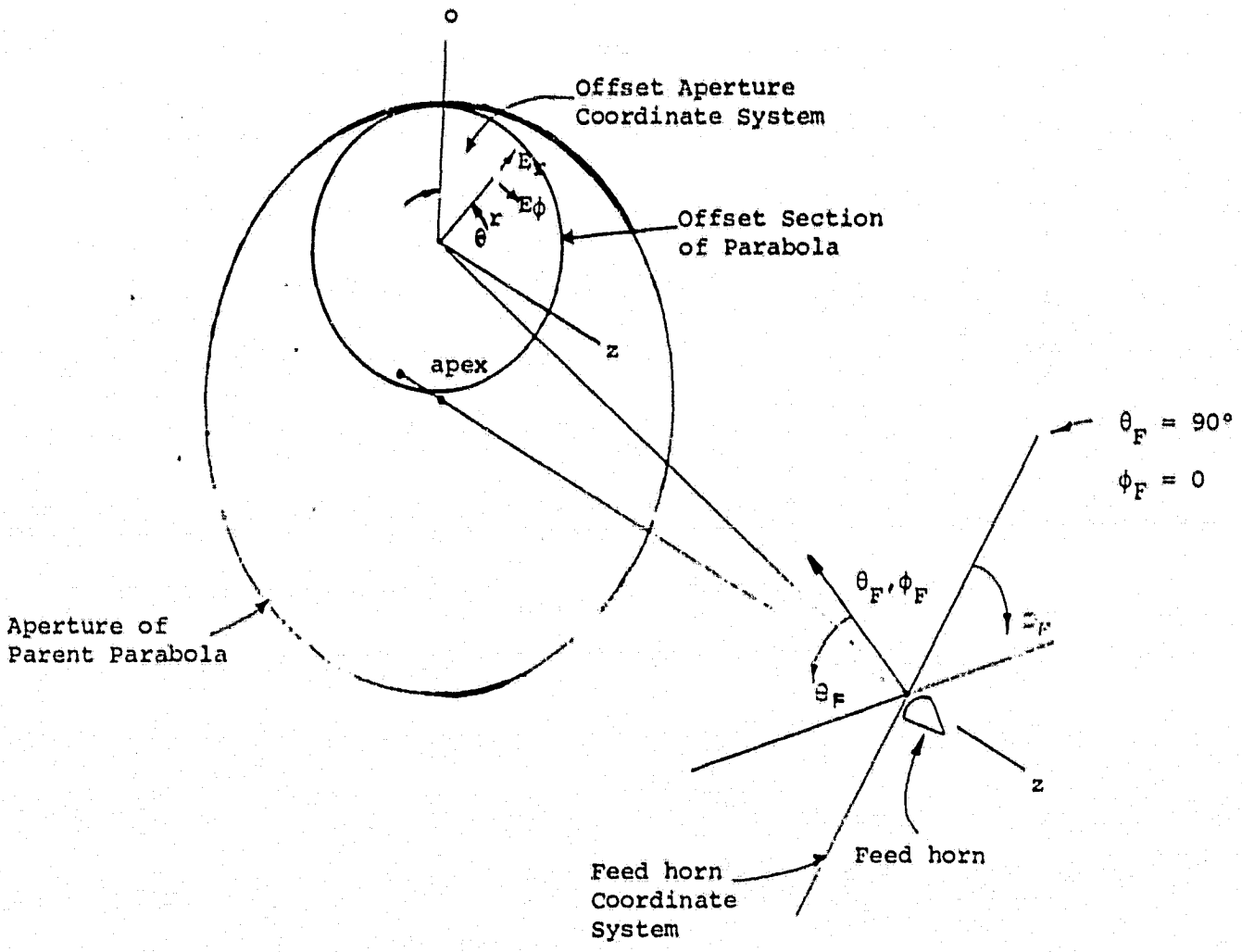

Figure A-1. DEFINITION OF COORDINATE SYSTEMS FOR RELATING FEED HORN FAR-FIELD PATTERNS TO AN ARBITRARY APERTURE DISTRIBUTION IN OFFSET SECTION.

Table A-1. COORDINATE SYSTEM DEFINITION

I. Feed horn centered coordinate system:	Spherical, centered on z_F axis with components ρ, θ_F, ϕ_F
II. Offset Aperture coordinate system:	Cylindrical, centered on aperture plane and z axis on reflected ray for $\theta_F = 0$ (θ angle) with components z, r, ϕ
III. Parent parabola aperture coordinate system:	Cylindrical, with origin at aperture center, on axis, with components z, r , ϕ
IV. Parent parabola focus coordinate system:	Spherical, with origin at focus, with components, ρ, θ_ρ, ϕ_ρ

SUMMARY OF RESULTS

Let $E_{\hat{r}}^{(r)}$ and $E_{\hat{\phi}}^{(r)}$ be the aperture plane components of the electric field in polar coordinates centered on the (circular) aperture with the direction towards the feedhorn being π, (-180°). ($E_{\hat{r}}$ and $E_{\hat{\phi}}$ are the components for the orthonormal basis $\underline{e}_{\hat{r}}$, $\underline{e}_{\hat{\phi}}$, where $\underline{e}_{\hat{r}}$ and $\underline{e}_{\hat{\phi}}$ are unit vectors parallel to the r and ϕ directions respectively).

The far field of the feedhorn has components $E_{\hat{\Theta}_F}$ and $E_{\hat{\Phi}_F}$ for the orthonormal basis $\underline{e}_{\hat{\rho}}$, $\underline{e}_{\hat{\Theta}_F}$, $\underline{e}_{\hat{\Phi}_F}$. The radiation travels in the direction $\pm\, \underline{e}_{\hat{\rho}}$ as given by geometrical optics.

$$\left(\underline{k} = \pm \frac{2\pi}{\lambda} \underline{e}_{\hat{\rho}} \right)$$

In terms of the aperture field $E_{\hat{r}}(r,\phi)$ and $E_{\hat{\phi}}(r,\phi)$ (these are given), we can obtain the feedhorn radiation field by the relation:

$$\begin{pmatrix} E_{\hat{\Theta}_F} \\ E_{\hat{\Phi}_F} \end{pmatrix} = -\left[\frac{1 + \cos\Theta_p}{2f}\right] \begin{pmatrix} A & +B \\ -B & A \end{pmatrix} \begin{pmatrix} \cos(\phi-\phi') & -\sin(\phi-\phi') \\ \sin(\phi-\phi') & \cos(\phi-\phi') \end{pmatrix} \begin{pmatrix} E_{\hat{r}}(r,\phi) \\ E_{\hat{\phi}}(r,\phi) \end{pmatrix}$$

where
$$\left.\begin{aligned} r &= (r'^2 + b^2 - 2br'\cos\phi')^{\frac{1}{2}} \\ \sin\phi &= \frac{r'}{r}\sin\phi' \\ \cos\phi &= \frac{r'\cos\phi' - b}{r} \\ b &= \frac{2f\sin\Theta_c}{1+\cos\Theta_c} + b_o \end{aligned}\right\}$$

$$\left.\begin{aligned} r' &= \frac{2f\sin\Theta_p}{1+\cos\Theta_p} \\ \phi' &= \phi_p \end{aligned}\right\}$$

$$\left.\begin{aligned} \cos\Theta_p &= \cos\Theta_F \cos\Theta_c - \sin\Theta_F \cos\phi_F \sin\Theta_c \\ \sin\Theta_p \sin\phi_p &= \sin\Theta_F \sin\phi_F \\ \sin\Theta_p \cos\phi_p &= \sin\Theta_F \cos\phi_F \cos\Theta_c + \cos\Theta_F \sin\Theta_c \end{aligned}\right\}$$

and where A and B are given by:

$$\left(\sin\Theta_p = \sqrt{1 - \cos^2\Theta_p} \right.$$

$$A = \frac{\sin\Theta_F \cos\Theta_c + \cos\Theta_F \cos\phi_F \sin\Theta_c}{\sin\Theta_p}$$

$$B = \frac{\sin\phi_F \sin\Theta_c}{\sin\Theta_p}$$

A and B satisfy $A^2 + B^2 = 1$

f is the focal length of the parabolic reflector

Θ_c is the inclination angle of the feedhorn (see Figure 1)

b_o is the offset distance from the point on the aperture plane that ray traces to (Θ_F, ϕ_F) b_o is > 0 for offsets in the direction away from the feedhorn

Far-field feed horn patterns were calculated for a range of aperture distributions based on the $J_1(u)/u$ function in which the edge illumination taper was varied from 15 to 30 dB. Figure A-2 shows the far-field pattern for two principal planes, the 0 and 90° plane for an f/D of the parent parabola of 0.5 in a 25 dB edge taper. The beam required for perfect generation of this particular aperture illumination function is elliptical and narrower in the $\phi = 0$ and 180 plane than the ±90° plane. This is intuitively obvious from an inspection of the projected cross-section of a circular aperture onto the focal point of the parent parabole. More importantly, the extent of the ellipticity is extremely small; at the edge of the dish, the differential amplitude is approximately 4 dB.

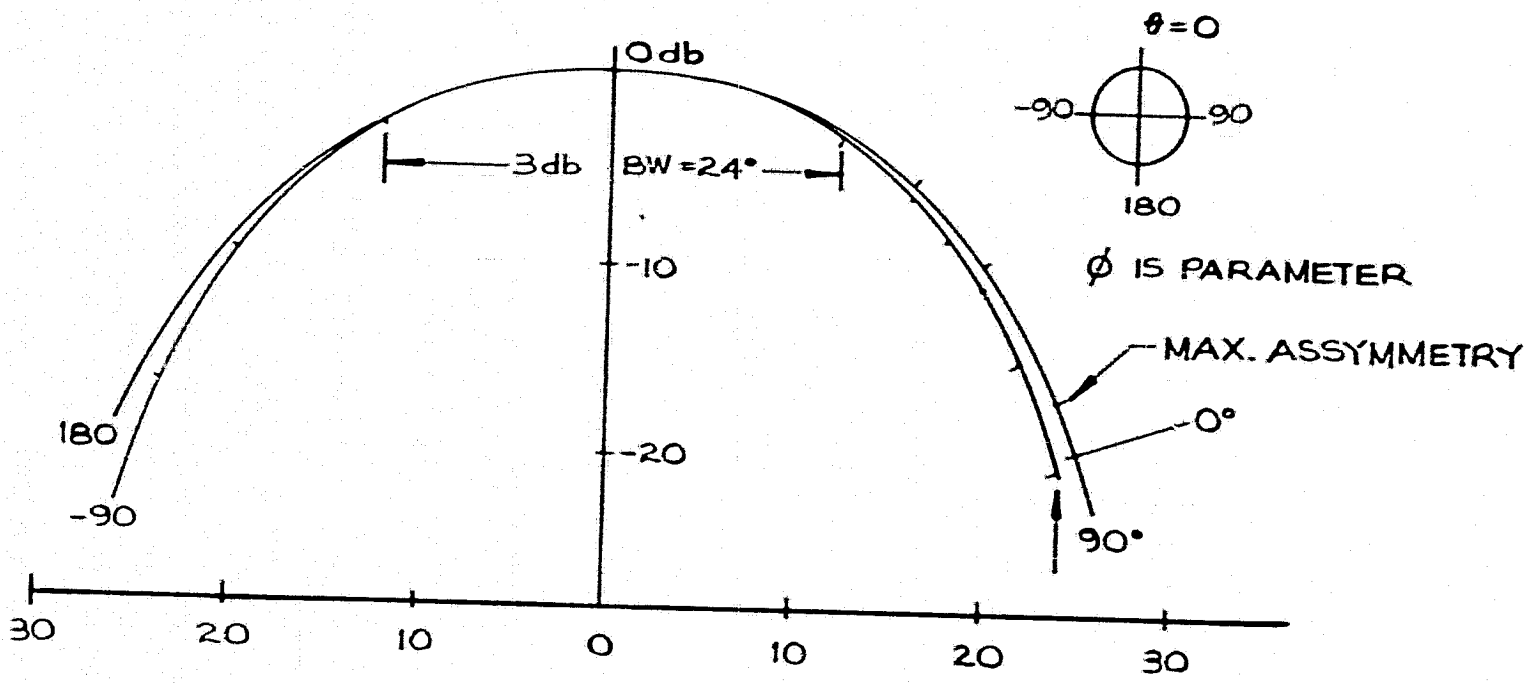

Figure A-2. COMPUTED FEED FAR-FIELD PATTERN TO OBTAIN $J_1(u)/u$ IN APERTURE.

$f/D = 0.5$ A=3.6 (25 dB EDGE TAPER)

Table A-2. FAR-FIELD FEED HORN DATA FOR GENERATION OF A $J_1(u)/u$ APERTURE DISTRIBUTION WITH A 25 dB EDGE ILLUMINATION TAPER

Parent Parabola f/D = 0.5 A = 3.6

θ_F	ϕ_F	$E_{\theta F}$	$E_{\phi F}$	$10 \log (E_{\theta F}^2 + E_{\phi F}^2)$	$\tan^{-1}(\frac{E_{\theta F}}{E_{\phi F}})$
2.000	.000	-.495	.000	-.100	-89.943
4.000	.000	-.482	.000	-.338	-89.943
6.000	.000	-.460	.000	-.748	-89.943
8.000	.000	-.429	.000	-1.342	-89.943
10.000	.000	-.392	.000	-2.142	-89.943
12.000	.000	-.348	.000	-3.175	-89.943
14.000	.000	-.299	.000	-4.483	-89.943
16.000	.000	-.247	.000	-6.131	-89.943
18.000	.000	-.195	.000	-8.220	-89.943
20.000	.000	-.142	.000	-10.932	-89.943
22.000	.000	-.093	.000	-14.645	-89.943
24.000	.000	-.048	.000	-20.412	-89.943
26.000	.000	.000	.000	-74.000	.000
28.000	.000	.000	.000	-74.000	.000
30.000	.000	.000	.000	-74.000	.000
2.000	30.000	-.428	.250	-.100	-59.747
4.000	30.000	-.415	.245	-.337	-59.493
6.000	30.000	-.395	.235	-.745	-59.238
8.000	30.000	-.368	.221	-1.336	-58.980
10.000	30.000	-.335	.204	-2.128	-58.719
12.000	30.000	-.297	.182	-3.150	-58.456
14.000	30.000	-.255	.158	-4.441	-58.189
16.000	30.000	-.211	.132	-6.060	-57.919
18.000	30.000	-.167	.105	-8.106	-57.646
20.000	30.000	-.122	.078	-10.746	-57.369
22.000	30.000	-.081	.052	-14.326	-57.089
24.000	30.000	-.043	.028	-19.767	-56.803
26.000	30.000	.000	.000	-74.000	.000
28.000	30.000	.000	.000	-74.000	.000
30.000	30.000	.000	.000	- .000	.000
2.000	60.000	-.244	.431	-.099	-29.568
4.000	60.000	-.235	.421	-.335	-29.131
6.000	60.000	-.221	.404	-.738	-28.692
8.000	60.000	-.204	.379	-1.318	-28.250
10.000	60.000	-.184	.348	-2.092	-27.806
12.000	60.000	-.161	.312	-3.084	-27.357
14.000	60.000	-.138	.272	-4.328	-26.906
16.000	60.000	-.113	.228	-5.876	-26.450
18.000	60.000	-.089	.183	-7.811	-25.991
20.000	60.000	-.066	.139	-10.271	-25.526

TABLE A-2 (continued)

θ_F	ϕ_F	$E_{\theta F}$	$E_{\phi F}$	10 log $(E_{\theta F}^2 + E_{\phi F}^2)$	$\tan^{-1}\left(\frac{E_{\theta F}}{E\phi_F}\right)$
22.000	60.000	-.045	.096	-13.529	-25.057
24.000	60.000	-.026	.056	-18.241	-24.583
26.000	60.000	.000	.000	-74.000	.000
28.000	60.000	.000	.000	-74.000	.000
30.000	60.000	.000	.000	-74.000	.000
2.000	90.000	.004	.495	-.099	.501
4.000	90.000	.008	.482	-.333	1.001
6.000	90.000	.012	.461	-.729	1.503
8.000	90.000	.015	.432	-1.295	2.005
10.000	90.000	.017	.396	-2.045	2.509
12.000	90.000	.019	.354	-2.998	3.014
14.000	90.000	.019	.309	-4.183	3.520
16.000	90.000	.018	.261	-5.642	4.029
18.000	90.000	.017	.212	-7.442	4.540
20.000	90.000	.014	.164	-9.690	5.054
22.000	90.000	.011	.117	-12.587	5.570
24.000	90.000	.008	.074	-16.568	6.090
26.000	90.000	.004	.035	-22.954	6.614
28.000	90.000	.000	.000	-74.000	.000
30.000	90.000	.000	.000	-74.000	.000
2.000	120.000	.251	.427	-.099	30.435
4.000	120.000	.248	.414	-.330	30.866
6.000	120.000	.240	.394	-.719	31.295
8.000	120.000	.228	.368	-1.273	31.724
10.000	120.000	.212	.337	-2.000	32.151
12.000	120.000	.193	.302	-2.917	32.578
14.000	120.000	.171	.264	-4.048	33.005
16.000	120.000	.148	.224	-5.427	33.431
18.000	120.000	.123	.184	-7.107	33.858
20.000	120.000	.098	.144	-9.174	34.285
22.000	120.000	.074	.106	-11.778	34.713
24.000	120.000	.050	.071	-15.221	35.141
26.000	120.000	.028	.040	-20.271	35.571
28.000	120.000	.000	.000	-74.000	.000
30.000	120.000	.000	.000	-74.000	.000
2.000	150.000	.430	.246	-.099	60.247
4.000	150.000	.420	.238	-.328	60.495
6.000	150.000	.403	.226	-.713	60.741
8.000	150.000	.379	.210	-1.257	60.985
10.000	150.000	.350	.192	-1.968	61.229
12.000	150.000	.317	.172	-2.861	61.471
14.000	150.000	.280	.151	-3.954	61.713
16.000	150.000	.241	.128	-5.279	61.953
18.000	150.000	.201	.106	-6.881	62.193
20.000	150.000	.161	.084	-8.832	62.433

TABLE A-2 (continued)

θ_F	ϕ_F	$E_{\theta F}$	$E_{\phi F}$	10 log $(E_{\theta F}^2 + E_{\phi F}^2)$	$\tan^{-1}(\frac{E_{\theta F}}{E_{\phi F}})$
22.000	150.000	.122	.063	-11.254	62.672
24.000	150.000	.085	.044	-14.384	62.911
26.000	150.000	.052	.026	-18.767	63.150
28.000	150.000	.000	.000	-74.000	.000
30.000	150.000	.000	.000	-74.000	.000
2.000	180.000	.496	.000	-.098	89.943
4.000	180.000	.483	.000	-.327	89.943
6.000	180.000	.462	.000	-.710	89.943
8.000	180.000	.434	.000	-1.251	89.943
10.000	180.000	.400	.000	-1.957	89.943
12.000	180.000	.361	.000	-2.840	89.943
14.000	180.000	.319	.000	-3.921	89.943
16.000	180.000	.275	.000	-5.227	89.943
18.000	180.000	.229	.000	-6.802	89.943
20.000	180.000	.184	.000	-8.713	89.943
22.000	180.000	.140	.000	-11.075	89.943

REFERENCES

[1] James M. Janky, William T. Zaumen, Lin-Shan Lee, "On Attaining Lower Sidelobes and New Antenna Envelopes for Better Orbit Spectrum Utilization in Satellite Broadcasting," IEEE Transactions on Broadcasting, Sept. 1979; see also final report under NASA Contract NAS5-25302.

[2] Final Acts of WARC-1977, The World Broadcasting Satellite Administrative Radio Conference, Geneva, 1977, published by International Telecommunications Union.

[3] Private communication from Mr. John E. Miller of NASA Goddard Space Flight Center under NASA Contract NAS5-25302.

[4] C.A. Mentzer, P.H. Pathak, and L. Peters, Jr., "Pattern Analysis of an Offset Fed Parabolic Reflector Antenna," Final Report 3220-2, NASA Contract N00178-71-C-0264, June 1972.

[5] P.J.B. Clarricoates and P.K. Saha, "Propagation and Radiation Behavior of Corrugated Feeds, Part II: Corrugated Conical Horn Feed," Proc. of IEEE, Vol. 118, pp. 1177-1186, Sept. 1971.

[6] M.S. Narasimhan and B.V. Rao, "Diffraction by Y-Flare-Angle Corrugated Conical Horns," Electronic Letters, 23 July 1970.

[7] Y. Rahmat-Samii, "Useful Coordinate Transformations for Antenna Applications," IEEE Transactions on Antennas and Propagation, Vol. AP-27, No. 4, pp. 571-574, July 1979.

[8] D.L. Gish and P. Graham, "Characteristic Impedance and Phase Velocity of a Dielectric-Supported Air Stripline with Side Walls," IEEE Transactions on Microwave Theory Antenna Techniques, March 1970.

[9] A.W. Rudge and N.A. Adtia, "Offset-Parabolic-Reflector Antennas: A Review," Proc. of IEEE, Vol. 66, No. 12, Dec.1978.

[10] A.W. Rudge and N.A. Adtia, "New Class of Primary Feed Antennas for Use with Offset Parabolic Reflector Antennas," Inst. Elec. Eng. Electronic Letter, Vol. 11, pp. 597-599, 1975.

[11] A.W. Rudge and N.A. Adtia, "Matched Feed for Offset Parabolic Reflector Antennas," Proc. 6th European Microwave Conf. (Rome, Italy), pp. 143-147, Sept. 1976.

[12] D.J. Bem, "Electric Field Distribution in the Focal Region of an Offset Paraboloid," Proc. of IEEE, Vol. 116, No. 5, p. 6.

[13] A.R. Valentino and P.P. Toulios, "Fields in the Focal Region of Offset Parabolic Antennas," IEEE Transactions on Antennas and Propagation, pp. 859-865, Nov. 1976.

SELECTED BIBLIOGRAPHY

OFFSET-FED ANTENNA SYSTEMS

1. A.W. Love, "Reflector Antennas," IEEE Press, IEEE Standard Book No.: 0-87942-104-5, John Wiley & Sons, Inc., 1978.

2. A.W. Rudge and N.A. Adatia, "Offset-Parabolic-Reflector Antennas: A Review," Proceedings of the IEEE, Volume 66, No. 12, pp. 1592 - 1618, Dec. 1978.